

IN VIVO QUANTIFICATION OF BONE STRONTIUM USING
X-RAY FLUORESCENCE

IN VIVO QUANTIFICATION OF BONE STRONTIUM USING
X-RAY FLUORESCENCE

By
Christopher Heirwegh, B.Sc.

A Thesis
Submitted to the School of Graduate Studies
In Partial Fulfillment of the Requirements
For the Degree
Master of Science

McMaster University
2008

© Copyright by Christopher Heirwegh, December 2008

Master of Science (2008)
(Medical Physics)

McMaster University
Hamilton, Ontario

TITLE: *In vivo* Quantification of Bone Strontium Using X-Ray Fluorescence

AUTHOR: Christopher Heirwegh, B.Sc. (McMaster University)

SUPERVISOR: Dr. David R. Chettle

NUMBER OF PAGES: xiv, 151

ABSTRACT

Strontium (Sr) is an element naturally present in the human skeleton and is acquired through dietary means. Exposure to strontium has been linked to both harmful and beneficial effects on skeletal health. Recently, the administration of strontium has been shown to induce a therapeutic effect of increasing bone strength and bone mineral density in women suffering from post-menopausal osteoporosis. The advent of this new therapy has warranted the continued development of an energy dispersive x-ray fluorescence (EDXRF) system that may be used as a diagnostic tool for non-invasive measuring and monitoring of *in vivo* bone strontium levels.

This device is currently housed at McMaster University and has been previously optimized to measure bone strontium *in vivo*. One shortcoming with this system is the inability to quantify absolute amounts of bone strontium *in vivo* due to Sr x-ray absorption by soft-tissue overlying bone. This work describes an attempt to examine several imaging modalities to determine which modality may provide overlying tissue thickness readings with an acceptable range of accuracy to correct for Sr x-ray absorption.

A performance comparison between magnetic resonance imaging, x-ray computed tomography, 8, 25 and 55 MHz ultrasound, in estimating the tissue thickness of seven cadaver fingers, illustrated that 55 MHz ultrasound provided a superior range of accuracy at 3.2%. It further indicated that the currently used 8 MHz ultrasound may be used to accurately estimate tissue thickness, though with a diminished accuracy of 6.6%.

EDXRF measurements were performed on cadaver fingers *ex vivo*. Analysis of results indicated that quantification might be achieved if signals are normalized to the 35 keV coherent scatter peak and correction of both soft-tissue absorption of Sr x-rays and differences in ^{125}I excitation source activity are carried out.

Four EDXRF measurements were performed on a strontium citrate supplemented individual starting six months after Sr medicating had begun. Analysis of strontium levels revealed that bone strontium was already at a plateau by the first measurement and that these levels did not change in the 6 months following.

Acknowledgements

I wish to express my sincere thanks to my supervisor, Dr. David R. Chettle, for the encouraging academic and moral support he has shown to me throughout my entire project. Thank you!

I also extend my sincere appreciation to my committee member, Dr. Ana Pejović-Milić for imparting upon me both her expertise and passion for the strontium project.

To my committee members, Dr's Richard Butler and Colin E. Webber, I thank for their guidance and professional opinions and inputs toward the completion of this study.

With great appreciation I express my gratitude to Mariangela Zamburlini Ph.D. who repeatedly gave of her time to introduce and guide me through the complexities of this project. Her patience was much appreciated.

My thanks goes out to the institutions who permitted me to use their imaging technologies in my studies and to the many individuals who have lent me their wisdom, personal time and technical support throughout: I thank Dean Inglis, Ph.D. of The Centre for Appendicular MRI Studies, Chantal Saab and Rod Rhem of the McMaster Centre for Pre-Clinical and Translational Imaging, Malka Glasner and Regy Mathew of the Mohawk-McMaster Institute of Applied Health Sciences, Sara Iradji and Michael Kolios, Ph.D. of the Department of Physics, Ryerson University and Jason Falladown and Scott McMaster of the Tandem Accelerator Building.

I thank both the Educational Anatomy lab of McMaster University for donation of the tissue samples used in this work and the anatomy support staff for providing anatomical guidance. I further thank the staff of the Hamilton Health Sciences Research Ethics Board for their advice and consideration toward my research.

To the volunteers who selflessly gave of their time to participate in my research, I am grateful. To Fiona Ahlang, Vera Iarossi and our department administrators, I thank you for the exceptional work you have done in organizing the critical details of my progress through the program. To the many members of our office building, you made

my master's experience one filled with a balance of thoughtful discussion, light-heartedness and friendship. For that, I thank you.

I thank my sisters, Danielle and Whitney Heirwegh, for openly supporting my interest in this program. To my parents, Mike and Laurie Heirwegh, I sincerely thank you both for your continued support and encouragement. You have taught me the importance of achieving one's maximum potential in life and to persevere through all obstacles. These principles, I hold dear and lay credit to how I have made it this far.

I also heartedly thank my girlfriend, Meagan Mojeski, for the warm-hearted support she has provided to me every step of the way. Thank you!

Table of Contents

1. INTRODUCTION	
1.1. Strontium	1
1.2. Strontium Metabolism	2
1.3. Therapeutic effects of administered strontium on bone health	6
1.4. Measurement of <i>in vivo</i> bone strontium using non-invasive techniques	7
1.5. Photon interactions in strontium x-ray fluorescence spectrometry	9
1.5.1. Selection of ^{125}I brachytherapy excitation source for <i>in vivo</i> bone strontium measurements	11
1.6. System optimization for <i>in vivo</i> bone strontium measurements	14
1.7. Proposed method of quantification of bone strontium measurements using soft-tissue correction and normalization to coherent scatter	17
2. SOFT-TISSUE CORRECTION USING IMAGING MODALITIES	
2.1. Introduction	19
2.1.1. Attenuation properties	19
2.1.2. Previous soft-tissue correction attempts	20
2.1.3. Monte Carlo modelling of cylindrical finger geometry	22
2.1.4. Analysis of observed strontium K_{α} to K_{β} x-ray ratios	24
2.1.5. Cross-examination of imaging modalities for optimization of soft-tissue correction	26
2.2. Materials and Methods	29
2.2.1. Gold standard finger soft-tissue thickness	29
2.2.2. Cadaver finger imaging	30
2.2.3. Re-evaluation of 8 MHz ultrasound performance	35
2.3. Results and Discussion	37
2.3.1. Gold standard finger soft-tissue thickness	37
2.3.2. Cadaver finger imaging and modality performance	38

2.3.2.1. Evidence of thickness estimation bias	44
2.3.2.2. Accuracy of imaging modalities	50
2.3.3. Re-evaluation of 8 MHz ultrasound performance	53
3. COHERENT NORMALIZATION AND XRF MEASUREMENTS	
3.1. Introduction	57
3.1.1. Coherent scatter normalization	57
3.1.2. Measurement of strontium supplementing individuals	62
3.2. Materials and Methods	67
3.2.1. Strontium doped plaster of Paris calibration	67
3.2.2. <i>Ex vivo</i> finger XRF measurements	70
3.2.2.1. <i>Ex vivo</i> tissue intact XRF measurements	70
3.2.2.2. <i>Ex vivo</i> bare bone XRF measurements	71
3.2.3. Analysis of the K_{α} ; K_{β} ratio	72
3.2.4. Strontium quantification attempts and system performance	72
3.2.5. <i>In vivo</i> XRF measurements of Sr supplementing individuals	74
3.3. Results and Discussion	76
3.3.1. Strontium doped plaster of Paris calibration	76
3.3.2. <i>Ex vivo</i> K_{α} and K_{β} properties and ratios	78
3.3.3. Creation of an experimental soft-tissue correction relationship	89
3.3.4. Attempts to quantify <i>ex vivo</i> bone strontium using Monte Carlo soft-tissue correction model	94
3.3.5. Evaluation of system performance and measurement reproducibility	106
3.3.6. <i>In vivo</i> XRF measurements of a strontium supplementing individual	108
4. CONCLUSIONS AND FUTURE WORK	
4.1. Conclusions	114
4.1.1. Comparison of imaging modalities	115
4.1.2. Analysis of observed K_{α} and K_{β} ratios	116
4.1.3. Creation of an experimental soft-tissue correction model	116
4.1.4. Attempts to quantify <i>ex vivo</i> bone strontium	117

4.1.5. Evaluation of system performance and measurement reproducibility__	118
4.1.6. <i>In vivo</i> XRF measurements of a strontium supplementing individual_	118
4.2. Future Work_____	119
4.2.1. Finger bone composition analysis_____	119
4.2.2. Creation of a new calibration standard_____	120
4.2.3. Optimization of a new DCC x-ray optical system_____	121
4.2.4. Measurement of strontium kinetics in strontium supplementing individuals_____	122
REFERENCES_____	124
APPENDIX A_____	130
APPENDIX B_____	134
B.1. Soft-tissue correction and bone strontium quantification calculations_____	134
B.2. Ex-vivo bone strontium concentration estimation example_____	143
B.3. Examination of the influence of ignoring the uncertainties inherent to the soft-tissue calibration line_____	149

List of Figures

- Figure 1.1** Natural decay scheme of ^{125}I
- Figure 1.2** Spectra obtained by Si(Li) detector using brachytherapy Prostaseed® source on a plaster of Paris phantom
- Figure 2.1** Transverse image of the dorsal side of a human index finger using MR
- Figure 2.2** Sagittal image of a human index finger produced by 65 kVp CT
- Figure 2.3** Transverse image of a human index finger produced using 65 and 75 kVp voltage
- Figure 2.4** Sagittal image of a human index finger produced using 8 MHz ultrasound
- Figure 2.5** Transverse image of a human index finger using 8 MHz ultrasound
- Figure 2.6** Sagittal image of a human index finger using 25 MHz ultrasound
- Figure 2.7** Transverse image of a human index finger using 25 MHz ultrasound
- Figure 2.8** Sagittal image of a human index finger using 55 MHz ultrasound
- Figure 2.9** Transverse image of a human index finger using 55 MHz ultrasound
- Figure 2.10** Image modality tissue thickness readings of seven cadaver fingers
- Figure 2.11** Differences from mean soft tissue thickness: evidence for biasing of image modalities to either underestimate or overestimate soft tissue thickness ($\pm\text{SEM}$)
- Figure 2.12** Plot of average difference of finger and ankle ultrasound thickness measurements performed two years apart
- Figure 3.1** Sample spectra of non-supplementing Caucasian and Asian individuals and a strontium supplementing individual
- Figure 3.2** Results obtained from Sr EDXRF measurements performed on finger and ankle sites of a strontium supplementing individual (reproduced with permission)

- Figure 3.3** Depiction of detector and *in vivo* bone strontium measurement setup using 180° interaction geometry (side view) with axial view of human finger positioning
- Figure 3.4** Zero strontium added plaster of Paris phantom spectra: K_{α} (left) and K_{β} (right) peaks fitted with Marquardt non-linear least squares fitting routine
- Figure 3.5** Depiction of detector and *in vivo* bone strontium measurement setup using 180° interaction geometry (head-on view)
- Figure 3.6** Sample plaster of Paris K_{α} and K_{β} calibration curves created from raw peak areas where each data point is the average of three measurements performed on each phantom
- Figure 3.7** Relative strontium intensities of 7 measured cadaver fingers expressed as the K_{α} peak area normalized to the coherent scatter peak with associated overlying finger soft tissue thicknesses displayed above the corresponding intensity
- Figure 3.8** Tissue intact observed average K_{α} /coherent vs. average K_{β} /coherent
- Figure 3.9** K_{α} : K_{β} ratio observed from intact cadaver fingers with error bars representing the one standard deviation in the spread of observed ratios
- Figure 3.10** Observed K_{α} and K_{β} ratios from ten measurements performed on each of seven intact cadaver fingers plotted against corresponding soft-tissue thickness
- Figure 3.11** Observed K_{β} vs. K_{α} ratios from bare bone EDXRF measurements
- Figure 3.12** Semi-logarithmic plot of the ratio of all observed tissue intact intensities to bare bone intensities for K_{α} (A) and K_{β} (B), corrected for live time differences and plotted against overlying tissue thickness
- Figure 3.13** Experimental model of x-ray intensity on tissue thickness using EDXRF data from 7 cadaver finger measurements
- Figure 3.14** Experimental model data plotted with trend lines of the theoretical relationship data
- Figure 3.15** Comparison of tissue intact to bare bone EDXRF quantifications using soft-tissue correction and coherent normalization

- Figure 3.16** Comparison of tissue intact to bare bone EDXRF quantifications using soft-tissue correction, source activity correction and coherent normalization
- Figure 3.17** Comparison of tissue intact to bare bone EDXRF quantifications using soft-tissue correction and live time correction
- Figure 3.18** Comparison of tissue intact to bare bone EDXRF quantifications using soft-tissue correction, live time correction and source activity correction
- Figure 3.19** Concentration estimates of strontium in finger bone measured starting six months after strontium supplementation was begun
- Figure 3.20** Concentration estimates of strontium in ankle bone measured starting six months after strontium supplementation began
- Figure B.1** An example extraction of strontium concentration from a plaster of Paris K_{α} calibration line, with a non-zero intercept, using a low count peak area
- Figure B.2** An example extraction of strontium concentration from a plaster of Paris K_{α} calibration line, with a zero intercept, using a low count peak area
- Figure B.3** Plaster of Paris phantom calibration line of K x-ray peak area normalized to coherent scatter peak area versus added strontium

List of Tables

- Table 1.1** Various estimates of human bone strontium concentrations: (T) – trabecular bone, (C) – cortical bone
- Table 1.2** Strontium K-shell x-rays with intensities per 100 shell vacancies
- Table 1.3** Photons and Prostaseed® ^{125}I brachytherapy source information
- Table 2.1** Attenuation properties of strontium x-rays and selected source photons through bone^a and skin^b
- Table 2.2** 1 Tesla MR parameters
- Table 2.3** Philips HDI 5000 L12-5 50mm system specifications
- Table 2.4** Vevo 770™ transducer specifications by VisualSonics
- Table 2.5** Ultrasound 25 & 55 MHz operation parameters
- Table 2.6** Caliper tissue thickness measurements
- Table 2.7** Raw modality tissue thickness estimates
- Table 2.8** Evidence for image modality biasing to underestimate or overestimate tissue thickness
- Table 2.9** Standard T-test examination of modality bias
- Table 2.10** Image modality accuracy results
- Table 2.11** Inter-study comparison of ultrasound measurements on ankle and finger of returning participants
- Table 3.1** Observed $K_{\alpha}:K_{\beta}$ ratios from (N = 10) EDXRF measurements performed on cadaver fingers with tissue intact
- Table 3.2** Observed $K_{\alpha}:K_{\beta}$ ratios from EDXRF measurements performed on cadaver fingers with tissue intact and after soft-tissue thickness correction has been applied

Table 3.3	Comparison of average intact finger strontium concentration estimates from K_{α} and K_{β} peaks, after tissue correction and coherent normalization
Table 3.4	Observed K_{α} : K_{β} ratios from EDXRF measurements performed on cadaver fingers bare bones
Table 3.5	Comparison of tissue intact to bare bone EDXRF quantifications using soft-tissue correction and coherent normalization
Table 3.6	Comparison of tissue intact to bare bone EDXRF quantifications using soft-tissue correction, source activity correction and coherent normalization
Table 3.7	Comparison of tissue intact to bare bone EDXRF quantifications using soft-tissue correction and live time correction
Table 3.8	Comparison of tissue intact to bare bone EDXRF quantifications using soft-tissue correction, live time correction and source activity correction
Table 3.9	Comparison of the range of finger bone strontium concentration estimates obtained using each of the four correction trials
Table 3.10	Comparison of the covariance associated with using each correction trial for tissue intact measurements
Table 3.11	K_{α} : K_{β} ratios from an <i>in vivo</i> bone strontium XRF measurement of a strontium supplementing individual before and after soft-tissue correction
Table 3.12	Bone strontium concentration estimates of finger and ankle measurement sites of a strontium supplementing individual

Chapter 1

INTRODUCTION

1.1 Strontium

Strontium is the 38th element on the periodic table. It is an alkaline earth metal, situated between calcium and barium, and shares in common with these elements a 2+ valence charge. Strontium is generally known for its four existing stable isotopes and associated natural abundances: ⁸⁴Sr (0.56%), ⁸⁶Sr (9.86%), ⁸⁷Sr (7.00%) and ⁸⁸Sr (82.58%). In the 1950's it was discovered that radioactive isotopes ⁸⁹Sr ($t_{1/2} = 50.53$ days) and ⁹⁰Sr ($t_{1/2} = 28.79$ years) were formed as byproducts of atomic bomb testing and were present in the fall-out. The potential health hazards associated with Sr-90 prompted numerous investigations into the behavior and metabolism of strontium in biological systems and in humans (MacDonald *et al.*, 1951; Comar *et al.*, 1957; Schroeder *et al.*, 1972).

Strontium is a naturally occurring element on earth but is not typically found in pure form as it is highly reactive and readily oxidizes. The two most common mineral forms of strontium are celestite, also known as strontium sulfate (SrSO_4) and strontianite (SrCO_3) (Hurlbut and Sharp, 1998). Both minerals may be found together and with limestone deposits. Commercial uses are few but strontium may be used as a separating agent of sugar from molasses and in signal flares and pyrotechnics for the red flame it produces (Hurlbut and Sharp, 1998). Strontium is the 15th most abundant element in the earth's crust and has an average soil concentration of 450 ppm (Schroeder *et al.*, 1972). Strontium is ubiquitous throughout the earth's crust and is found in soil with concentrations that vary according to the particular geographical region (Schroeder *et al.*, 1972). It is present in both fresh water and sea water sea but in much higher concentration in sea water; strontium is the most abundant ocean trace element having a concentration of 8000 ppb. Bodies of fresh water and American municipal water supplies are comparably less concentrated having a median concentration of 110 ppb (range 2 –

410 ppb). The greater strontium concentration in sea water is likely due to strontium salts being more highly soluble in salt water (Schroeder *et al.*, 1972).

1.2 Strontium Metabolism

In humans, primary exposure to strontium is through the food chain via the gastrointestinal tract (Comar *et al.*, 1957; Cabrera *et al.*, 1999). The ubiquitous and abundant nature of strontium in soil and water, combined with its chemical similarity to calcium, permits it to be subsequently taken up by plant and aquatic life. In plants, strontium is taken up from the soil through the root system and deposited within living tissues. Strontium is further taken up in the mammalian system primarily through intestinal absorption of ingested plant life (Comar *et al.*, 1957). To a lesser extent, it is also acquired through the passage between mother and fetus, in the milk of most mammals and in minerals derived from grains; total dietary intake is estimated at 2.5mg Sr/day (Schroeder *et al.*, 1972) and ranges between 2.0 – 4.0 mg Sr/day (Marie *et al.*, 2001). Evidence suggests that plant life may only be able to discriminate only marginally against strontium, in favour of calcium, and so concentrations in some plants are similar to those found in soils (Comar *et al.*, 1957). On the other hand, the mammalian digestive system seems predisposed to discriminate against absorption of strontium in favour of calcium and may explain why Sr/Ca ratios found in humans are less than those in plants or in soil (Comar *et al.*, 1957; Alexander and Nusbaum, 1959). Intestinal absorption of strontium may be hindered as the calcium binding protein binds strontium to a lesser degree than calcium (Schrooten *et al.*, 1998). Such discrimination suggests a need for the mammalian metabolism to regulate absorption of strontium in favour of calcium.

In the early half of the twentieth century, a number of studies were carried out to determine the potential role strontium plays in a biological system. When rats were fed on a diet of strontium carbonate, they became rachitic (Sobel *et al.*, 1935). This indicated that strontium could interfere with the natural calcification mechanism in a mammalian model and cause a weakening of the skeletal structure. Injections of radiolabeled isotopes: strontium (^{89}Sr) and calcium (^{45}Ca) into adult white mice illustrated that calcium

is preferentially taken up over strontium, but also that both elements deposit in similar locations within the body, namely, the skeleton (Pecher, 1941). This strongly suggested that strontium behaves similarly to calcium and that it may be mistaken for it during intestinal absorption and deposition into bodily tissues. Of the total strontium content retained in the human body, 99% resides within the skeleton, indicating that bone is the primary storage organ of strontium (Schroeder *et al.*, 1972).

The continuous process of bone remodeling is considered one mechanism of how strontium may be incorporated into the human skeleton (Dahl *et al.*, 2001). The apposition or formation of new bone and resorption of old bone provides a mechanism of uptake of trace elements that continues into adulthood. However, this occurs at a far slower rate in adulthood than is found in neonatal or young mammals. In the adult skeleton, two further mechanisms of strontium deposition have been hypothesized: rapid surface ionic exchange with calcium and slow ionic substitution with calcium deep into bone (MacDonald *et al.*, 1951; Cohen-Solal, 2002). Rapid surface exchange occurs at bone surfaces in direct contact with blood supply while in ionic substitution, strontium slowly migrates inwards through the entire bone volume, by exchanging with calcium. The latter is considered the primary mechanism of uptake of trace elements into the adult skeleton (O’Flaherty, 1992).

The ability of strontium to migrate inward into bone may be explained partially if we consider Sr uptake at the hydroxyapatite (HAp) crystal level. Using Cynomolgus monkey models, Boivin *et al.* (1996) found that absorption and exchange at the crystal surface was the only mechanism of deposition observed in old bone. However, in newly formed bone, strontium was found to deposit through both surface absorption and heteroionic substitution with calcium, deeper into the HAp matrix (Boivin *et al.*, 1996). This might explain how strontium is able to solidify a relatively permanent residence within the skeleton, even after exposure has ceased.

Many studies have been performed to estimate the approximate concentration of strontium in the human skeleton using *ex vivo* bone tissue. A summary of these findings have been well documented by Zamburlini (2008) and is presented in table 1.1.

Table 1.1^a: Various estimates of human bone strontium concentrations: (T) – trabecular bone, (C) – cortical bone

Source	N	Bone site	Age of Individual	Concentration
ICRP 23 (1975)	150	Rib	N/A	32 µg Sr/g bone
Hodges <i>et al.</i> (1950)	20	Parietal	(8 mos. - 75 yrs.)	230 µg Sr/g bone ash
		Rib		220 µg Sr/g bone ash
		Vertebrae		220 µg Sr/g bone ash
		Femur		220 µg Sr/g bone ash
Thurber <i>et al.</i> (1958)		Various		450 µg Sr/g Ca
Zaichick (2006)	81	Iliac crest	(15 - 55 yrs)	308 ± 18 µg Sr/g dry bone(C)
				235 ± 18 µg Sr/g dry bone(T)
		Femoral neck	(15 - 55 yrs)	260 ± 18 µg Sr/g dry bone(C)
				212 ± 20 µg Sr/g dry bone(T)
Carvalho <i>et al.</i> (1998)	60	Skull	N/A	147 ± 55 µg Sr/g dry bone
Rosenthal <i>et al.</i> (1972)	3 - 5	Clavicle, tibia, ulna	(40 - 60 yrs.)	460 ± 50 µg Sr/g bone ash
Samudralwar and Robertson (1993)	12	Rib	(60 - 82 yrs.)	62 ± 18 µg Sr/g dry bone(C)
				58 ± 17 µg Sr/g dry bone(T)
Turekian and Kulp (1956)	277	N/A	N/A	600 µg Sr/g bone ash
Aras <i>et al.</i> (2000)	12(C), 9(T)	Iliac Crest	(15-50)	110 ± 22 µg Sr/g dry bone

a) Zamburlini (2008)

It is interesting to note that bone turnover is higher in trabecular than in cortical bone and consequently, high levels of administered in addition to dietstrontium will predominantly deposit in trabecular bone (Boivin *et al.*, 1996; Dahl *et al.*, 2001).

The effects of excessive exposure to strontium have been studied. High doses of strontium were found ultimately to distort the HAp crystal structure of SrCl₂ injected rats (MacDonald *et al.*, 1951). A substitution of Sr for Ca may cause lattice expansion of the HAp crystal due to the larger atomic radius of the strontium atom versus the calcium atom (1.13 vs. 0.99 Å) (Boivin *et al.*, 1996; Christoffersen *et al.*, 1997). A larger atomic radius implies a greater Sr to hydroxyl group bond distance than that of the Ca to hydroxyl group. This would decrease bond energy and cohesion and may consequently weaken overall crystal structure (Boivin *et al.*, 1996). Verberckmoes *et al.* (2004) examined this effect *in vitro* by introducing variable amounts of strontium to newly forming hydroxyapatite crystals. They found that very high concentrations of strontium

caused a severe reduction in the final HAp crystal size, while lower doses of strontium produced minimal to no size reduction (Verberckmoes *et al.*, 2004). They concluded that high levels of strontium exposure severely inhibit the formation of new HAp crystals while low levels produce minimal to no reduction in expected growth.

An excessive substitution of the larger strontium ions for calcium in the building materials of HAp is thought to decrease the likelihood of forming a stable HAp crystal structure. However, if low level strontium exposure only marginally stunts crystal growth, but does not affect total mineral density, this might improve bone strength. Smaller crystals, imply greater surface area for the organic bone matrix to bond with and thus, would improve bone rigidity (Paschalis *et al.*, 1997). In turn, this has been proposed as one reason that low doses of strontium may alternatively be beneficial and improve bone strength (Marie *et al.*, 2001). Hence, there is evidence to support both detrimental and beneficial effects of strontium exposure in biological systems.

Some detrimental effects on human health have been attributed to strontium exposure. Diseases such as rickets in children and osteomalacia in adults have been correlated with excessive exposure to strontium. An increased prevalence of strontium induced rickets was observed in children living in a region of Turkey with elevated soil strontium levels in which grains from this area were the primary food source (Özgür *et al.*, 1996). Rickets is a disorder in which the mineralization of the organic bone matrix in growing bone is defective. Rat models suggest that high levels of strontium might inhibit parathyroid glands thus, reducing the kidney's production of vitamin D required for calcium absorption (Özgür *et al.*, 1996).

Abnormally high strontium exposure has also been linked as a contributor to osteomalacia in rats and humans suffering from end stage renal failure (Schrooten *et al.*, 1998; Cabrera *et al.*, 1999). A loss of renal function prevents the body from clearing heavy metals including strontium and subsequent accumulation disturbs bone metabolism, thereby increasing risk of developing osteomalacia (Schrooten *et al.*, 1998; Cabrera *et al.*, 1999; D'Haese *et al.*, 2000). However, in chronic renal failure cases, osteomalacia may not be solely caused by strontium as other heavy elements may also

accumulate in abnormally high quantities (Cohen-Solal, 2002). One primary limitation of these studies is that they do not confirm what threshold level of strontium exposure may be linked to inducing detrimental effects. As yet, it is not fully understood what levels of strontium exposure may be toxic (Nielsen, 2004a).

Positive effects on bone health were observed in rats fed with low doses of strontium. An overall increase in bone mineralization and number of bone forming sites were observed yet, strontium did not seem to affect the rate of bone apposition or indicate any additional detrimental effects (Grynopas *et al.*, 1996). This strongly suggested that beneficial effects from low doses of strontium are not matched with detrimental effects in overall bone matrix mineralization.

1.3 Therapeutic effects of administered strontium on bone health

Researchers have hypothesized on the potential benefits of low dose strontium exposure as a treatment to bone mineral diseases such as osteoporosis. Osteoporosis is characterized as an estrogen deficiency induced imbalance in the rate of bone turnover in which the relative rate of bone resorption exceeds that of new bone formation. The result is typified with an increased risk of osteoporotic induced fracture which is most predominantly seen in trabecular bone (Lentle and Worsley, 2006). Typical diagnosis of osteoporosis is done by measuring bone mineral density (BMD) using DEXA where a BMD [g/cm^2] at 2.5 standard deviations lower than that of the average healthy 25 year old may be considered osteoporotic (WHO, 1994). Low doses of strontium are thought to improve bone mineral density (BMD) by increasing bone forming preosteoblastic activity (Canalis *et al.*, 1996) and decreasing resorption by the osteoclasts (Takahashi *et al.*, 2003). Thus, strontium may enact a therapeutic effect by rebalancing the natural rates of bone turnover. Additionally, new bone takes up strontium more readily than old bone and greater quantities are taken up in newly forming trabecular bone than in new cortical bone (Boivin *et al.*, 1996; Cohen-Solal, 2002).

Strontium lactate was first reportedly administered by McCaslin and Janes (1959) and Shorr and Carter (1952) to patients suffering from osteoporosis. In both cases, a

decrease in bone fracture incidence, skeletal defects and patient morbidity were reported (McCaslin and Janes, 1959). It was not until the early 1980's that strontium was again examined for its therapeutic properties. Marie *et al.* (1985) found that strontium could stimulate bone formation in rats without altering resorption rates. Recently, these effects have been observed in two large scale, blinded, human studies: Spinal Osteoporosis Therapeutic Intervention (SOTI) (Meunier *et al.*, 2004) and Treatment of Peripheral Osteoporosis (TROPOS) (Reginster *et al.*, 2008). Long-term effects of Strontium Ranelate (SR, S12911-Protelos®)(Marie, 2006) orally administered to post-menopausal osteoporosis patients were examined. Compared to the placebo groups, the SR patients had significantly reduced risk of new vertebral (SOTI) and non-vertebral (TROPOS) osteoporotic fractures, an increased BMD, and no differences in adverse health effects experienced during the trials (Meunier *et al.*, 2004; Reginster *et al.*, 2008).

As yet, the mechanisms by which SR exerts its therapeutic properties are not fully understood (Marie, 2006). This in addition to the many questions on the role of strontium in metabolic bone diseases such as osteomalacia and osteoporosis might be answered if a non-invasive method to measuring strontium *in vivo* could be developed (Wielopolski *et al.*, 1983). This method may be used as a diagnostic tool to monitor strontium levels in patients that are suffering from bone disease and to follow-up on individuals taking strontium medication (Pejović-Milić *et al.*, 2004).

1.4 Measurement of *in vivo* bone strontium using non-invasive techniques

Dual photon absorptiometry (DPA) and x-ray fluorescence (XRF) spectrometry are two methods that have been examined as a means to detect and measure *in vivo* bone strontium, non-invasively. For almost 30 years, XRF has been investigated and applied to the *in vivo* measuring of high Z trace elements such as lead (Ahlgren *et al.*, 1976). The feasibility of using XRF to quantify uranium in bone has also been investigated by O'Meara *et al.* (1997). Quantification of bone lead *in vivo*, using XRF, was first realized by Somervaille *et al.* (1985) and later refined by Nie *et al.* (2004). Given the success of measuring high atomic number (Z) elements using XRF, it has been postulated that the

same goals of quantification may be achieved in the measurement of *in vivo* bone strontium.

Nielsen *et al.* (2004) examined dual photon absorptiometry (DPA) as a means to measure strontium *in vivo*. This method utilizes the unique attenuation properties of two radiation sources, of differing energies ^{241}Am (59.5 keV) and ^{133}Ba (356 keV), to determine Sr/Ca ratios in HAp crystals. One limitation with this method was the need to immerse the measured appendage in water, to overcome soft-tissue geometrical differences, in which it had to be assumed that the photon attenuation through the appendage soft-tissue is the same as for water. This may not actually be the case and hence, the DPA method may only provide an indirect measure of bone strontium. Additionally, DPA did not have the sensitivity to measure natural levels of *in vivo* bone strontium. Even when large count statistics were used, slight errors in detection counts were found to increase the error in quantification drastically. The high quantification uncertainties could only be reduced if *in vivo* quantities were much higher than actually found *in vivo* (Nielsen *et al.*, 2004). Hence, the DPA method was not a feasible method to measure *in vivo* bone strontium.

Early attempts to measure strontium *in vivo*, using x-ray fluorescence spectroscopy, were performed by Snyder and Secord (1982) and Wielopolski *et al.* (1983) on rabbits and humans respectively. *In vivo* levels were detectable when measured from superficial bone sites: rabbit skull and human tibial shaft. However, small thicknesses of overlying skin and soft tissue thickness were found to absorb strontium x-rays significantly. Thus, absolute quantification of bone strontium was deemed theoretically possible only if soft tissue attenuation of the strontium x-rays is corrected for in the final spectral analysis (Snyder and Secord, 1982; Wielopolski *et al.*, 1983).

Pejović-Milić *et al.* (2004) and Zamburlini *et al.* (2006) re-examined the use of XRF to measure *in vivo* bone strontium and hypothesized this to be a promising method if signal normalization and soft tissue attenuation corrections can be successfully applied. The bulk of the work presented in this manuscript is built on this hypothesis and utilizes the detection system and set-up optimized by Zamburlini *et al.* (2007).

1.5 Photon interactions in strontium x-ray fluorescence spectrometry

The XRF process involves induced photoelectric effect followed by emission of a characteristic x-ray. When an incident photon strikes an inner orbit electron of an atom, and has enough energy to overcome the electron shell binding energy, the electron is subsequently ejected from the atom as a photo-electron. The vacancy left in the shell orbital is filled by the de-excitation of an electron from a higher energy orbital. To conserve energy in de-excitation, either a characteristic x-ray photon is emitted, or an Auger electron from a higher energy shell is released. Each mode of de-excitation is possible and the probability of either occurring depends on the atomic number of the associated atom. Auger emission predominates as the primary means of de-excitation in low Z elements while x-ray emission predominates in large Z atoms.

Detection of x-rays, of known energies, indicates the presence of a specific element in the sample. In energy dispersive x-ray fluorescence (EDXRF), collected x-rays will be counted into a peak on an energy spectrum. Peak area is directly proportional to elemental concentration level of the element being measured. In principle, peak area is used to quantify elemental concentration, when compared against a calibrated reference.

In the case of strontium, x-rays from the K lines demonstrate high enough energy and intensity to be practically used in spectroscopic analysis for work *in vivo*. The K shell fluorescence yield of strontium is quite high; 70.3% of all atomic de-excitations result in a characteristic K x-ray emission. Electronic de-excitation from an L ($n = 2$) shell to the K ($n = 1$) shell results in a K_{α} x-ray line and direct transition from the higher M ($n = 3$) shell to K shell produces a K_{β} x-ray line. Table 1.2 summarizes K line characteristic x-rays that strontium is known to fluoresce and includes the energy of the K-shell photoelectric edge.

Table 1.2^b: Strontium K-shell x-rays with intensities per 100 shell vacancies

Line	Energy (keV)	Intensity $\pm \sigma$
K_{α_1}	14.165	39.1 ± 1.4
K_{α_2}	14.098	20.3 ± 0.7
K_{β_1}	15.836	5.63 ± 0.20
K_{β_3}	15.825	2.91 ± 0.10
K_{β_2}	16.085	1.00 ± 0.04
K - edge	16.105	

b) Firestone (2005)

The energy of the K- edge is the minimum incident photon energy required to break the K-shell binding energy to free one electron from this shell. At best, energy resolution of typical lithium doped silicon (Si(Li)) commercial detectors is of the order of 140-170 keV (Knoll, 1999) which means that the individual alpha or individual beta lines cannot be resolved. In a typical strontium spectrum, the $K_{\alpha_{1,2}}$ lines will be grouped into a single strontium K_{α} peak at about 14.14 keV and the $K_{\beta_{1,3}}$ lines grouped into single K_{β} peak at about 15.83 keV. The K_{β_2} line sits about 250 eV above the $K_{\beta_{1,3}}$ lines and is partially distinguishable as a small upper energy shoulder on the right side of the K_{β} peak. Both K_{α} and K_{β} peak areas may be used to analyze *in vivo* strontium concentration.

Atomic excitation may be caused by either a charged particle or photon interaction with an atomic shell electron; both x-ray and gamma ray photons may produce this effect. However, in the source based system used throughout this work, only photons are present as an excitation source. The probability of photoelectric absorption increases the closer the incident photon energy is to that of the K-edge. In Sr XRF, excitation sources must be chosen so that coherent and Compton scatter energies are close above the photoelectric edge, to maximize interactions, but not overlap with the strontium x-ray energies. An overlap of two peaks in a spectrum will complicate analysis or make peak area extraction impossible. To optimize spectrum counts and cleanliness of the background under the strontium peaks, the chosen excitation source should be close in energy above the K-edge

but far enough so that the source Compton and coherent scatter do not overlap the strontium peaks.

1.5.1 Selection of ^{125}I brachytherapy excitation source for *in vivo* bone strontium measurements

This section summarizes the system and choice of parameters as optimized by Zamburlini *et al.* (2006) and Pejović-Milić *et al.* (2004) which has been implemented in this work. In a comparison of potential excitation sources, Pejović-Milić *et al.* (2004) demonstrated Iodine-125 to be ideal for measuring *in vivo* bone strontium. The Prostaseed® ^{125}I brachytherapy source consists of a titanium cylindrical capsule 4.5 mm in length by 0.8 mm diameter housing five silver spheres coated with ^{125}I . The decay sequence of ^{125}I is illustrated in Figure 1.1 below and is described as follows (Kereiakes and Rao, 1992). ^{125}I decays by electron capture (E.C.) to Tellurium metastable $^{125\text{m}}\text{Te}$ daughter nuclide with an atomic shell vacancy. This vacancy is filled by the atomic de-excitation of an electron from a higher orbital causing the release of either a characteristic Te x-ray or an Auger electron. For $^{125\text{m}}\text{Te}$ the probability of a K-shell vacancy by E.C. is 0.797 and the fluorescence yield (ω_K) is 0.878; this corresponds to a 0.692 or 69.2% probability of K x-ray production via E.C.

The nuclear de-excitation of $^{125\text{m}}\text{Te}$ to ^{125}Te occurs shortly after atomic de-excitation through two possible mechanisms. The nucleus may de-excite either through the production of a 35.49 keV gamma photon (6.67% probability) or by process of internal conversion (I.C.) of an inner shell electron (93.3% probability). As in the case of E.C., the atomic vacancy produced by I.C. is filled by de-excitation of a higher energy electron which similarly produces a characteristic x-ray or liberates an Auger electron. Thus, both the E.C. and I.C. steps in the decay of ^{125}I may go on to produce Te x-rays which are useful as an excitation source of strontium. Auger electrons are primarily absorbed in the titanium casing. The decay scheme of ^{125}I is illustrated in figure 1.1.

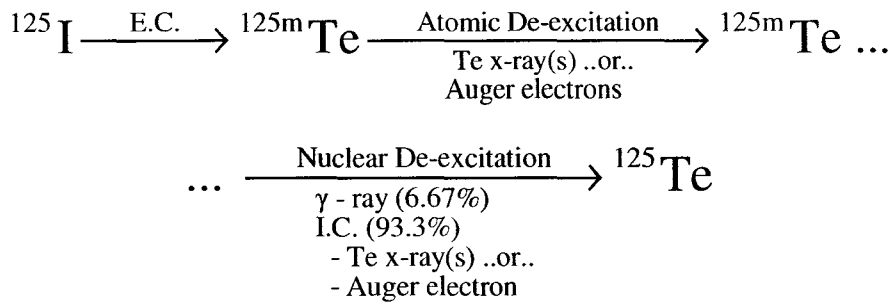


Figure 1.1: Natural decay scheme of ${}^{125}\text{I}$

The probability ratio of K-shell electron internal conversion to gamma emission in ${}^{125\text{m}}\text{Te}$ is $e_K/\gamma = 11.0$ (Lederer et al., 1967). Through internal conversion, the proportion of all de-excitations, through gamma or electron emission, of the metastable ${}^{125\text{m}}\text{Te}$ nucleus that result in a K-shell vacancy is 0.688. Factoring in the aforementioned fluorescence yield gives a total characteristic x-ray emission of 0.604 or 60.4% following the de-excitation of ${}^{125\text{m}}\text{Te}$ to stable ${}^{125}\text{Te}$. Total K x-ray yield is the sum of the yields from both the atomic and nuclear de-excitations. Therefore, a single decay of ${}^{125}\text{I}$ has an expected total Te K x-ray yield of 1.296 or 129.6% which suggests this to be an efficient excitation source.

The inclusion of the silver spheres in the construction of the Prostaseed® Brachytherapy ${}^{125}\text{I}$ seeds provides an added advantage to the excitation of bone strontium. The gammas and Te x-rays produced in the decay of ${}^{125}\text{I}$ may either escape the ${}^{125}\text{I}$ seed or interact with the silver spheres within the capsule and consequently cause production of silver x-ray lines. The presence of silver x-rays, as an excitation source, further enhances the excitation of strontium as Ag x-ray energies are closer to the photoelectric absorption edge of strontium than that of the tellurium x-rays or ${}^{125}\text{I}$ γ -rays (Zamburlini *et al.*, 2006). The ${}^{125}\text{I}$ photons that substantially contribute to the excitation of strontium are summarized in table 1.3. Intensities have been determined by Zamburlini *et al.* (2007) using XRF on the source to observe the proportions of photons emerging from each line.

Table 1.3: Photons and Prostaseed® ^{125}I brachytherapy source information

	Half-life, days	Energy ^c , keV (relative Intensity) ^e	Photo-electric ^d (μ/ρ) _{abs} for Sr, cm ² /g	Energy of Main compton (180°), keV
^{125}I	59.41	35.49 (3.906%)	13.1	31.2
Te x-rays		27.202 & 27.472 (58.18%)	27.0	24.7
		30.944 & 30.995 (11.625%)	19.2	27.6
		31.704 (2.557%)	18.0	28.2
Ag x-rays		21.990 & 22.163 (18.47%)	48.3	20.3
		24.912 & 24.943 (4.398%)	34.9	22.7
		25.455 (0.865%)	33.0	23.1

c) Firestone (2005)

d) Berger *et al.* (2005)e) Zamburlini *et al.* (2007)

Table 1.3 illustrates that all source photons, including Compton scatter energies, are well above the strontium x-ray energies and hence, do not interfere with the strontium spectra. Line intensities were determined using XRF on the Prostaseed® source (Zamburlini personal correspondence). Figure 1.2 depicts a sample strontium spectrum obtained using the Prostaseed® ^{125}I brachytherapy source incident upon a bare plaster of Paris phantom with zero added strontium. The strontium signal seen in this spectrum is the result of the inherent strontium contamination found in gypsum, the building material of plaster of Paris.

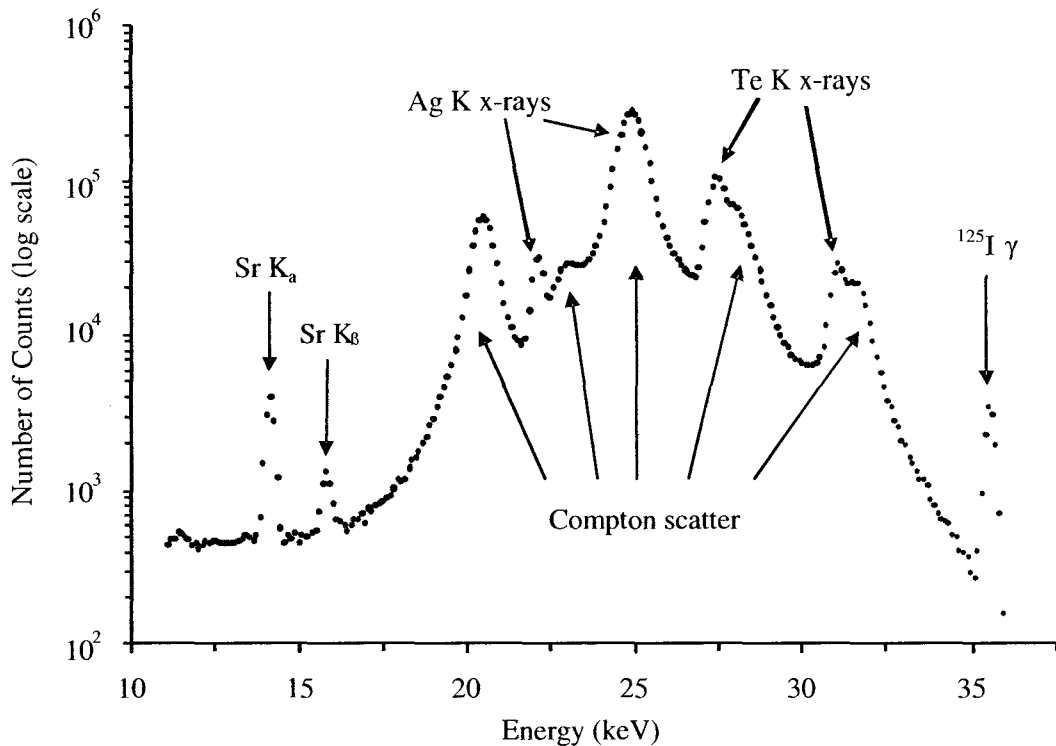


Figure 1.2: Spectra obtained by Si(Li) detector using brachytherapy Prostateed® source on a plaster of Paris phantom

1.6 System optimization for *in vivo* bone strontium measurements

To effectively measure bone strontium using XRF, a measurement must be performed at a superficial bone site with thin overlying skin and soft tissue. To locate the most superficial site, Pejović-Milić *et al.* (2002) examined the overlying soft tissue thickness of four anatomical sites on 10 individuals. The finger, forehead, tibia and heel were each imaged using a 12 MHz maximum frequency ultrasound system to measure total skin and soft tissue thickness overlying bone. Thickness results were: finger (2.9 ± 0.7 mm), forehead (3.6 ± 0.7 mm), tibia (4.8 ± 2.0 mm) and heel (8.4 ± 1.7 mm). The index finger had the lowest average thickness and was considered the ideal measurement site for low energy *in vivo* bone XRF (Pejović-Milić *et al.*, 2002). An *in vivo* pilot study by Zamburlini *et al.* (2007) for measuring bone strontium confirmed that satisfactory count statistics could be obtained by measuring at the dorsal side of the middle phalanx of

the index finger. Also, an adequate signal was obtained by measuring at the middle of the medial malleolus of the ankle (Zamburlini *et al.*, 2007). Measuring both finger and ankle sites adds an advantage in which the signals are indicative of predominantly cortical and trabecular bone types, respectively.

An examination by Zamburlini *et al.* (2006) of potential source-target-detector geometries was carried out to optimize reproducibility and minimum detectable limit (MDL) on a measurement. The two positioning angles tested were the 90° versus 180° geometry; the geometry is the angle between the source-to-target path and the target-to-detector path. 90° geometry was found to produce only marginally superior MDL, (MDL₉₀ 42.6 ± 0.6 µg Sr/g Ca) versus (MDL₁₈₀ 44.6 ± 0.6 µg Sr/g Ca) but relied heavily on proper positioning to ensure Sr x-ray acquisition in the 90 degree direction (Zamburlini *et al.*, 2006). For its superior reproducibility, the 180° geometry was implemented in the experiments described in this thesis.

The weak signal obtained from low energy strontium x-rays requires a detector that is capable of resolving low energy spectra and handling a high count rate without sacrificing efficiency. Hyperpure germanium (HPGe) detectors are normally implemented for use in K XRF detection of energies higher than 30 keV while Si(Li) detectors specialize in L XRF detection of low energy photons from high atomic number elements ($Z > 50$) or K XRF detection from low atomic number elements (Pejović-Milić *et al.*, 2004). A comparison of HPGe and Si(Li) detector performance of acquiring strontium spectra was done by Pejović-Milić *et al.* (2004). The strontium spectra, obtained from an HPGe detector, was complicated by prominent escape peaks situated about 10 keV below each measured peak.

An escape peak is formed as a result of incomplete photon energy deposition in a detector crystal. A photon may undergo multiple interactions within a detector crystal and transfer its energy into the excitation of electrons to the conduction band. Collection of these electrons provides a direct indication of the energy deposited by the photon in the crystal and hence, the number of ionizations to the conduction band is proportional to energy. However, if this photon scatters with enough energy to escape the detector

crystal, the remaining energy is not deposited and, as a result, a count is added to the observed spectrum at a lower energy channel than the full energy of the incident photon. If this occurs frequently, and for a common proportion of energy not being collected, then a peak at this energy will appear in a spectrum. For low energy photons, this effect is amplified in HPGe detector in comparison to Si(Li) detectors as a result of the difference of detector composition. Since germanium is a higher Z number than silicon, the probability of photoelectric and Compton interactions are greater and so the average penetration distance of photons into a Ge crystal is reduced. Thus, interactions occur closer to the crystal surface thereby increasing the probability that a scattered photon will leave the crystal volume cause the production of an escape peak.

In a strontium spectra produced using a HPGe detector, an escape peak from the silver 24.9 keV peak was positioned in between the strontium K_{α} and K_{β} peaks and partly overlapped the K_{β} peak. The disruption of the strontium spectra by this escape peak would severely complicate spectral analysis. Escape peaks in the Si(Li) produced spectra were very small and would not significantly interfere with analysis. Figure 1.2 illustrates how the strontium peaks are undisturbed by artifacts when a Si(Li) detector is used for photon collection. Thus, Si(Li) detection was deemed superior to carry out *in vivo* strontium measurements using XRF (Pejović-Milić *et al.*, 2004).

To study further the feasibility of using XRF to measure *in vivo* bone strontium, consideration toward participant safety in the presence of a radioactive source was examined by Pejović-Milić *et al.* (2004) and Zamburlini *et al.* (2007). Pejović-Milić *et al.* (2004) simulated radiation dose to skin for a 30 minute XRF measurement using a collimated cadmium-109 source positioned 2.5 cm from the dosimeter. The dose delivered to this small area of skin was calculated to be 0.46 mGy or 80×10^{-6} mSv total body effective dose. This was well within the limits of the 10 mGy upper limit for a dose to skin and has risk equivalent to receiving 20 minutes of natural background radiation (Pejović-Milić *et al.*, 2004). Zamburlini *et al.* (2007) examined the dose to finger and ankle phantoms for a 30 minute XRF measurement using a collimated 30 MBq Prostateed® ^{125}I brachytherapy source. Calculation included the portion of dose to the

subject received simply from being within the vicinity of the source during the measurement. Whole body effective doses from ankle and finger measurements were calculated to be $(49.08 \pm 0.05) \times 10^{-6}$ mSv and $(87.32 \pm 0.09) \times 10^{-6}$ mSv respectively (Zamburlini *et al.*, 2007). In context, the annual natural background dose in North America is 3 mSv/year and that received from a standard chest x-ray is about 0.1 mSv. Thus, dose limits are well within acceptable range to implement XRF safely to measure bone strontium *in vivo*.

1.7 Proposed method of quantification of bone strontium measurements using soft-tissue correction and normalization to coherent scatter

Despite the previous achievements of measurement sensitivity and system optimization, the ability to quantify an *in vivo* strontium measurement has still not been met. Quantification has been proposed as possible using a two-step normalization process. The first step would be to correct for bone shape and geometrical differences, between subjects, using a coherent normalization procedure. This procedure involves dividing the K x-ray peak areas over a source coherent scatter peak and is an effective procedure for measurement of high Z elements such as lead and uranium (Somervaille *et al.*, 1985; O'Meara *et al.*, 1997).

In vivo quantification of high Z elements such as these may be accomplished without having to correct for photon absorption by overlying soft tissue. The source and photon energies associated with these measurements are high enough that the difference in the proportion of soft tissue attenuation observed by the K_{α} x-rays (Eg: Pb $E_{\alpha} = 74$ keV) and the coherent scatter (^{109}Cd $E_{\gamma} = 88$ keV) is small. Also, the soft tissue is not a significant source of coherent scatter at 88 keV. Thus, normalization using step one alone, for high atomic number elements, will allow for full quantification *in vivo*.

However, the much lower strontium x-rays energies experience substantial attenuation through as little as several millimeters of overlying soft tissue. At these energies, even a small difference in source photon (Ag $E(K_{\alpha}) = 22.1$ keV) to Sr x-ray (Sr $E(K_{\alpha}) = 14.2$ keV) energy will constitute a large difference in the proportion attenuated

by overlying soft tissue. Also, soft tissue does contribute to a non-negligible fraction of the source coherent scatter, even at 35 keV. Thus, a second step must be added to the normalization procedure to correct for signal attenuation by the overlying soft tissue. The problems associated with attempts at tissue correction have been examined and explained in detail in Chapter two of this manuscript. This includes attempts made by the author to correct for soft tissue thickness by investigating various imaging modalities at accurately estimating overlying tissue thickness. Application of the two step correction mentioned above is carried out *ex vivo* in chapter three.

Chapter 2

SOFT TISSUE CORRECTION USING IMAGING MODALITIES

2.1 Introduction

2.1.1 Attenuation properties

Soft tissue photon attenuation is a problem unique to *in vivo* bone XRF studies involving the measurement of L-shell x-rays from high atomic number medium, or K-shell x-rays of low atomic number medium such as strontium. When dealing with photons of energies less than 20 keV, soft tissue thickness, on the order of several millimeters, will impart noticeable attenuation to travelling photons.

To understand the attenuation effect that soft tissue imparts on x-rays of these energies, we may examine the attenuation and propagation properties of the strontium x-rays and excitation source photons. The linear attenuation coefficients (μ , mm^{-1}) and mean free paths (λ , mm) of source photons and Sr x-rays, in skin and cortical bone tissues, have been provided in table 2.1. The data in table 2.1 illustrate how the attenuation of the strontium x-rays differs from that of the source photons.

Table 2.1: Attenuation properties of strontium x-rays and selected source photons through bone^a and skin^b

Photon	Energy, keV	Bone ($\rho = 1.92 \text{ g/cm}^3$)		Skin ($\rho = 1.09 \text{ g/cm}^3$)	
		μ , mm^{-1}	λ , mm	μ , mm^{-1}	λ , mm
Sr K_α	14.14	1.98	0.51	0.215	4.7
Sr K_β	15.83	1.48	0.70	0.158	6.3
Ag K_α	22.10	0.559	1.8	0.071	14
Te K_α	27.38	0.313	3.2	0.047	21
$^{125}\text{I } \gamma$	35.49	0.163	6.1	0.033	30

a) ICRP 89 (2002)

b) Berger *et al.* (2005)

Mean free paths represent the travel distance at which 63.2% of the original signal is attenuated. Given that the natural adult human index finger skin and soft tissue thickness may range from 2.0 to 4.8 mm, attenuation of Sr x-rays by skin is quite substantial.

In adult human index fingers, the cortical bone thickness is about 1.5 mm at the middle dorsal side of the middle phalanx. Table 2.1 illustrates that in bone, source photons are able to penetrate deep into the cortical matrix to excite strontium almost uniformly throughout. In contrast, the mean free path of the low energy strontium x-rays suggest that the greatest contribution to the detected strontium signal are those photons emitted from strontium atoms near the surface of the cortical bone. Strontium x-rays from deep within the bone matrix are much more likely to be attenuated on their way out of the bone and are thus less likely to make it to the detector to be counted.

The passage through skin by the ^{125}I source photons is characterized with only marginal attenuation which means that most get through without being absorbed. The story is different for the strontium x-rays. If attenuation of Sr K_{α} x-rays is calculated for the two limits of human finger soft tissue thickness, then 35% are attenuated by 2mm of skin and 64% are attenuated by 4.8 mm of skin. Thus, soft tissue attenuation of x-ray signals cannot be ignored and must be corrected for in order to achieve *in vivo* strontium quantification.

2.1.2 Previous soft-tissue correction attempts

Snyder and Secord (1982) were the first to report on the necessity of correcting for soft tissue absorption of strontium x-rays in order to quantify in absolute terms. While they were unable to achieve this goal, they proposed a correction method that utilized the ratio of the Rayleigh to Compton scatter (N_R/N_C) observed from an *in vivo* XRF measurement. For a single rabbit, they artificially altered the soft tissue by furrowing and stretching the skin and performed an XRF measurement at each thickness. From this they constructed a linear plot of arbitrary Sr concentration vs. the observed (N_R/N_C) found at

each skin thickness. Using this graph they computed an average Rayleigh to Compton ratio $\overline{(N_R/N_C)}$ and intercept abscissa $(N_R/N_C)_0$ corresponding to zero strontium content. Individual strontium content values (N_R/N_C) could then be corrected for soft tissue by multiplying with expression:

$$\frac{\overline{(N_R/N_C)} - (N_R/N_C)_0}{N_R/N_C - (N_R/N_C)_0}$$

Several limitations with this method exist. First is that multiple measurements of the same subject must be taken to calculate the average and abscissa Rayleigh to Compton values; this has the added difficulty of having artificially to change soft tissue thickness for each reading. Second, this method provides only a relative correction value to soft tissue absorption on the same subject and thus, cannot provide an absolute quantification of bone strontium.

Alternatively, Wielopolski *et al.* (1983) proposed the use of 7 MHz ultrasound to image tibial soft tissue and determine thickness to an accuracy of 0.3 mm. Ultrasound has been used by Pejović-Milić *et al.* (2004) and Zamburlini *et al.* (2007) in attempts to apply soft-tissue thickness corrections in pilot studies measuring *in vivo* bone strontium content. The ultrasound system used in each study had a maximal frequency of 12 MHz, an approximate 8 MHz centre frequency, and point resolution of 200 microns (Pejović-Milić *et al.*, 2002; Zamburlini *et al.*, 2007). Pejović-Milić *et al.* (2004) applied an exponential attenuation correction to both silver K x-ray lines, being the most abundant source photons, and the strontium x-rays from bone. Later, Zamburlini *et al.* (2007) applied a detailed analytical tissue correction that accounted for both incoming and outgoing photons. To account for the polyenergetic nature of the Prostateed® ^{125}I source, the correction was applied to all types of photons emitted by the source. This model included flux from the source, probability of source photon attenuation, and the probability of photoelectric interaction with strontium. This correction method assumes planar geometry and has the formula:

$$B_{\text{att}} = \frac{\sum_i \Phi_i \exp(-\mu_i d) \sigma_i}{\sum_i \Phi_i \sigma_i} = \frac{N \sum_i p_i \exp(-\mu_i d) \sigma_i}{N \sum_i p_i \sigma_i} \quad (\text{E1})$$

where, Φ_i is the flux of photons of energy E_i emitted by the source, p_i is the probability of emission for a photon of energy E_i , N is the total flux of photons emitted in the source (hence $\Phi_i = N \cdot p_i$), μ_i is the absorption coefficient of skin, d is the soft tissue thickness and σ_i is the photoelectric cross section of strontium at energy E_i (Zamburlini *et al.*, 2007).

The primary limitation with this model is that it does not take into account photons that may interact with soft tissue, through inelastic scattering, that may further contribute to the fluorescing of strontium (Zamburlini *et al.*, 2007). Additional limitations with this model may lie within the composition of the finger itself. Finger soft tissue is known to have two layers, one of skin and the other an assortment of largely adipose tissue intermixed with connective tissues, microvasculature, thin tendon and periosteum lining over bone. The attenuation properties for both layers are different with the linear attenuations for strontium K_α and K_β x-rays being 1.76 and 1.72 times bigger for skin than in adipose tissue. (Zamburlini *et al.*, 2008a) Thus, the assumption of homogenous soft tissue may cause a miscalculation in the amount of true attenuation observed in a given measurement and invalidate the tissue correction. A further limitation is the intersubject variability in soft tissue density and tissue composition which may introduce additional uncertainties to correction procedures. Lastly, if the ultrasound thickness measurement is performed inaccurately, these errors will manifest into an incorrect quantification of bone strontium (Zamburlini *et al.*, 2008a).

2.1.3 Monte Carlo modelling of cylindrical finger geometry

The correction factor seen in (E1) works for the ankle site, as the ankle may be assumed to be approximately planar, but correction of a finger measurement must take into account the finger's inherent cylindrical geometry. This problem may not be solved

analytically and contribution from tissue Compton scatter, as an excitation source, still needs to be addressed. To overcome both of these limitations, Zamburlini (2008) implemented the use of Electron Gamma Shower 5 (EGS5) Monte Carlo simulation program. The human finger was modeled as a cylinder of bone (C1), 9 mm in diameter, encompassed within a larger cylinder (C2) representing overlying soft tissue. All photons associated with the Prostateed® ^{125}I excitation source were included. Diameter C2 was varied to produce a relationship of strontium x-ray attenuation to overlying soft tissue. This model was plotted for K_α x-ray attenuation and fitted with a linear function as illustrated by Zamburlini (2008). These same conditions were used to produce a final set of soft-tissue correction relationships for the K_α and K_β photon attenuations in soft tissue as seen in E2 and E3 (Zamburlini, unpublished work).

$$\text{K}_\alpha: \quad \ln\left(\frac{I}{I_0}\right) = (-3.58 \pm 0.04)T + (0.156 \pm 0.006) \quad (\text{E2})$$

$$\text{K}_\beta: \quad \ln\left(\frac{I}{I_0}\right) = (-2.86 \pm 0.04)T + (0.162 \pm 0.006) \quad (\text{E3})$$

Where I_0 is the initial intensity of strontium x-rays emitted from the bone surface and I is the intensity of strontium x-rays after passage through soft tissue of thickness, T [cm]. Uncertainties were not provided with this particular model so the uncertainties from the simpler model, presented by Zamburlini (2008), were substituted for both K_α and K_β models.

The degree of attenuation seen in this model is higher than that of the linear attenuation coefficients for skin at these energies. For Sr K_α and K_β x-rays, total signal attenuation predicted by the model is 3.58 cm^{-1} and 2.86 cm^{-1} respectively, while the fundamental linear attenuation of skin of these respective photons are 2.15 cm^{-1} and 1.58 cm^{-1} , as seen in table 2.1. The attenuation effect predicted by the model is greater since it accounts for the attenuation of the primary photons from the source in addition to attenuation of the Sr K_α and K_β x-rays (Zamburlini, 2008). This model also accounts for

the more realistic cylindrical geometry of a human finger as opposed to the simple planar geometry case. The complexity of this geometry could produce the effect of increasing the travel distance through soft tissue for a proportion of strontium x-rays, depending on the location of emergence from bone. The physical setup used in the model is explained in detail in the Materials and Methods section of Chapter 3.

2.1.4 Analysis of observed strontium K_{α} to K_{β} x-ray ratios

To ascertain the effectiveness of an applied soft tissue correction, the ratio of observed intensities of the K_{α} to K_{β} has been used as an indicator by Zamburlini *et al.* (2007). The higher energy K_{β} photon is less attenuated per unit length than K_{α} photon and so by varying the thickness of a medium of propagation, the ratio of intensities will change. The theoretical emission probability of a K_{α} photon is 7 times higher than for a K_{β} photon making a K_{α} : K_{β} ratio of 7. In the case of an infinitely thick hydrated cortical bone sample, if strontium is assumed evenly distributed throughout this bone sample, and the source photon interaction rate is also evenly distributed inward, then the Sr K_{α} : K_{β} ratio emerging from the bone surface is 5.2. If these photons must then pass through overlying skin and soft tissue, the ratio is further reduced as the K_{α} photons become increasingly more attenuated than the K_{β} photons.

Theoretically, if a tissue correction is performed in planar geometry, for an *in vivo* Sr XRF measurement, the peak ratio, after correction, should be brought back to that of bare bone, namely 5.2. When this correction was applied to ankle measurements performed on 22 *in vivo* participants, Zamburlini *et al.* (2007) found that the correction only raised the ratio to approximately 3.0 which is not as high as expected. It was also observed that the variability of K_{α} : K_{β} ratios between subjects was quite high. This is likely caused by the large uncertainty in the counting statistics of the K_{β} peak associated with *in vivo* measurements performed on the population. This variability indicated that a K_{α} : K_{β} ratio could not be used as a means for tissue correction for a given measurement. However, K_{α} : K_{β} ratio was useful in indicating that the applied corrections might not be sufficient and require further study.

To help explain this observation, Zamburlini *et al.* (2007) theorized that if strontium was not uniformly distributed, radially throughout cortical bone, then this might impact the observed ratio. To test this hypothesis, five cadaver fingers were used to examine $K_{\alpha}:K_{\beta}$ ratios observed from EDXRF performed on fingers, with tissue intact, and on bare finger bones. The results of a Monte Carlo simulation of bare bone XRF measurements, predicted a $K_{\alpha}:K_{\beta}$ ratio of 4.4 ± 0.4 ; the simulation assumed evenly distributed bone strontium. This value was confirmed when EDXRF was performed on the five cadaver finger bare bones and a ratio of 4.4 ± 0.3 , which ranged between 3.9 and 5.0, was observed (Zamburlini, 2008). EDXRF performed on soft-tissue intact cadaver fingers produced $K_{\alpha}:K_{\beta}$ ratios between 2.6 to 3.2, after soft tissue correction, and did not agree with the ratios predicted by bare bone measurements and simulations. However, these ratios did agree with the findings in the *in vivo* pilot study by Zamburlini *et al.* (2007).

Micro particle induced x-ray emission (micro - PIXE) analysis on cadaver finger bone samples confirmed that strontium is uniformly distributed, radially inward in human finger cortical bone. This was in agreement with the findings of Boivin *et al.* (1996) in monkeys and strongly suggested against non-uniform strontium distribution as a possible reason to explain why the $K_{\alpha}:K_{\beta}$ ratios did not match the theoretical ratio of 5.2 (Zamburlini, 2008). It was also speculated that the difference of observed to expected ratios could result from the high attenuation of an unaccounted absorbing layer other than skin (Zamburlini, 2008). The thin layer of tendon overlying bone has been sparsely studied in terms of composition and attenuation properties and may contribute far more to absorption than is currently assumed.

Finally, it was hypothesized that perhaps the tissue thickness (d) used in the correction, was inaccurate. Consideration was given to the possibility that tissue thickness was being underestimated using the 12 MHz ultrasound imaging technique, or that the tendon overlying the bone was mistaken for the bone itself when performing the thickness reading (Zamburlini, 2008). This would produce a reduced estimate of the total overlying tissue thickness and consequently affect the $K_{\alpha}:K_{\beta}$ ratio after correction. This

speculation provided a benchmark to the investigation of soft tissue thickness measurement accuracy that is examined in this work. If it may be verified that the prior *in vivo* thickness measurements were underestimated, then this might explain why observed $K_{\alpha}:K_{\beta}$ ratios were lower than expected. This may be done by re-imaging the original 22 *in vivo* participants measured in the study by Zamburlini *et al.* (2007) and comparing the results to the original thickness estimates. Otherwise, if thickness measurement taking is verifiably correct, then this may be ruled out as a cause of the disparity between expected and observed $K_{\alpha}:K_{\beta}$ ratios.

The importance of accurately measuring thickness may be illustrated using the Zamburlini model (E2) for a measured finger thickness of 3.5 mm. If the precision of a 12 MHz ultrasound measurement is ± 0.2 mm, then the uncertainty of a K_{α} tissue correction alone is approximately 7.1%. This figure does not include the additional relative errors associated with peak analysis and quantification. If the measurement precision could be reduced to ± 0.1 mm, then the K_{α} tissue correction uncertainty could be lowered to 3.6%; this would provide a marked improvement in the uncertainty of the final estimate of strontium concentration. The challenge remains to ensure that tissue thickness may be repeatedly measured both accurately and with high precision to help reduce the inherent error in absolute quantification. If these two aspects may be met, then we might determine if the unexpected $K_{\alpha}:K_{\beta}$ ratios are the result of improper estimation of soft tissue thickness or that further investigation to correction procedures are needed.

2.1.5 Cross-examination of imaging modalities for optimization of soft-tissue correction

As yet, it is uncertain if the tissue correction problem is the result of the particular ultrasound imaging modality used by Zamburlini *et al.* (2007) and Pejović-Milić *et al.* (2004). The demand to produce accurate and precise tissue thickness measurements warrants an investigation into the performances of imaging modality alternatives, including the former ultrasound system, in an effort to uncover an optimal modality. The modalities chosen should have the capability to distinguish skin to bone interfaces, have

an image resolution that is comparable or superior to that of the previously used ultrasound system and be safe and available to the subject. Any well established imaging modalities such as standard x-ray computed tomography (CT), magnetic resonance imaging (MRI) and high frequency ultrasound (US), that met the aforementioned criteria, would be worth examining.

MRI is well known for its ability to image and distinguish differing soft tissues. To achieve the resolution required of this tissue correction problem, a system with a strong magnetic field, such as 3 Tesla, is favourable. However, the availability of these systems is, in general, quite limited. In an effort to find a system with a greater accessibility, Appendicular MRI's have been considered to satisfy this requirement. Small bore MRI systems, of 1.0 Tesla field strength, have been found to require only small spaces for storage, minimal shielding, have an increased level of availability and produce images of comparable quality to those from larger magnets (Inglis *et al.*, 2007). Thus, when considering reproducibility for imaging persons undergoing a strontium measurement, the one Tesla Appendicular MR systems may be acceptable.

In contrast to MR, CT is typically implemented for imaging bone structure within a subject. Intra-soft tissue differentiation is not easily acquired using CT; however, the total soft tissue thickness overlying bone may still be visualized by this modality and prove useful in measuring total thickness. One limitation of CT is the consideration for radiation dose that the patient may receive from undergoing this imaging procedure.

High frequency ultrasound (> 15 MHz) has seen a renewed interest in recent years for its ability to provide high resolution images with tissue differentiation approaching the cellular level (Brand *et al.*, 2008). Higher frequency ultrasound has the capability to image and determine overlying soft tissue thickness to a high level of accuracy and reproducibility (Nouveau-Richard *et al.*, 2004). Ultrasound imaging has a fundamental property in which wave frequency is directly proportional to the resolution, or image quality, but is inversely proportional to the depth of penetration. Thus, the move to higher frequency will improve the detail of the image but will decrease the depth of wave penetration into tissue. Ultrasound is also highly attenuated by dense materials such as

bone and calcium deposits; this modality cannot produce an image beyond the bone surface. However, in the case of a human finger, the image needs only to penetrate down to this surface and will be sufficient for the purposes of this study. To apply this technique to the finger, the chosen frequencies should maximize resolution yet, penetrate deep enough to image the total distance from finger surface to bone surface.

For the practical purposes of this study, ultrasound is in many ways superior to MR and CT imaging modalities. Ultrasound units are far less expensive and are easy to implement and operate. They offer a greater portability, do not require special shielding or consideration for dose and have a quick image acquisition time. Additionally, the system may be used in other *in vivo* trace element applications where tissue correction is required.

Ideally, a comparison of imaging modality performances should be carried out on human physiology rather than phantoms. This way, a system's ability to image living human finger thickness may be directly predicted. The use of human cadaver fingers over living test subjects has many advantages. First, there is no risk to a subject's well being during this examination when considering factors such as comfort or radiation dose to the patient from CT scanning. Second, in the case of studying soft tissue effects on Sr XRF measurements, cadaver fingers may be altered or dissected as required to carry out XRF in the absence of tissue; this is a clear advantage over the use of living human fingers. Third, without the use of living human subjects, cadaver fingers still provide the closest anatomical model in which experimental results will be highly indicative of system performances on living humans.

If a cross-examination of modality performances may be carried out, then it might be determined if prior ultrasound imaging was underestimating soft tissue thickness. This might answer the question on whether the $K_{\alpha}:K_{\beta}$ ratio discrepancy was due to inaccurate imaging or an altogether different reason. It will also provide a critical examination of system performances that may bring forth an imaging modality with a level of measurement accuracy superior to the currently used ultrasound system.

2. 2 Materials and Methods

2.2.1 Gold standard attempts

Ethics approval for the use of human cadaveric tissue was sought from Hamilton Health Sciences Research Ethics Board (HHSREB). Approval was granted for the use of human cadaver index fingers to study the efficacies of imaging modalities in determining soft tissue thickness with great accuracy. The cadaver fingers acquired were all from Caucasian individuals between 65-90 years of age at the time of death.

In an effort to cross-examine accuracies of finger soft tissue thickness estimates obtained from different imaging modalities, several attempts were made to arrive at a gold standard or “true” tissue thickness value of each finger. This value would be used as an absolute reference thickness to which results from each modality may be directly compared. The first attempt was to implement a cutting technique that would produce a finger cross section that could be measured with a fine scale ruler to arrive at thickness. It was accepted that any cutting of the soft tissue may result in tissue compression that would alter the reporting of the true tissue thickness.

To reduce this effect a histological embedding procedure was examined. By infiltrating the finger samples with paraffin wax, compression might be minimized. This technique was applied to an embalmed cadaver finger donated by the Educational Anatomy and Bequeathal Program of Hamilton Health Sciences (EABPHHS). Prior to the procedure, the measurement location of the middle phalanx of the finger was marked. At that location, the total finger thickness from the dorsal to ventral side was measured and later used to determine if the thickness changed as a result of either the cutting or histological procedure. Five millimeter cross-sectional disks of each middle phalanx were cut using a scalpel and bandsaw to cut through soft-tissue and bone. These cuts were made on either side of the spot marked for examination and meant that the marked spot would be cut only by a microtome after embedding.

The tissue samples further were fixed in a 10% formalin solution. The disk sample was then immersed in a decalcification solution for 24 hours to de-mineralize the

bone so that the finger cross-sections could be cut. With the bone decalcified, the sample was placed in cassettes and imbedded in paraffin wax. Cross-sections were cut at 5 μ m thickness each and 20 serial sections were created. Each section was mounted on a glass slide, stained with haematoxylin and eosin (H&E) to differentiate tissue and tissue thickness measured.

A second attempt to arrive at a gold standard was performed direct onto seven donated cadaver fingers used throughout the work in this manuscript. Seven index fingers, embalmed and fixed for preservation, were obtained from the (EABPHHS). Thirty caliper readings of dorsal to ventral total finger thickness were taken of the intact finger. The dorsal tissue was then completely excised down to bone so that another 30 measurements of the total bare bone to anterior surface thickness could be collected. This process was repeated for all seven fingers. For each finger, an average was calculated for each set of measurements and a subtraction of the latter from the former set was performed to obtain an estimate of the dorsal tissue thickness. This entire process was carried out after imaging and EDXRF trials were performed on the fingers.

2.2.2 Cadaver Finger Imaging

The seven index fingers obtained from the EABPHHS were wrapped in small cloths and stored in labeled plastic containers that housed a preserving moistening fluid; this fluid was composed of Dettol® antiseptic, phenol, sodium acetate, formaldehyde and thymol in a 92% water base. Each finger was removed by sectioning at the knuckle between the metacarpal hand bone and proximal phalanx. An ink marking was placed on the dorsal tissue surface, midway along the middle phalanx of each finger to mark the centre point of the bone and to indicate where future image thickness and EDXRF measurements would be made. It is at this location along the finger bone that it is necessary to know the skin surface to bone surface tissue thickness.

The imaging modalities tested were: 1 Tesla magnetic resonance imaging (MRI), 65 & 75 kVp x-ray computed tomography (CT) and 8, 25 & 55 MHz ultrasound (US). Ultrasound of 8 MHz US was included to provide a benchmarking with prior experiments

done by Zamburlini *et al.* (2007) and Pejović-Milić *et al.* (2004). This device has an approximate 8 MHz center frequency but was previously reported according to its maximum frequency at 12 MHz. Note that all ultrasound frequencies mentioned from this point on refer to the centre frequency of the transducer as this is the most intense wave frequency the transducer will emit. Prior to marking, the ink was checked for strontium contamination and was verified strontium free.

MRI was carried out using an OrthoOne® 1.0 Tesla small bore extremity MR imaging system at the Centre for Appendicular MRI Studies, Hamilton, ON. This system's smallest available coil size, at 80mm in diameter, was used in an effort to surrender the best possible image resolution. Cadaver fingers were doubly sealed in plastic seal bags to maintain cleanliness of the site. Imaging parameters were optimized by the technician to bring out the best soft tissue contrast of the cadaver fingers. All seven cadaver fingers were imaged under these parameters, with the primary axis of the beam aligned along the dorsal surface of the middle phalanx bone. See Table 2.2 for parameters used.

Table 2.2: 1 Tesla MR parameters

Parameter	Specifics
Fat/water weighting	3D Gradient water peak echo
Slice size	22 slices @ 1.5mm / slice
Slice gap	0 mm
Frequency x Phase	256 x 256
Field of view (FOV)	40 x 40mm
Pixel width	156 x 156 mm
Number excitations (NEX)	2
TR/TE	40/17.7
Bandwidth	20 kHz
Flip angle	45°
Scan time	7.5 minutes

CT imaging was carried out at the McMaster Centre for Pre-Clinical and Translational Imaging (MCPTI). A Gamma Medica – Ideas X-SPECT™ system was used to obtain standard CT x-ray images. In order to bring out the best inter-tissue contrast, a low operating voltage was used. The lowest possible voltage available for this

particular situation was 65 kVp; the imaging was repeated using 75 kVp to see if any difference in contrast or quality would result from a difference in voltage. Each 3 dimensional image data set was constructed using 1024 projections over 360° to construct a voxel matrix of 512 x 512 x 768 to cover the entire middle phalanx of each finger. The image resolution produced by this system is in the range of 80 – 100 µm and each voxel is of size 50 x 50 x 50 µm. Hounsfield units for each voxel were also included. Cobra_Exxim was used to reconstruct the raw CT data and in-house software used to acquire Hounsfield units. Image viewing and file saving was made possible through Amide v.8.15.1 freeware software. Tissue thickness readings were done using Image Processing and Analysis in Java (ImageJ) for both the MR and CT images.

A Philips HDI 5000 system with a L12-5 50 mm linear probe was used to acquire 2 dimensional (b-mode) images of the cadaver fingers. This system was made available through the Mohawk-McMaster Institute of Applied Health Sciences. The HDI 5000 has an approximate 8 MHz centre frequency with 12 MHz maximum frequency and has a point resolution of 200 µm (Philips Healthcare Tech. Support). The image plane was oriented so that both transverse and sagittal b-mode US images were taken of the dorsal side of the middle phalanx of each index finger. Standard transducer gel was used at the interface of the *ex vivo* samples to propagate sound waves and minimize noise artifacts. Care was taken to ensure the transducer did not touch the fingers at anytime so that tissue compression would not be an issue.

A line tool built into the system was used to measure the separation of the skin and bone surfaces and reported to the nearest 0.1 mm significant figure. A single reading of thickness was obtained from each of the transverse and longitudinal images to provide two estimates of soft tissue thickness at the same measurement site. Table 2.3 summarizes the features inherent with this system.

Table 2.3^c: Philips HDI 5000 L12-5 50mm system specifications

Parameter	Specification
Center Frequency	8 MHz
Axial Resolution	0.250 mm
Lateral Resolution	0.390 mm
Focal Length	12 mm
Field of View	51.2 mm

c) Philips Technical support: Personal Communication by Email

Additionally, cadaver fingers were imaged using a VisualSonics Vevo 770™ High Resolution *in vivo* Micro-Imaging System with 25 MHz (RMV-710B) and 55 MHz (RMV-708) transducers. Use of this system was made possible through Dr. Michael Kolios of the Department of Physics, Ryerson University. Availability of a higher frequency ultrasound system was utilized in addition to the Philips HDI 5000 system as the higher frequency was expected to yield a better spatial resolution and hence, provide a more precise estimate of soft tissue thickness. Both 25 and 55 MHz were used as it was uncertain how either would perform as far as resolution and penetration depth in the 55 MHz transducer case. Also this system offered an additional advantage of acquiring both b-mode and 3 dimensional image data sets.

Three dimensional imaging is made possible using a mechanical arm, designed by VisualSonics, that slowly guides the transducer along a linear path. As the arm moves in an x-direction, the transducer takes a series of b-mode images in the y,z-plane and the Vevo software ultimately constructs a 3-D image data set that may be viewed using built-in Vevo software. Both 25 and 55 MHz b-mode and 3-D volume renderings of each finger were acquired. The technical specifications and transducer resolutions, as reported by VisualSonics, are summarized in table 2.4.

Given that the transducer would be made to move across the surface of the finger, a water bath was used to provide a sound propagation interface medium between finger and transducer. Water was chosen over transducer gel so that 3-D volume renderings could be obtained without concern of losing the gel-surface contact as the transducer passes over the finger surface. To accomplish this, cadaver fingers were fully submerged

in a salt water bath with the dorsal surface of the middle phalanx being oriented to face upward or parallel to the table.

There was concern that submersing the fingers in water alone would result in tissue swelling or shrinkage. To overcome this potential problem, a 0.9% by weight amount of pure sodium chloride (NaCl) was added to the water bath. This was done to mimic the sodium content in preservation fluid in which the fingers are stored. Given that swelling would be almost exclusively governed by a salt concentration gradient, it was expected that this addition of NaCl would prevent any water exchange and hence, prevent a change in tissue thickness.

Table 2.4: Vevo 770™ transducer specifications by VisualSonics¹

Parameter	Transducer Model	
	RMV-710B	RMV-708
Center Frequency	25 MHz	55 MHz
Axial Resolution	0.070 mm	0.030 mm
Lateral Resolution	0.140 mm	0.070 mm
Focal Length	15 mm	4.5 mm
Depth of Field	2.7 mm	1.4 mm

1. VisualSonics 700-Series RMV™ Scanhead Selector Manual

Operations parameters associated with these measurements are provided in table 2.5.

Table 2.5: Ultrasound 25 & 55 MHz operation parameters

Parameter	Transducer Model	
	RMV-710B	RMV-708
Transducer speed	4 Hz	5 Hz
Field of View	18 mm	8 mm
Speed of Sound in Medium	1540 m/s	

The processing of each image data set for all 5 modalities had to be done such that a single operator produced all measurements and without bias or preference to any given modality. This was to ensure that the reading was done with the positioning of line tool end points at the same interfaces each time. Additional care was taken to make sure that the line tool was drawn completely normal to the bone surface so that the shortest path

difference from bone to skin surfaces was found. If the path difference is traced on a slight diagonal, this would artificially increase the soft tissue thickness reading. Lastly, for the inter-modality comparison of thickness readings to be possible, the same centre point along the middle phalanx had to be carefully located on each image to make the measurement. This was typically done by measuring the distance between each knuckle of the middle phalanx and marking the halfway point in between as the measurement site. All measurements were made on the dorsal surface of the finger.

The transverse views of each image were first used to determine the most dorsal point along the bone of each finger. From this marker, a longitudinal view was selected and the point-to-point thickness measurement was carried out. This was done for each of the CT, US-25 MHz and US-55 MHz imaging modalities. The thickness measurement was repeated 2 more times to collect 3 estimates of tissue thickness per image. As there were two image sets for the CT modality being done using 65 and 75 kVp, both were analyzed so that the thickness reading from CT was calculated from the average of 6 readings per finger as opposed to 3. In the MR data sets, only the transverse view of each slice was available to make a thickness reading. Of the 22 slices obtained, slices 11 and 12 are representative of the middle part of the finger bone. Three measurements, from both image slices, were taken and averaged to get one estimate of finger thickness.

The 8 MHz ultrasound measurements were done on site using the software built into the Philips HDI 5000 system. One measurement was done of the thickness reading in the transverse view and another was taken of the finger in the sagittal view to give two estimates of tissue thickness per finger.

2.2.3 Re-Evaluation of 8 MHz ultrasound performance

The question of whether the 8 MHz ultrasound imaging modality was underestimating true tissue thickness was examined here to put to rest any speculation of its involvement in affecting the expected $K_{\alpha}:K_{\beta}$ ratios seen in Zamburlini *et al.* (2007). Since the original ultrasound images were no longer available to be re-analyzed, a re-measuring of the original study subjects was necessary. This study began with subject

recruitment from the original 22 individuals involved in the *in vivo* strontium measurement pilot study from the spring of 2006, reported by (Zamburlini *et al.*, 2007). Out of the 22 individuals, 9 were recruited to be re-measured in the summer of 2008, at the same anatomical sites and using the same 8 MHz ultrasound as before. The examined measurement sites were the middle phalanx of the right index finger and the medial malleolus of the right ankle; both of the right appendages were measured in the prior study in the spring of 2006.

A small ink mark was made on each measurement site to guide the transducer to the appropriate site. A gel pad was interposed between the finger and transducer to reduce the effects of direct compression to the measurement site by the transducer. Transducer gel was applied to both sides of the pad to connect each interface for sound propagation. As in the case of the cadaver finger imaging using 8 MHz ultrasound, both sagittal and transverse images slices were taken to provide two estimates of tissue thickness other than one. It was assumed that if no weight gain or loss occurred in the population being measured, then finger size would be the same now as it was in 2006.

2.3 Results and Discussion

2.3.1 Gold standard finger soft tissue thickness

In the attempt to create a gold standard true tissue thickness value for each cadaver finger, it was deemed that the method of using histological processing would not satisfactorily allow for a reliable gold standard. Brief analysis of the prepared microscope slide sections revealed that the samples had undergone an alteration in their structural integrity and had in most cases, shrunk from the initial thickness of the finger measured prior to the cutting. Some segments had shrunk more than others and a few of the finger cross sections were up to 2 mm smaller in diameter than the diameter of the uncut finger. Hence, this idea was abandoned.

The second method used in attempt to obtain a gold standard, although not completely successful, proved somewhat helpful in verifying the thickness readings from the 5 modalities. Illustrated in table 2.6 are the averages and percent uncertainties (\pm SD) calculated from the raw caliper measurements. Although the relative uncertainty of each caliper trial was only about 1% of the total thickness, when the two values were subtracted, and the uncertainties added in quadrature, the uncertainty increased to a 5-10% range. Since the uncertainty is so high, it is not possible to use these readings as a gold standard. However, they do provide an additional estimate of soft tissue thickness. Hence, the caliper results were added to the 5 modality results as a sixth modality which provided a sixth estimate of true tissue thickness.

Table 2.6: Caliper tissue thickness measurements

Finger ID	Total Intact, mm	Uncert., % (\pm SD) N=30	Tissue Removed, mm	Uncert., % (\pm SD) N=30	Subtraction	Uncert., %
1	15.96	\pm 0.92	13.36	\pm 1.27	2.60	\pm 8.64
2	18.74	\pm 1.02	14.49	\pm 1.14	4.25	\pm 5.94
3	17.75	\pm 1.51	14.31	\pm 1.48	3.44	\pm 9.96
4	16.76	\pm 0.99	12.85	\pm 1.07	3.91	\pm 5.52
5	17.44	\pm 0.96	13.65	\pm 0.72	3.79	\pm 5.13
6	18.56	\pm 0.90	14.60	\pm 0.89	3.96	\pm 5.35
7	17.44	\pm 1.24	13.97	\pm 0.96	3.47	\pm 7.35

2.3.2 Cadaver finger imaging and modality performance

A sample image from each modality performed on finger 4 has been provided to illustrate the level of image quality that has been produced. Attention has been given to the dorsal side of the index finger where the tissue thickness measurements are performed. Here, bone and skin surfaces and tendon have been marked according to the legend in figure 2.1. Figures 2.1 through to 2.9 provide sagittal and transverse image slice examples of all five imaging modalities tested in this study: MR, CT, US 8 MHz, US 25 MHz and US 55 MHz.

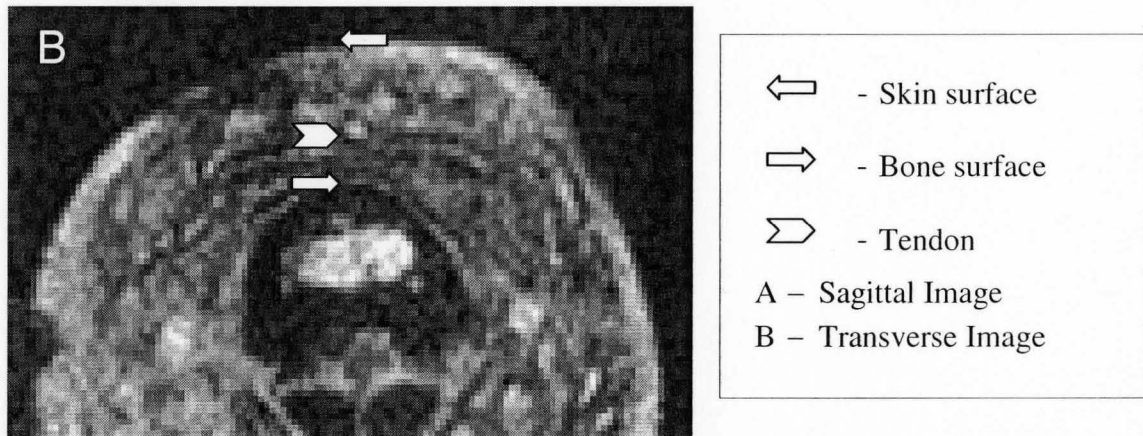


Figure 2.1: Transverse image of the dorsal side of a human index finger using MR

The tendon sheath is visible in the MR image seen in Figure 2.1. Only transverse slices were available from the MR images produced.

Of the CT images examined, there was no noticeable difference in image quality between the 65 and 75 kVp produced images. The unusual grey scale colouring of these images was chosen as it was found to bring out the best inter-tissue contrast. In the CT transverse view seen in figure 2.3, tendon was barely visible. However, tendon was not always discernible in obtained cadaver finger CT images.

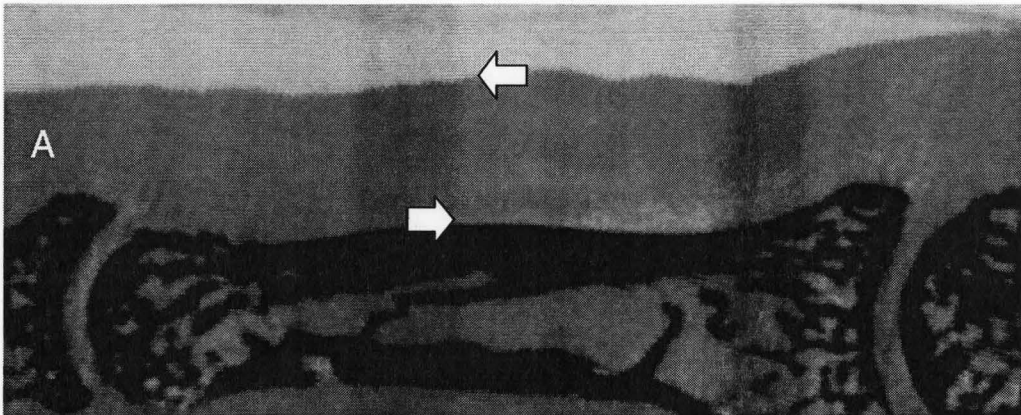


Figure 2.2: Sagittal image of a human index finger produced by 65 kVp CT

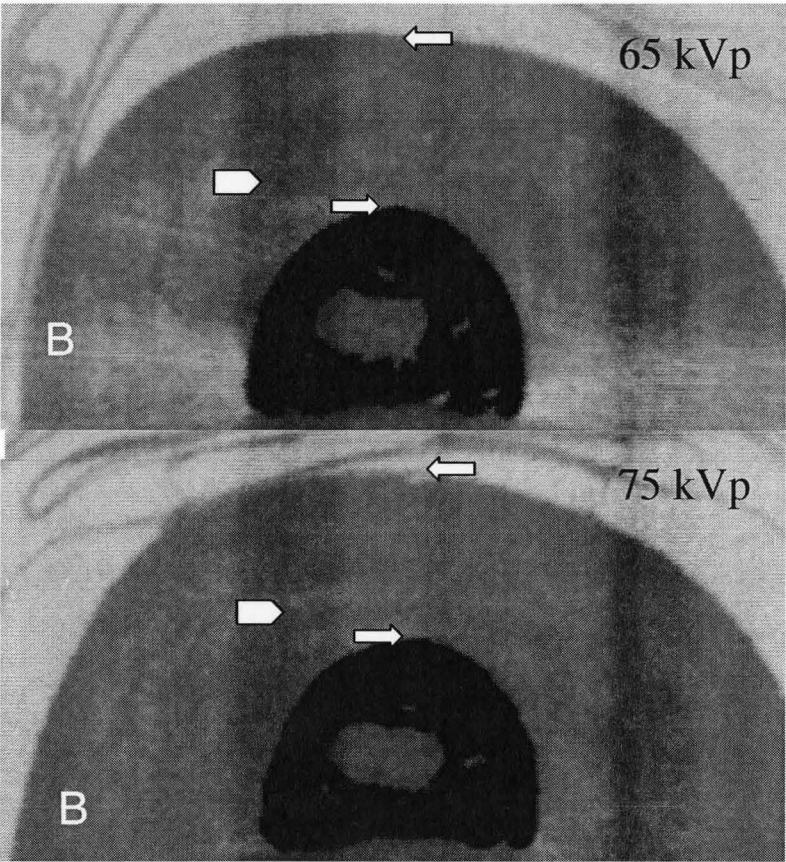


Figure 2.3: Transverse image of a human index finger produced using 65 and 75 kVp voltage

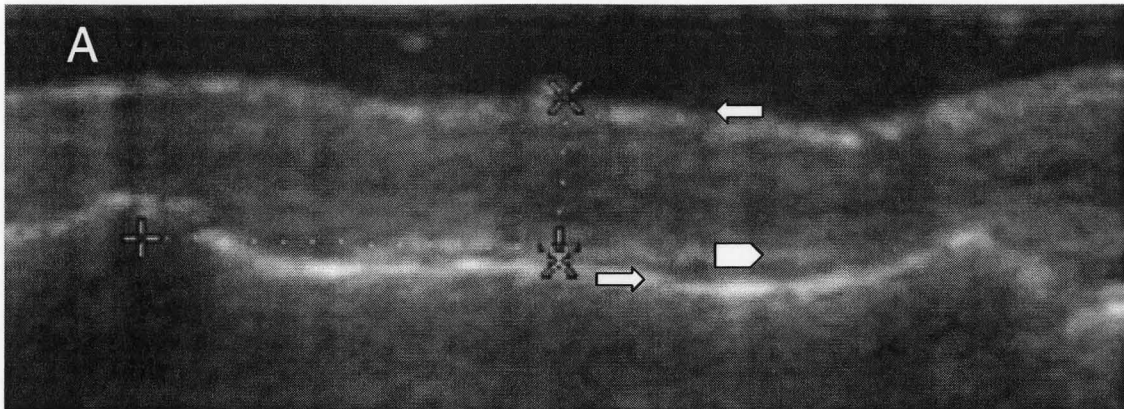


Figure 2.4: Sagittal image of a human index finger produced using 8 MHz ultrasound

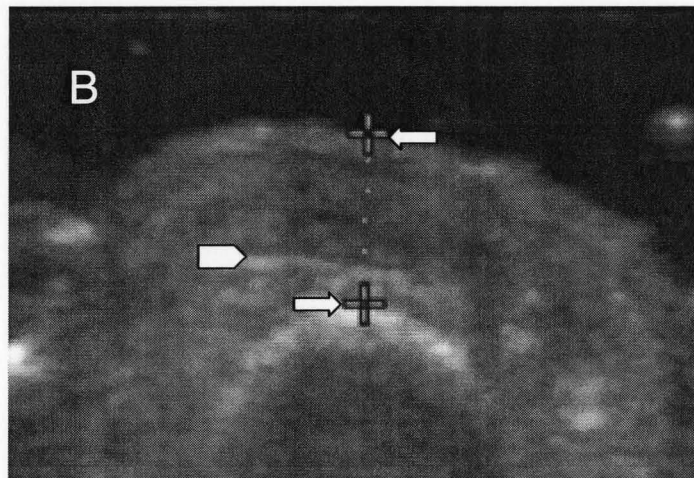


Figure 2.5: Transverse image of a human index finger using 8 MHz ultrasound

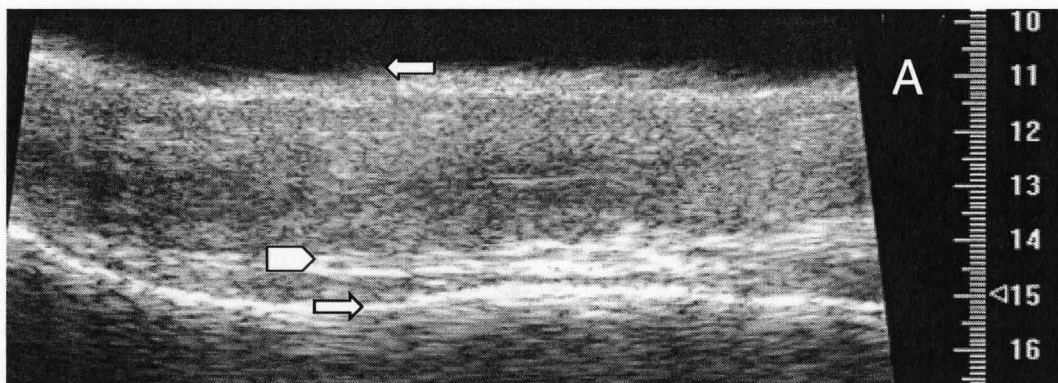


Figure 2.6: Sagittal image of a human index finger using 25 MHz ultrasound

Bone surface was clearly visible in all three frequency images and tendon was best distinguished from bone using the 55 MHz ultrasound

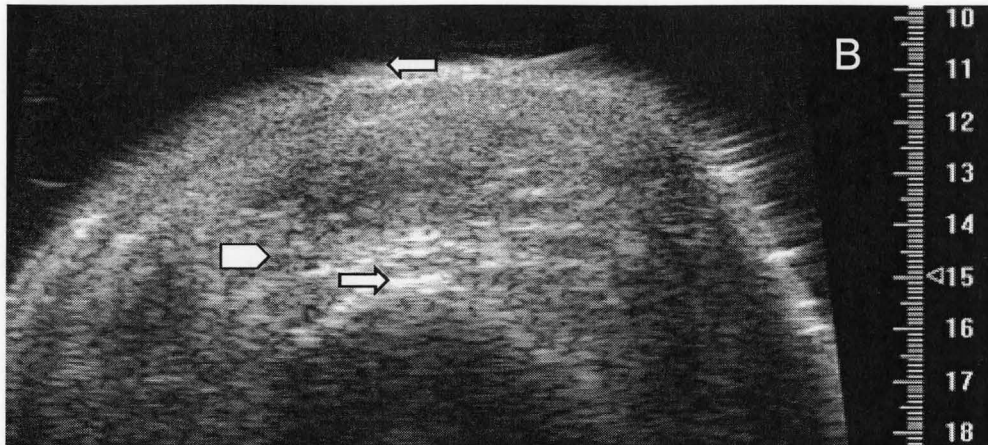


Figure 2.7: Transverse image of a human index finger using 25 MHz ultrasound

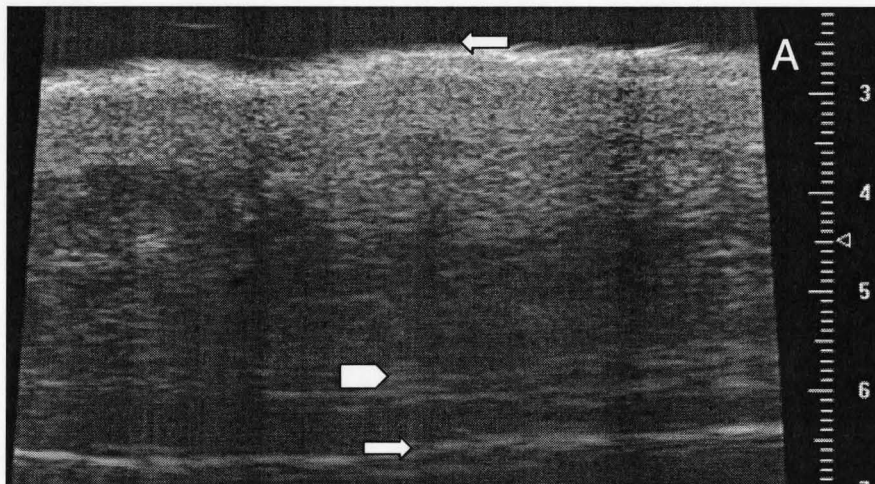


Figure 2.8: Sagittal image of a human index finger using 55 MHz ultrasound

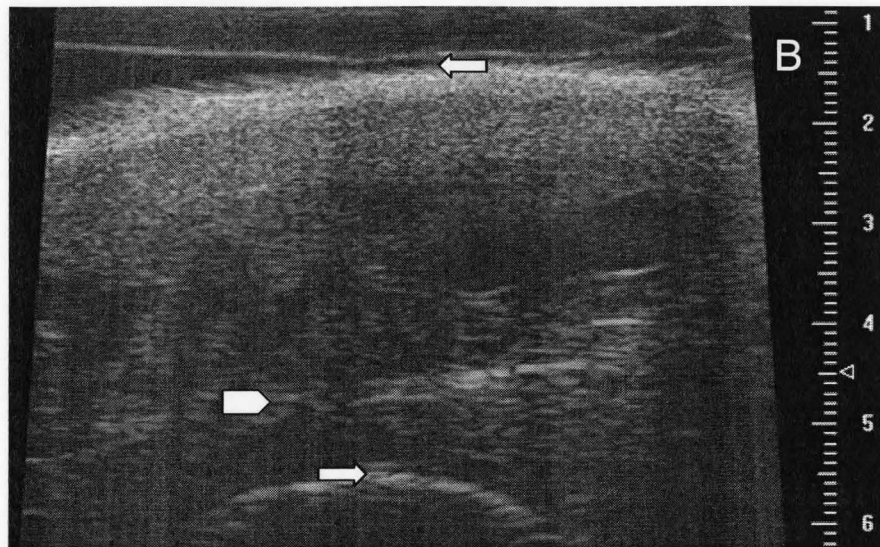


Figure 2.9: Transverse image of a human index finger using 55 MHz ultrasound

The results for the tissue thickness measurements of all modalities on all seven fingers are tabulated in table 2.7. The average and standard deviations for all 6 modalities have also been provided in this table. Uncertainties for the 5 imaging modalities are given as the standard deviation of multiple measurements made on one finger by one modality except in the case of 8 MHz US. Since only two readings were taken from this modality, the system resolution was used over the standard deviation. Uncertainty was taken as half the smallest scale division of the resolution (0.125 mm) and added as the square root of the sum of squares to account for the uncertainty of both ends of the line tool.

Each of the ultrasound resolutions reported in table 2.7 are the axial resolutions reported for each system. Each line tool measurement of skin surface to bone surface is made axially to the position of the transducer. In other words, the line measurement is made perpendicular to the face of the transducer and is consequently perpendicular to both tissue interfaces. Hence, it may be assumed that only the axial resolution has relevance to the discerning of tissue boundaries and placement of the measurement line tool. Note also that the total uncertainty of the tissue thickness of a finger estimated by an imaging modality may be higher than the resolution of the image given that there is

uncertainty associated with the positioning of each end of the line tool and that multiple measurements may produce a spread that is larger than the resolution.

Table 2.7: Raw modality tissue thickness estimates

Finger ID	CT	MR	Thickness $\pm \sigma$ (Thickness) [mm]			Caliper (\pm SD)	Average (\pm SD)
			US 8	US 25	US 55		
1	2.708 \pm 0.080	2.480 \pm 0.174	3.000 \pm 0.177	2.813 \pm 0.061	2.750 \pm 0.034	2.599 \pm 0.224	2.725 \pm 0.179
2	3.908 \pm 0.109	4.140 \pm 0.125	4.450 \pm 0.177	4.240 \pm 0.049	4.273 \pm 0.041	4.248 \pm 0.252	4.210 \pm 0.179
3	3.710 \pm 0.084	3.895 \pm 0.113	3.600 \pm 0.177	3.743 \pm 0.107	3.740 \pm 0.034	3.441 \pm 0.343	3.688 \pm 0.154
4	3.570 \pm 0.122	3.872 \pm 0.121	3.900 \pm 0.177	3.947 \pm 0.055	3.850 \pm 0.027	3.908 \pm 0.216	3.841 \pm 0.137
5	3.623 \pm 0.081	3.938 \pm 0.122	4.200 \pm 0.177	4.137 \pm 0.052	3.980 \pm 0.034	3.794 \pm 0.195	3.945 \pm 0.214
6	4.067 \pm 0.083	4.373 \pm 0.132	4.400 \pm 0.177	4.730 \pm 0.076	4.593 \pm 0.030	3.965 \pm 0.212	4.355 \pm 0.295
7	3.713 \pm 0.229	3.593 \pm 0.153	4.050 \pm 0.177	3.800 \pm 0.067	3.820 \pm 0.021	3.472 \pm 0.255	3.741 \pm 0.200

The results of the tissue thickness values reported in table 2.7 are illustrated graphically in figure 2.10. Finger thicknesses are independent of each other and this histogram was created to illustrate how each imaging modality estimates the thickness of one finger for a total of 7 fingers. It also indicates the relative size of error associated with each finger thickness as reported by each modality.

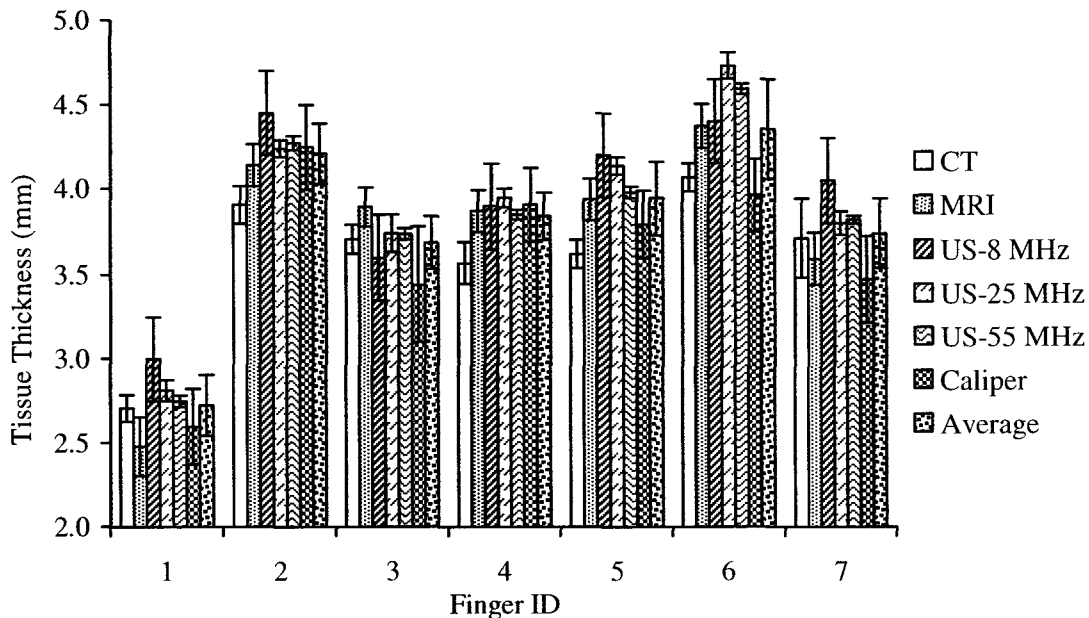


Figure 2.10: Image modality tissue thickness readings of seven cadaver fingers

Figure 2.10 demonstrates that the caliper uncertainties are quite large in comparison to most of the other modalities and further verifies that it cannot be used as a gold standard reference. Of all the modalities presented, the 55 MHz ultrasound provided the smallest range of error on a given measurement. Note that the MR resolution was approximated as the pixel size of the image as no readily available resolution data were available on this particular system.

2.3.2.1 Evidence of Thickness Estimation Bias

Given that no gold standard value of true finger tissue thickness could be found, the 6 modality data sets available had to be manipulated so that the associated measurement performance of each modality could be examined. This was done by taking advantage that 6 different modalities were used to estimate the same unknown. The average of the thickness estimates may be thought to approach the true tissue thickness value and subsequently approximate the formerly sought gold standard thickness value. The choice not to include in the average, the estimate from the modality being tested, was

made to keep the tested modality an independent variable in the calculation. Each modality had to be analyzed individually in this type of calculation.

To help answer the question posed by Zamburlini (2008) on whether the 8 MHz ultrasound has a tendency to underestimate soft tissue thickness, each modality has been examined for bias toward either overestimating thickness or underestimating thickness. Multiple measurements to provide an average thickness estimate for each finger (μ_i), from modality (i), are compared against the average thickness of that finger as estimated by the other 5 remaining modalities (μ_-). To examine one modality, the difference in finger soft tissue thickness from the average, as observed from the other 5 modalities, is calculated for each of the $j = 1..7$ cadaver fingers. This produces the average difference (AD) as follows:

$$AD = \frac{1}{N} \sum_j (\mu_i - \mu_-)_j. \quad (E4)$$

An average and standard error of the mean (SEM) of the $N = 7$ cadaver fingers calculated differences are then computed. SEM is calculated as $SD/\sqrt{N-2}$ since both the mean and standard deviation (SD) are estimated from the data at hand. The average difference divided by the standard error of the mean is assessed for significance using a student t-test at 90% confidence for $N-2 = 5$ degrees of freedom. The results of this calculation are provided in table 2.8.

Table 2.8: Evidence for image modality biasing to underestimate or overestimate tissue thickness

Modality	Average Difference, μm	SEM, μm	T-statistic, AD/SEM	Bias, $\alpha = 0.10$ None, OE, UE
Caliper	-185.0	88.8	-2.083	UE
US-55MHz	85.8	41.4	2.071	OE
US-25MHz	155.1	64.6	2.399	OE
US-8MHz	187.6	80.7	2.326	OE
MRI	-36.7	77.3	-0.475	None
CT	-206.8	83.4	-2.480	UE

Legend: AD – average difference
SEM – standard error of the mean
OE – overestimate
UE - underestimated

At 95% confidence, there was no evidence of bias for any modality. At 90% confidence, only the average difference of MR was not significantly different from zero. Of all the tested modalities, CT produced the highest difference from the mean as it appeared to underestimate the true tissue thickness while ultrasound was found to possibly overestimate tissue thickness. It is possible that the caliper measurements were lower than average due to compression of the caliper arms on the tissue surface. Despite the care taken to make the measurements very gently, changes of thickness on the order of hundreds of microns are very likely to manifest through contact. However, at only 90% confidence, evidence of bias is not entirely clear. Figure 2.11 illustrates these results graphically, with error bars indicating the standard error of the mean (SEM) for each modality.

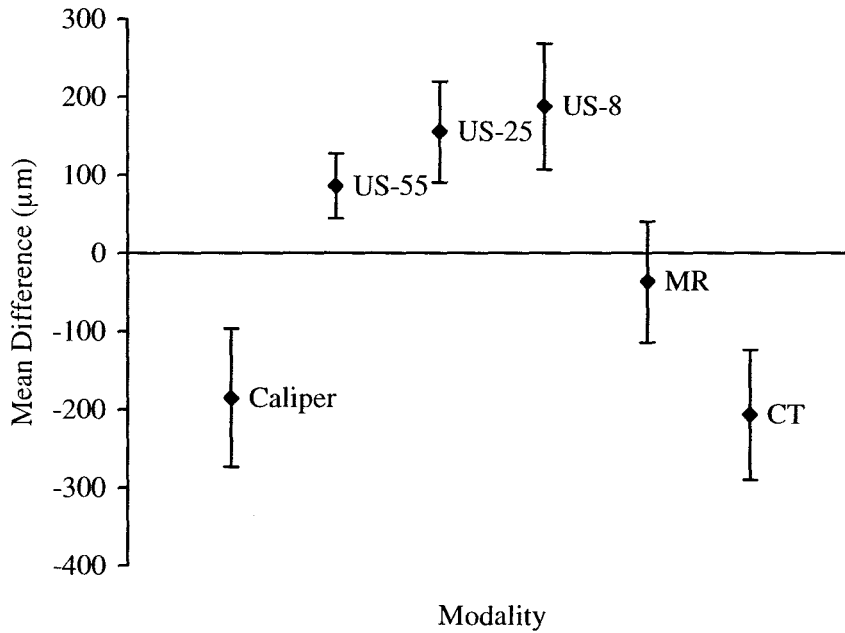


Figure 2.11: Differences from mean soft tissue thickness: evidence for biasing of image modalities to either underestimate or overestimate soft tissue thickness (\pm SEM)

To obtain more conclusive results regarding modality bias, a standard t-test between two means may be used to assess how the performance of each modality compares to the exclusive weighted means from all other modalities. An unequal sample size is accounted for in this calculation and the difference between true means is assumed to be zero ($\mu_{T_i} - \mu_{\bar{T}} = 0$). The unbiased estimator of the variance ($\sigma_{i,j}^2$) between observed and average measurement, is calculated as follows:

$$\sigma_{i,j}^2 = \left(\frac{(n_{T_{i,j}} - 1)\sigma_{T_{i,j}}^2 + (n_{\bar{T}_{i,j}} - 1)\sigma_{\bar{T}_{i,j}}^2}{(n_{T_{i,j}} - 1) + (n_{\bar{T}_{i,j}} - 1)} \times \frac{n_{T_{i,j}} + n_{\bar{T}_{i,j}}}{n_{T_{i,j}} n_{\bar{T}_{i,j}}} \right) \quad (E5)$$

where: $T_{i,j}$ - is the estimate of tissue thickness of finger (i) averaged from (h) many repeated measurements using modality (j) such that:

$$T_{i,j} = \frac{1}{n_{T_{i,j}}} \sum_{h=1}^{n_h} T_{h,i,j}$$

$n_{T_{i,j}}$ - is the number of single measurements taken, per image, to estimate thickness of finger (i) by modality (j),

$\bar{T}_{i,j}$ - is the average thickness of finger (i), as estimated by the other ($n_{\bar{T}_{i,j}} = 5$) remaining modalities. Note that:

$$\bar{T}_{i,j} = \frac{1}{n_{\bar{T}_{i,j}}} \sum_{k=1, k \neq j}^6 T_k$$

k - is the number of the modality being tested = 1..6

$\sigma_{T_{i,j}}^2$ - is the variance of the (h) observed estimates of thickness of finger i using modality j.

$\sigma_{\bar{T}_{i,j}}^2$ - is the variance of the exclusive average $\bar{T}_{i,j}$

This value may be used to calculate the t-statistic to determine if a significant difference exists between the observed and average thickness for modality j and will further indicate if the difference is biased toward over or underestimation. The t-statistic and degrees of freedom (D.O.F.) for modality j is calculated as follows:

$$t_j = \frac{1}{n_i} \sum_{i=1}^7 \left(\frac{T_{i,j} - \bar{T}_{i,j}}{\sigma_{i,j}} \right), \quad \text{D.O.F.} = n_{T_{i,j}} + n_{\bar{T}_{i,j}} - 2 \quad (\text{E6})$$

where: n_i - is the number of fingers used to estimate the t-score t_j .

This calculation process was performed for each measurement individually to produce 6 t-test scores. To evaluate the t-score of one modality, all 7 finger t-scores pertaining to that modality were averaged. The final t-scores are presented in table 2.9 and are compared against tabulated two-tailed t-values at 95% confidence.

Table 2.9: Standard T-test examination of modality bias

Modality	$n_{T_{i,j}}$	$n_{\bar{T}_{i,j}}$	D.O.F.	Table T (+/-),	Observed t_j ,	Bias
				$\alpha = 0.05$	t-score	
Caliper	30	5	33	1.96	-1.60	None
US-55 MHz	3	5	6	2.45	0.52	None
US-25 MHz	3	5	6	2.45	1.05	None
US-8 MHz	2	5	5	2.57	0.95	None
MRI	6	5	9	2.26	-0.22	None
CT	6	5	9	2.26	-2.48	sig. lower

This method indicates that the CT method was biased to underestimate the true tissue thickness, on average. However, it does not indicate any sort of bias in any of the other modalities. This is contrary to the results suggested in table 2.8 at 90% confidence. Scanning using CT may have also imparted compression as the fingers had to remain in plastic bags while being inserted into a small holding chamber. In the case of CT, there was no difference in the appearance of soft tissue contrast between finger images produced using the 65 and 75 kVp voltage. However, it was observed that the tissue-to-air boundary was not clearly defined in each image as this interface appeared to spread across 3 to 4 pixels prior to terminating.

CT thickness measurements were done by placing the line tool end at the outer edge of the last fully tinted pixel of the tissue-air boundary. It is possible that this may not represent the true location of this boundary if we consider partial volume effects on voxel image reconstruction. For example, if the tissue boundary terminates in the middle of a voxel, the reconstructed image will be the average of the signal received from both air, in one half of the voxel, and tissue, in the other half. This would produce the effect of creating a lighter tinted pixel with a reduced overall density. Additionally, since the system resolution (80-100 μm) is about twice as large as the pixel size (50 μm), this effect may be spread across multiple pixels and explain why the boundary termination gradually occurs over 3-4 pixels. Thus, if the true tissue-air boundary is several pixels higher than that assumed in this experiment, this would constitute an underestimation of the total tissue thickness.

Surprisingly, 8 MHz ultrasound produced the largest average estimate of soft tissue thickness which is in contrast to results previously reported (Zamburlini, 2008). Zamburlini (2008) observed that estimates of soft tissue thickness, using a Philips HDI 8 MHz ultrasound system, were less than expected and could not be fully explained.

Each of the ultrasound devices used in this study was capable of imaging and discerning the overlying tendon layer from other tissues. The bone layer was also distinguishable from tendon using all systems. However, only the 55 MHz ultrasound was able to show possible inter soft tissue detail (see Figure 2.9); this may prove useful if future tissue correction work requires differentiation between the layers of soft tissues and estimates of layer thickness. The surface of the finger appeared as a brightly coloured, homogenous band of near uniform thickness; it was suggested by Richard Butler Ph.D. of the McMaster University Anatomy Department that this may represent the epidermal, dermal and hypodermal layers of skin. The globular, inhomogeneous, darkly coloured region under this layer and surrounding tendon was more indicative of the complex matrix of adipose and connective tissues underlying skin. Since adipose tissue may be localized in pockets throughout the connective tissues, this may help explain why the image of this region appeared highly globular.

2.3.2.2 Accuracy of imaging modalities

To determine the accuracy of one modality, the thickness estimate from this modality was once more compared against the average of the estimates from the other five modalities. In this case however, to arrive at a maximal estimate of measurement variation from the mean, a square of difference had to be calculated. Equation (E7) calculates the accuracy of an imaging modality, in units of length. A sample calculation of accuracy for one modality is provided below; this example illustrates accuracy calculated for the CT estimate of total soft tissue thickness:

$$\text{Accuracy}_{\text{Modality}(j)} = \left[\frac{\sum_{i=1}^{7 \text{ fingers}} \left(\text{Mod}_{i,j} - \frac{\sum_{k=1, k \neq j}^6 \text{Mod}_{i,k}}{N_k - 1} \right)^2}{N_i} \right]^{1/2} \quad [\text{mm}] \quad (\text{E7})$$

- Where:
- N_k = number of modalities tested = 6
 - N_i = number of fingers modality used on = 7
 - $\text{Mod}_{i,j}$ = thickness reading given by modality(j), $j = 1, \dots, 6$ of finger(i)
 - $\text{Mod}_{i,k}$ = thickness reading given by modality(k), $k = 1, \dots, 6$ of finger(i)

Sample Calculation:

- If:
- Modality (1) = MR
 - Modality (2) = CT
 - Modality (3) = US8
 - Modality (4) = US25
 - Modality (5) = US55
 - Modality (6) = caliper

$$\text{Accuracy}_{\text{Modality}(2)} = \sqrt{\frac{\sum_{i=1}^{7 \text{ fingers}} \left(\text{Mod}_{i,2} - \frac{\text{Mod}_{i,1} + \text{Mod}_{i,3} + \text{Mod}_{i,4} + \text{Mod}_{i,5} + \text{Mod}_{i,6}}{5} \right)^2}{7}}$$

The results of this calculation are listed below in table 2.10. All figures are given as absolute uncertainties of tissue thickness. To apply these accuracy quantities to future measurements of tissue thickness readings, the uncertainties must be converted into

relative error quantities. This is done by dividing the uncertainty over the average finger soft-tissue thickness calculated using all six modality estimates of seven cadaver fingers. Tissue thickness estimates from seven cadaver fingers suggests an average population index finger soft tissue thickness of 3.79 mm. The calculated uncertainties converted to relative error using this value are displayed in Table 2.10. Even if the average human soft tissue thickness may differ from this in the normal population, this estimate still serves to relate the relative magnitude of the uncertainty associated with using each modality. Relative uncertainties will be highly useful in determining error of quantification as they may be simply added to the total uncertainty associated with the rest of the quantification process.

Table 2.10: Image modality accuracy results

Modality	Accuracy Range, mm	% Accuracy Range (% Relative Error)
Caliper	0.261	6.9
US-55 MHz	0.121	3.2
US-25 MHz	0.205	5.4
US-8 MHz	0.251	6.6
MR	0.164	4.3
CT	0.269	7.1

Note: % Accuracy = $100 * (\text{Accuracy, mm}) / (3.79 \text{ mm})$

The results in table 2.10 indicate that the 55 MHz ultrasound imaging would have the lowest associated uncertainty, at 3.2%, in estimating finger soft tissue thickness. This presents a two fold improvement over the accuracy of the 8 MHz ultrasound used in prior experiments. 55 MHz ultrasound was capable of imaging down to bone in even the upper limits of finger soft tissue thickness. MR imaging was found to be a close runner up to 55 MHz ultrasound at 4.3% and CT imaging was found to produce the highest level of uncertainty associated with a measurement of finger soft-tissue thickness. Given that these quantities of relative uncertainty would be added to total uncertainty, it further exemplifies the importance of reducing this uncertainty of a measurement by as much as possible.

It is interesting to note that the 8 MHz ultrasound did not underestimate tissue thickness as was previously found (Zamburlini, 2008). This suggests that in previous image measurement analysis, tendon may have been mistaken for bone which would thus, artificially reduce overlying soft tissue thickness. Hence, identification of the bone-tissue interface is of great importance. Additionally, meaningful estimates of overlying soft-tissue depend on the proper placement of the measurement tool cross-hairs. Specifically, it is vital that the cross-hairs be directly centered on the interfaces of the corresponding tissues and that the line tool is positioned such that it is perpendicular to bone. If these factors are acknowledged during measurement taking, then the 8 MHz ultrasound should be expected to provide a reliable indication of overlying soft-tissue thickness.

Magnetic resonance imaging was performed on a 1 Tesla instrument and produced an acceptable level of accuracy. This level of accuracy may be further improved if the scan time were to be increased so that a higher image quality may be obtained. If the image acquisition time were increased by a factor of four, then the acquired image information would be increased by a factor of four. This would effectively produce an image with a 512x512 pixilation, but in the same 40x40 mm FOV as the 256x256 pixel images gathered in this study. This might translate into an improved level of accuracy in a tissue thickness reading. The only disadvantage would be the four fold increase in scanning time to acquire this level of detail. This would put the total measurement time, which includes time for patient positioning, to well over half an hour. This would risk discomfort to the patient and increase the likelihood of patient movement during scanning time. Any movement whatsoever may ruin the resultant image. Additional means of improving MR image quality and possibly accuracy of measurement would be to use an MR instrument with a greater magnetization, say to 3.0 Tesla or to use a smaller diameter coil.

2.3.3 Re-evaluation of 8 MHz ultrasound performance

Both ankle and finger measurements of the 9 participating subjects have been reported. Both of the transverse and sagittal slices of each site have been averaged to

produce a single finger and ankle thickness value per person. It is important to note several limitations confronted this study. The first was that the individual ultrasound images were not available to be re-measured; had they been available, re-measuring the 22 individuals may not have been necessary in the first place. The second complication was that no body mass index (BMI) information of the subjects from the first study existed. This information would be advantageous to determine if subject body mass has changed over time as a means to check if changes in overlying soft-tissue thickness has occurred between the 2006 and 2008 studies; this would influence the final outcome of tissue thickness measurements.

In order to compare the results from the present study to the first one directly, it must be assumed that finger size has not changed. To assume this, we must be certain that a person did not experience any noticeable weight loss or gain in the past several years that would alter their finger or ankle soft tissue thickness. In the absence of BMI information, verbal confirmation of weight change had to be relied upon for evidence that thickness may have changed. For simplicity, individuals reporting weight change have been excluded from analysis. Subjects 14 and 19 reported undergoing weight gain or loss in the last several years and thus, were not included in this analysis. All other subjects did not report any noticeable change.

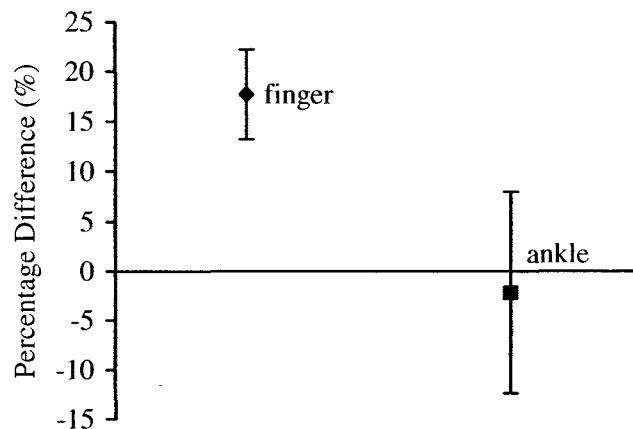
For each person, thickness readings from 2008 have been compared relative to those from 2006 in a percentage difference as follows:

$$\frac{T_{2008} - T_{2006}}{T_{2006}} \times 100$$

The average and standard deviation of these percentage differences for the seven participants were computed and summarized in table 2.11. These are further illustrated in figure 2.12 as the average percentage difference of each site with error bars representing the standard error of the mean for $N-2 = 5$ degrees of freedom.

Table 2.11: Inter-study comparison of ultrasound measurements on ankle and finger of returning participants

Site	Average Difference, mm	Average Difference, %	SD, %	SEM, % (d.o.f = 5)	t-statistic	Significance
Finger	0.48	17.70	10.09	4.51	3.92	higher ($\alpha = 0.025$)
Ankle	-0.19	-2.18	22.79	10.19	-0.21	Not different

**Figure 2.12:** Plot of average difference of finger and ankle ultrasound thickness measurements performed two years apart

Although this is a sample size of only seven, these results still serve as an indication of potential differences in measurements between the two studies. The percentage difference for the ankle measurement is well within zero indicating no significant difference while that of the finger is significantly above zero at 97.5 % confidence. This strongly suggests that the finger tissue thickness was underestimated in the 2006 study. This may be the result of mistaking tendon for bone which would artificially shorten the estimate of bone to skin surface distance.

Alternatively, real time ultrasound showed that even with the use of the gel pad, substantial compression from the transducer may still occur. This may have imparted compression to the finger thicknesses of the originally measured individuals and artificially thinned out the soft tissue. Even if a delicate touch is used, the gel pad may impart enough compression that it alters the natural tissue thickness by fractions of a

millimeter. This would provide a significant error in the correction for bone strontium content measured using EDXRF. Thus it is important to achieve minimal to no compression at all time. It is recommended that ultrasound measurements be done using liquid sound propagating media only, such as transducer gel or water baths. This is to ensure that the transducer never comes in contact with the skin.

Since it appears that ankle thickness measurements were done correctly in 2006, this is in disagreement with the prediction made by Zamburlini *et al.* (2007). At the time, it was thought that the observed $K_{\alpha}:K_{\beta}$ ratios from the tissue corrected ankle EDXRF measurements did not match expected ratios possibly because of an underestimation of soft tissue thickness overlying the ankle site. The percentage difference results bring evidence against this hypothesis. If the disparity of the $K_{\alpha}:K_{\beta}$ ratios cannot be linked to tissue attenuation alone, then perhaps some factor is affecting the peak areas observed. This observation is discussed in Chapter 3 in greater detail.

This study illustrated that 8 MHz ultrasound may accurately estimate soft tissue thickness, when the bone interface is properly identified. Thus, it may be subsequently used to continue imaging people for *in vivo* bone strontium measurements. However, 8 MHz ultrasound has a poorer precision of measurement and a reduced level of accuracy in comparison to other available imaging modalities. Regardless of the imaging modality that is used, efforts need to be made to reduce finger soft tissue compression during image acquisition. Implementation of a higher frequency ultrasound system, using a water bath sound propagation medium, would be beneficial to improving tissue thickness measurement accuracy. The 55 MHz ultrasound with three dimensional data reconstruction provided a twofold improvement in accuracy of measurement over the former 8 MHz system and of all modalities tested, has the highest level of accuracy. For the purpose of implementing an imaging modality to provide tissue thickness estimates for *in vivo* bone strontium measurements, high frequency ultrasound offers a superior image quality, portability and cost to implement. It is also user friendly and does not require consideration of radiation dose to the patient or operator.

Chapter 3

COHERENT NORMALIZATION AND XRF MEASUREMENTS

3.1 Introduction

3.1.1 Coherent scatter normalization

The ultimate goal in performing an *in vivo* bone strontium measurement is to achieve absolute quantification. This is a challenging procedure that requires correction of many variables if quantification is to be achieved. Variables include intersubject differences of overlying soft-tissue thickness, bone size and shape as well as variations in reproducing measurement trials.

The existing challenge is to take the Sr K x-ray peak areas, produced by an *in vivo* EDXRF bone strontium measurement, and convert them into an absolute concentration of bone strontium. Corrected measurements will reveal concentration when the reading is extracted from a strontium doped plaster of Paris calibration line. However, meaningful information may only be extracted if the following factors are corrected for: (1) the amount of bone volume being measured, which includes bone size and shape as well as collimation and detector positioning, (2) geometrical factors such as bone to source distance, (3) overlying tissue thickness absorption of associated photons and (4) consideration for duration of measurement, detector size and source strength (Zamburlini *et al.*, 2008b). While condition (3) may be met by carrying out a tissue correction procedure, as outlined in chapter 2, correction of the remaining factors present a rather tedious task to undertake if absolute concentration of bone strontium is to be determined.

In chapter 1, the concept of using the source coherent scatter peak, as a means of signal normalization, was briefly introduced. In the case of bone lead XRF measurements made using ^{109}Cd γ -rays as an excitation source, normalization of Pb K x-rays to the coherently scattered γ -rays has produced measurements that were independent of

overlying soft tissue thickness variations and differences in bone size, in addition to the other factors mentioned above (Somervaille *et al.*, 1985). This procedure was successful because the following criteria were met: (1) the x-ray and coherent photons are produced by the same incident fluence, (2) they exhibit similar absorption in overlying soft tissue, (3) the coherent signal arises from the same region as the x-ray signal and (4) the coherent cross section is uniform about the scattering angle (Zamburlini *et al.*, 2008b). Coherent normalization has also been modeled and found to be feasible for the case of correcting XRF measurements of bone uranium using a ^{57}Co source. Although the four conditions mentioned above were not strictly met in this case, the modeled procedure was satisfactory in correcting for bone size and shape, and producing a measurement that was independent of overlying soft tissue thickness (O'Meara *et al.*, 1997).

If all variable factors are corrected using the coherent scatter peak, then the only remaining factor to adjust is the difference of the coherent scatter differential cross-sections between cortical bone and plaster of Paris material in the phantoms used to construct the calibration line.

The success of the applied coherent normalization in the case of lead may be credited, in part, to the energy of the chosen excitation source. The ^{109}Cd incident γ -ray and lead K-edge share a close proximity of energy at 88.035 and 88.005 keV respectively. This means that an incident γ -ray may only Compton scatter to a maximum angle of 3.6° and still have the necessary energy to excite the K-shell of lead to fluorescence (O'Meara *et al.*, 1997). This ensures that the primary photon flux used to excite lead will be from the incident γ -rays rather than the Compton scatter and thus satisfies criterion (1) and consequently, criterion (4). Although the Pb K_α x-ray (72.8 keV) is more than 15 keV less than the ^{109}Cd γ -ray energy, the difference in soft-tissue mass attenuation coefficients between these photons is only 7% (ICRP 23, 1975; Berger *et al.*, 2005). This implies very similar absorption of source and x-ray photons through overlying soft tissue and satisfies criterion (2). For ^{109}Cd γ -rays, the differential cross-section of the coherent scatter in bone is about 30 times greater than in soft-tissue. Therefore, the detected

coherent scatter originates primarily from bone and since bone is also the source of the Pb x-rays, criterion (3) is thusly satisfied (O'Meara *et al.*, 1997).

In contrast to a bone lead measurement, correction of a bone strontium measurement, using coherent normalization, is more complicated. The lower energies associated with strontium excitation introduce a greater proportion of coherent scatter originating from soft-tissue relative to that from bone. The coherent scatter peaks produced by the Ag K_{α} x-ray (22.16 keV) line and the ^{125}I γ -ray (35.49 keV) have been examined for the potential to provide coherent normalization for *in vivo* bone strontium measurements; these peaks were selected because they are clearly defined in an energy dispersive spectrum. For Ag K_{α} x-rays and ^{125}I γ -rays the differential scattering cross sections of bone are only 1.8 (Zamburlini *et al.*, 2008b) and 3.1 (Appendix A) times greater than that of soft-tissue, respectively. Hence, the soft-tissue contribution to total observed coherent scatter may no longer be ignored if coherent normalization is carried out on a strontium measurement.

In consideration of the criteria satisfying successful coherent normalization, we may further examine the difference between soft-tissue attenuation of the source photons to strontium x-rays. The soft-tissue mass attenuation coefficient of Sr K_{α} x-rays is almost 3 times as large as that of Ag K_{α} x-rays and more than 6 times that of ^{125}I γ -rays. This is in stark contrast to the lead measurement case using a ^{57}Co γ -ray source (122 keV) to excite Pb K_{α} x-rays (72.8 keV). Despite the 50 keV difference in photon energy, the difference in soft-tissue attenuation between these two photon energies is only about 15% (Zamburlini *et al.*, 2008b). Therefore, it is questionable if normalization to coherent scatter will correct for differences in bone size and shape in the case of *in vivo* bone strontium measurements.

Zamburlini *et al.* (2008b) performed EGS5 Monte Carlo simulations to examine the use of both the Ag K_{α} x-ray and ^{125}I γ -ray coherent scatter peaks in their ability to correct for differences of bone size and shape in an *in vivo* bone strontium measurement. The physical situation of an *in vivo* strontium measurement was simulated using cylindrical finger geometry in which soft tissue thickness and bone strontium

concentration were fixed and the bone diameter made to vary between 7 and 14 mm. Results revealed that the Ag peak normalization only partially corrected for difference in bone size but that normalization with the ^{125}I peak fully corrected for differences of bone size within statistical uncertainty (Zamburlini *et al.*, 2008b). Additional modeling was carried out to determine the soft-tissue correction and ^{125}I coherent normalization dependency on variations in both soft-tissue thickness and bone diameter. For soft-tissue thicknesses up to 3.5 mm, the coefficients of variation of the measurements were within the statistical uncertainty of the model. Only at a tissue thickness of 4.5 mm was the coefficient of variation larger than the statistical uncertainty of the model. This was determined to be a result of the increased proportion of coherent scatter coming from the overlying soft tissue. In total, normalization to the ^{125}I coherent scatter was found to correct for differences in bone size, to within 10% uncertainty, and at the same time, eliminate the need for correction of source strength and system dead time, thus, simplifying an *in vivo* strontium correction (Zamburlini *et al.*, 2008b).

In theory, if we can assume that Sr K x-ray peak normalization to ^{125}I coherent scatter effectively corrects for bone size and shape, detector-to-source geometry, positioning differences, detector dead time and source activity, then the only additional correction that would be required to quantify *in vivo* bone strontium is the soft-tissue thickness correction covered in Chapter 2. Up to this point, such a correction has been modeled but has not experimentally been applied to examine the predictions of the model. An ideal test of this situation would be to perform EDXRF measurements on a human subject and apply both the soft-tissue absorption correction and the coherent scatter normalization correction. Then, concentration of strontium in bone may be extracted directly from a plaster of Paris calibration line, provided that the difference of coherent differential cross-sections between bone and plaster of Paris is taken in to account.

In order to verify the resultant concentration estimates, an accurate bone strontium reference value from the measured subject is required. Such a reference value might be possible if a bone biopsy on a living subject could harvest a large enough bone sample to permit compositional analysis. However, this procedure is not possible due to the

discomfort it would impart to the subject. Instead, the cadaver fingers used in the analysis of imaging modalities might supplant as they would provide both a close representation of a living human and the necessary bone sample for compositional analysis. EDXRF may be performed on the cadaver fingers, with the soft tissue intact, to provide a signal in which corrections may be applied and an estimated bone strontium concentration extracted. Then, with the soft tissue removed, EDXRF may be performed on the bare bones to extract bone strontium concentration that is representative of the true concentration in bone. This will provide the necessary bone strontium reference value to compare to the measurements in which the tissue was intact. If this procedure is followed, then it might be determined experimentally whether the coherent normalization correction, in conjunction with the aforementioned soft-tissue correction, can be used adequately to extract concentrations of *in vivo* bone strontium.

Currently, a Monte Carlo based soft-tissue correction model is used to correct for absorption due to soft-tissue. If EDXRF measurements are performed on the cadaver fingers, then it might be possible to construct a finger soft-tissue correction relationship based on experimental data rather than Monte Carlo theoretical data. This would have the advantage of providing a superior representation of true finger geometry and physiology, and the subsequent effect that these have on photon attenuation. Ultimately, this may prove to be a superior soft-tissue correction model.

In performing these measurements, we might also learn more about the EDXRF system performance and its reproducibility of measuring individuals from the population. Multiple measurements made on the same finger will allow us to determine the range of concentration estimates of bone strontium that we might expect in performing these measurements *in vivo*. The accuracy of this system may be determined if we use resultant measurements and perform an accuracy calculation similar to equation E7 in chapter 2 of this manuscript.

Acquired peak information may also be used to calculate $K_{\alpha}:K_{\beta}$ ratios observed in performing such measurements on cadaver fingers. Analysis of these ratios may provide an indicator to determine if the Zamburlini Monte Carlo model is effective in correcting

for overlying soft-tissue. Additionally, a comparison of modeled ratios to observed ratios will help verify if the current EDXRF system is behaving as predicted by modeling.

3.1.2 Measurement of strontium supplementing individuals

Recently, Pejović-Milić *et al.* orchestrated a pilot study to measure bone strontium incorporation and retention in individuals who are self administering bone strontium medication. These individuals are primarily women who are suffering from bone related diseases and disorders such as osteoporosis and have begun taking strontium based supplements as a potential treatment of these diseases. The most commonly found strontium based treatment in Canada is strontium citrate, a non-prescription supplement that may be purchased in select pharmacies and health food stores. This particular medication does not require a medical prescription and participants may choose either to control their own dosage and frequency of administration or be regulated under supervision of a bone health specialist.

As yet, supplements incorporating strontium ranelate are not approved by Health Canada for treatment of osteoporosis. Given the positive effects observed in human trials with the administration of strontium ranelate in Europe, the question arises as to whether or not strontium citrate may provide an equally effective substitute. Strontium citrate and strontium ranelate are both ionic compounds in which the strontium ion is released from the salt. Hence, it is possible that both compounds exhibit similar solubility and absorption and thus, provide an equally effective delivery of strontium to the human skeleton.

The advent of this new therapy has posed many questions on the kinetics and effects of this treatment in the human body. We wish to know if there is an optimum dosage that a person should take or how long a person's treatment should last. Questions such as these may be answered if it can be determined if a person's strontium levels will continue to rise indefinitely or eventually saturate despite continued strontium supplementation. If the study may be further complemented with periodic bone mineral density scans, then the efficacy of this treatment might be determined. In this case, the

results of bone mineral density scans must be corrected for the effects that high bone strontium levels have in artificially inflating resultant bone mineral density estimates. Since strontium ($Z = 38$) is a higher Z material than calcium ($Z = 20$), it will impart a stronger attenuation of x-rays and lead to an overestimation of the bone mineral content. To determine the proportion of BMD overestimation due to the presence of high levels of bone strontium, Nielsen *et al.* (1999) proposed the following relationship:

10% overestimation per 1.0 mol/mol % Sr

$$\text{where: } 1.0 \text{ mol/mol \% Sr} = 1.0 \left(\frac{\text{moles Sr}}{\text{moles (Sr + Ca)}} \times 100\% \right)$$

Nielsen *et al.* (1999) further illustrated that this correction may be used to adjust BMD estimates from DXA measurements *in vivo*, with consideration for overlying soft-tissue included, using the following formula:

$$\text{BMD}(adj) = \frac{\text{BMD}(scan)}{1 + C \cdot \text{SrL}}$$

where: $\text{BMD}(adj)$ - is the adjusted bone mineral density

$\text{BMD}(scan)$ - is the bone mineral density determined by DXA

C - is the correction factor (= 10% or 0.10)

SrL - is the molar percentage strontium level with respect to calcium as illustrated in brackets above

Use of this correction formula would require knowledge of the strontium levels present in the individual being studied. This would be possible if quantification of EDXRF bone strontium measurements is realized. This correction was found to be applicable to strontium levels in the range of 4 - 53 mg Sr/g Ca (Nielsen *et al.*, 1999)

which is well above concentrations found in the general population. However, the lower end of this range may encompass strontium levels found in strontium supplementing individuals. Thus, this correction technique might prove useful in the adjustment of BMD scan results.

The effect of long term strontium supplementation on bone health remains in question. It is unknown if a lengthy exposure to strontium will continue to improve bone strength and density indefinitely or if it might eventually prove detrimental to process of bone mineralization, as suggested by Verberckmoes *et al.* (2004). This would effectively cause the opposite of the desired effect of the drug. As yet, it is not fully known how long the rate of clearance from the skeleton is for strontium once administration is ceased altogether. It will also be interesting to learn if this clearance is faster in individuals suffering from bone disease. An investigation involving the monitoring of bone strontium levels and kinetics of these supplementing individuals is warranted to attempt to answer these questions.

Early measurements of Sr supplementing individuals have revealed bone strontium levels to be many times greater than the general population. Figure 3.1 illustrates the strontium K x-ray signals received by non-supplementing Caucasian and Asian individuals and a spectrum from a subject who is self-administering strontium citrate. Previous studies have shown strontium levels in individuals of Asian ethnicity to be 2 to 3 times higher than those found in Caucasian individuals (Zamburlini *et al.*, 2007). However, the levels found in strontium supplementing individuals may be as much as 8-10 times greater than those in found in Caucasian individuals. The signal intensity from such a person is illustrated in figure 3.1 where the K_{α} and K_{β} peaks are much larger than non-supplementing individuals.

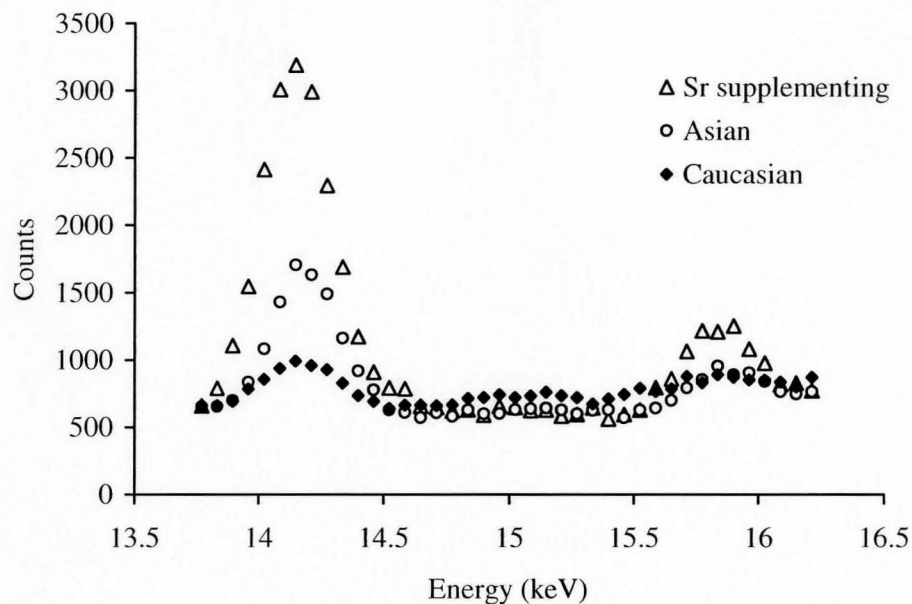


Figure 3.1: Sample spectra of non-supplementing Caucasian and Asian individuals and a strontium supplementing individual.

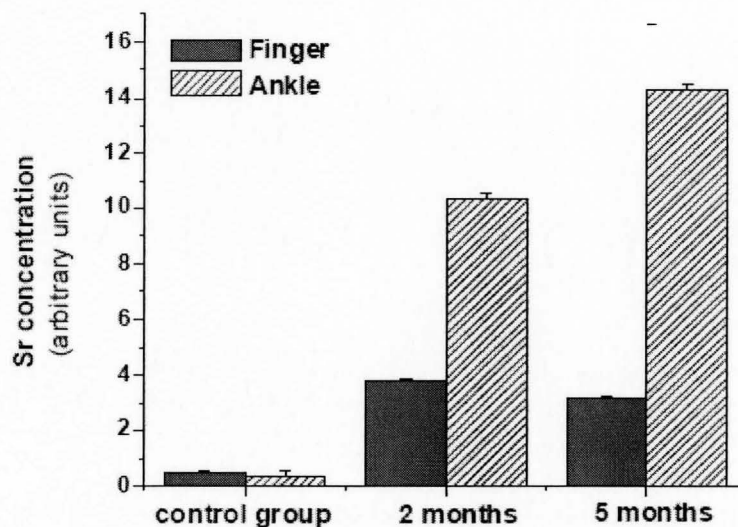


Figure 3.2: Results obtained from Sr EDXRF measurements performed on finger and ankle sites of a strontium supplementing individual (reproduced with permission)

The results of the first measurement set taken in this experiment are illustrated in figure 3.2 (Zamburlini, 2008). The first and second measurements were made two and five months respectively after strontium administration began. The concentration reading

from both measurements is higher in ankle than in finger which suggests that strontium uptake is higher in trabecular bone than in cortical bone. This is consistent with the findings of Dahl *et al.* (2001). Another interesting observation is that the concentration in the ankle increased over the three month period between the first and second measurement, however, the finger concentration did not. As yet, this effect is not fully understood and we may only speculate as to the cause. It is possible that the cortical bone strontium levels of this individual have reached a plateau or equilibrium with the rate of strontium clearance from the body.

Zamburlini (2008) has suggested further that the $K_{\alpha}:K_{\beta}$ ratio may be used to determine strontium distribution radially inward in bone. It is thought that strontium administered in concentrations exceeding that of exposure from daily diet would initially deposit on the cylindrical bone surface in direct contact with blood. Over time, it might come to reside deeper in the bone matrix through heteroionic substitution. This would constitute a higher bone Sr concentration on the bone surface than throughout the rest of the bone. If a Sr XRF measurement is performed, a higher Sr surface concentration would mean that more of the strontium K x-rays would emerge from the bone surface than from inside the bone and hence, would not be subject to attenuation by bone before leaving it. This would raise the $K_{\alpha}:K_{\beta}$ ratio above the theoretical 5.2 ratio predicted for measurements performed on evenly distributed strontium in infinitely thick bone. Hence, it can be expected that observed ratios after tissue correction will be higher in a Sr supplementing individual than those observed in the average population.

If another strontium supplementing individual may be measured multiple times, then the trends seen in figure 3.2 might be verified and more easily explained. An examination of observed $K_{\alpha}:K_{\beta}$ ratios might also indicate if supplemented strontium has been predominantly deposited on the bone surface. Ultimately, this will contribute knowledge toward the larger ongoing investigation of the incorporation and retention of strontium in human bone.

3.2 Materials and Methods

3.2.1 Strontium doped plaster of Paris calibration

In preparation for the EDXRF measurements to be performed on the cadaver fingers, a strontium doped plaster of Paris (poP), $\text{CaSO}_4 \cdot \frac{1}{2}\text{H}_2\text{O}$, calibration line was created. Seven phantoms of known added quantities of strontium were used. This was done using the Prostateed® ^{125}I brachytherapy excitation source with an approximate activity of 30 MBq and using 180° interaction geometry; an example of the detector setup and this geometry is provided in figure 3.3. EDXRF was performed on each phantom three times for 30 minute measurement periods using an Ortec® Ametek-AMT Si(Li) detector with a 16 mm diameter crystal and 220 eV resolution at 5.9 keV (User's Manual).

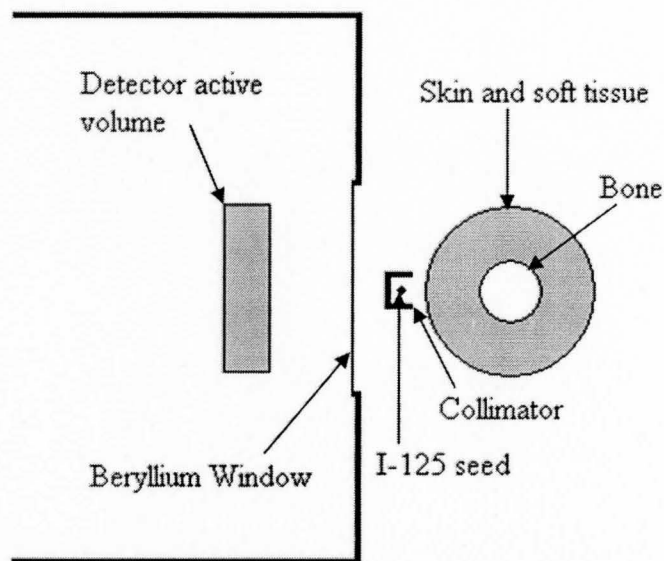


Figure 3.3: Depiction of detector and *in vivo* bone strontium measurement setup using 180° interaction geometry (side view) with axial view of human finger positioning

Pulse processing and count sorting was done using Ortec® DSPEC PLUS™ Digital Gamma Ray Spectrometer and Maestro™ software respectively. An in-house

Marquardt non-linear least squares program was used to fit the Strontium K_{α} and K_{β} peaks to extract peak area information. This program fits two Gaussian curves to these peaks and approximates the background as a slowly increasing exponential. Figure 3.4 illustrates a typical spectrum acquired in performing EDXRF on a plaster of Paris phantom, using the aforementioned conditions.

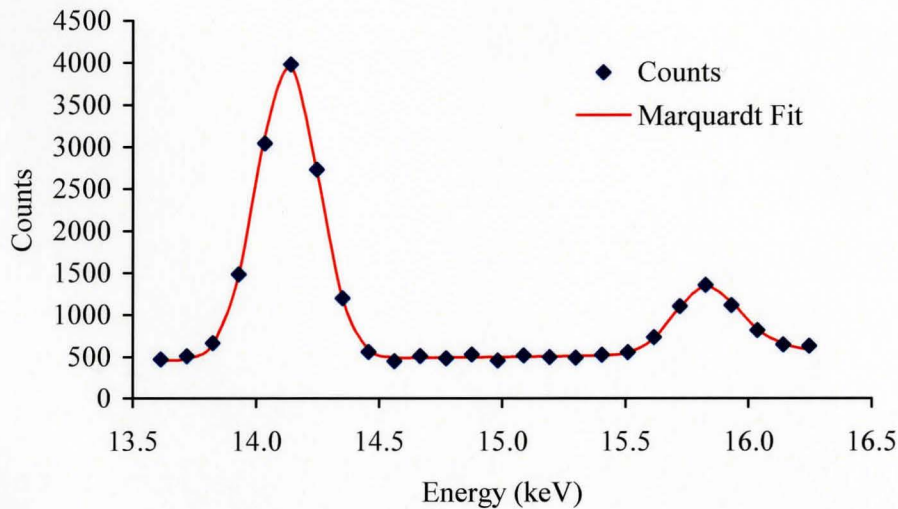


Figure 3.4: Zero strontium added plaster of Paris phantom spectra: K_{α} (left) and K_{β} (right) peaks fitted with Marquardt non-linear least squares fitting routine

Previously, a Si(Li) detector with a 10 mm diameter crystal was used to take phantom measurements. When phantom measurements were performed using this detector in the 180° geometry, Zamburlini *et al.* (2006) found that the source collimator substantially occluded the strontium photons from entering into the detector active volume, thereby weakening the observed signal. To combat this effect, an off-center collimator was designed both to approximate the effect of 180° geometry and prevent occlusion of the strontium signal. As reported in chapter 1, the combined MDL of this setup was found to be $44.6 \pm 0.6 \mu\text{g Sr/g Ca}$. The larger crystal of the 16mm diameter detector used in these experiments provides the capability of acquiring satisfactory count statistics with the source and collimator remaining on centre. Also, the larger active volume translates into an improved MDL for a finger measurement at $22.9 \pm 0.6 \mu\text{g Sr/g}$

Ca (Zamburlini *et al.*, 2007). The current setup for both a finger or phantom measurement is illustrated in both figures 3.3 and 3.5.

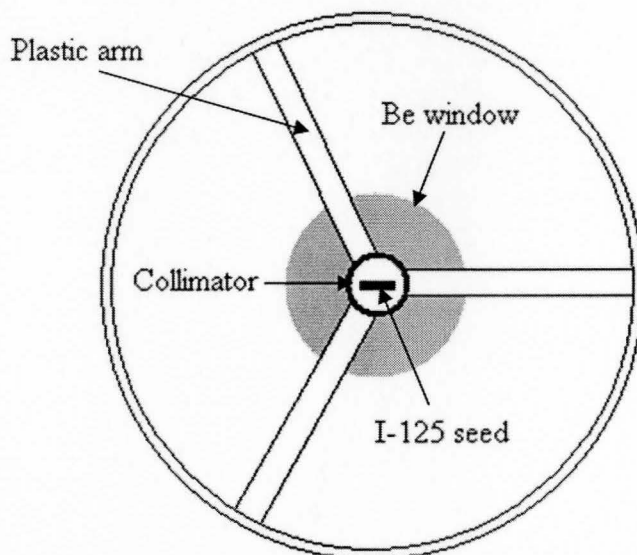


Figure 3.5: Depiction of detector and *in vivo* bone strontium measurement setup using 180° interaction geometry (head-on view)

The collimator illustrated in figure 3.5 is a hollow cylindrical piece of tungsten (W), 5 mm in diameter and is held in place by three thin plastic arms. The decision to use plastic was made because the low Z medium of plastic means that it will not absorb x-rays incident on the detector substantially. Also, low Z medium will not contribute x-rays of energies that could disrupt the strontium spectrum.

Each phantom was measured for 30 minute real-time count periods, three trials per phantom. Three trials were chosen as it was expected that the average of three would provide a better statistical estimate than one. Prior to positioning in the EDXRF system, the phantoms were removed from their vial containers. This was done to ensure that the signal would not be altered due to attenuation by the plastic covering the poP phantoms. Hence, the signal could be compared more directly to EDXRF measurements done on bare bone. Phantoms were placed approximately 3-4 mm from the edge of the collimator.

This separation was chosen so that the strontium x-rays would not be completely absorbed by the collimator as would be expected if the phantom were placed closer.

The calibration lines produced using the above said procedure provide a direct link of strontium peak area to the concentration of strontium within a phantom. Given that the lines of best fit for the points on the graph do not pass through the zero intercept point within error, it suggests that there is a degree of strontium contamination present in the un-doped poP material. A simple check for approximate contamination was made by dividing the calibration line intercept over its slope. This was done for both the K_{α} and K_{β} calibration lines and indicated that an approximate 430 $\mu\text{g Sr/g Ca}$ is already present in the poP raw material. This means that even the zero strontium added phantom will produce a peak signal representative of over 400 $\mu\text{g Sr/g Ca}$. Therefore, if a peak signal associated with a concentration less than 400 is to be analyzed, it would reveal a concentration of negative strontium content. This intuitively is not possible and so, the *in vivo* signals must be compared to only the slope of a calibration line; hence, the intercept (C_i) is artificially set to zero ($C_i = 0$). This correction is further explained in Appendix B.

3.2.2 *Ex-vivo* finger XRF measurements

3.2.2.1 *Ex-vivo* intact tissue XRF measurements

EDXRF was performed and repeated a total of ten times on each finger for one hour real time count periods. During each EDXRF measurement, the open tissue interface at the knuckle was wrapped in moistened fabric to prevent finger drying. One hour trials were chosen to obtain optimum count statistics. Each finger was oriented parallel to the face of the detector and set with a spacing of approximately 0.5-1 mm distance between the source collimator and the dorsal surface of the finger. The small spacing was chosen so that the finger could be as close to the excitation source as possible, thereby increasing the probability of strontium K x-ray collection, and at the same time, far enough away to keep the detector dead time under 50%. Average dead time was about 45%. The high dead time was not labeled a concern since it has been

generally accepted that measurements normalized to the coherent scatter peak do not require dead time correction. Fingers were promptly returned to their fluid filled storage containers at the conclusion of each trial to prevent drying.

3.2.2.2 Ex-vivo bare bone XRF measurements

The finger skin and soft-tissue were completely removed from the bones of each finger. A scalpel was used both to excise the tissue and to scrape away the periosteum sheath and synovial connective tissues that surrounded and connected each finger bone. Complete removal of any non-bone tissue was necessary to ensure that there would be no attenuation of x-rays, by soft tissues, during EDXRF measurements. All finger bones were returned to their respective, labeled containers.

EDXRF measurements were performed on middle phalanx of each finger a total of ten times per finger. The parameters used in the EDXRF measurements of the intact fingers were used in the bare bone measurements. However, the count durations were reduced to thirty minute real time trials as this was found to provide satisfactory count statistics. The bone was placed parallel to the detector face with the dorsal side facing the excitation source, as it would have faced during the intact tissue EDXRF measurements. A spacing of 3-4 mm was chosen between the bone surface and the collimator edge. This setting was chosen both to imitate the bone-to-collimator separation that would have existed during the intact tissue trials and to ensure that the collimator wouldn't completely shield all x-rays emitted from the bone. Bone width was, in some cases, as wide as the diameter of the collimator and it was thought that placing the bones too close would result in a substantial attenuation of Sr x-rays. Bone samples were stored in moistening fluid so that EDXRF measurements were carried out on wet-bone samples thus permitting all calculations to be done using well reported wet-bone composition reference values. It was found that the finger bones could lose up to 5-7% of their initial mass if they were allowed to air dry, over several days, despite being in sealed containers.

3.2.3 Analysis of the K_{α} : K_{β} ratio

Analyses of observed K_{α} to K_{β} ratios were carried out to compare with those observed in previous studies. This was done as it was expected that the K_{α} : K_{β} ratio can at least provide an indicator as to whether or not a soft-tissue correction is successfully applied. Calculations were made to determine ratios observed from EDXRF on fingers with tissue intact, ratios after soft-tissue correction and finally the ratios observed when EDXRF was performed on bare bone.

3.2.4 Strontium quantification attempts and system performance

At present, it is not conclusive if normalization to the ^{125}I (35.5 keV) coherent scatter peak is entirely effective in correcting for the various factors discussed. Attempts at quantification have been made in this chapter in which the coherent scatter normalization has been both implemented in several trials and left out in others. In the absence of coherent scatter, attempts were made to correct for differences of live time and source activity. However, information on other parameters such as bone size and positioning was not available from the measurements. At the time of the measurement taking, it was strongly believed by this author that the coherent scatter would fully correct for these factors so that changes in positioning from one trial to another would not matter or need recording.

A total of four analysis trials were made, all of which, involved correction of overlying soft-tissue using the Zamburlini Monte Carlo model introduced in chapter 2 in E2 and E3. In addition to this, the first trial utilized correction using (35.5 keV) coherent normalization. The second trial involved both coherent normalization and correction for source activity differences. The third and fourth trials involved a correction of only differences in live time and differences of live time and source activity respectively, in the absence of coherent normalization.

In order to make these corrections and then extract bone strontium concentration from calibration lines, the calibration lines also had to be corrected for corresponding

coherent normalization, live time and source decay to match the data being analyzed in each trial

Live time corrections are made by scaling the peak area observed from an associated measurement live time to the half hour (1800 s) real time measurement duration as follows:

$$(\text{Area})_{True} = (\text{Area})_{Obs} \times \frac{1800s}{\text{Live Time}}$$

where: $(\text{Area})_{True}$ - is the peak area that would be observed if detector dead time was zero

$(\text{Area})_{Obs}$ - is the observed peak area

Live time - is the total time in a measurement that the detector was live [s]

To make source activity corrections, we may theoretically need to account for time that has passed between assay date and the measurement and then account for the decay of the source during the measurement because this may affect the total observed fluorescence yield. However, in the case of ^{125}I , the 59.4 day half-life is long enough that the decay that the source experiences during a 30-60 minute measurement is very small (~0.05%). Therefore, calculations to correct for source decay are simplified to correct only for the difference between the assay date and the measurement date. Correction of both source activity and live time was done fundamentally as follows:

$$(\text{Area})_{True} = \frac{1800s}{\text{Live Time}} \times \frac{(\text{Area})_{Obs}}{I_0 \exp(-\lambda t)}$$

where: I_0 - is the initial activity of the source seed(s) used in the measurements

λ - is the decay constant of ^{125}I and

t - is time elapsed since assay date

This has the effect of correcting the peak area in terms of $[\text{MBq}^{-1}]$. This was necessary because time between tissue intact and bare bone measurements were several months apart and thus, two different iodine seed sets were used to perform these measurements, each having a different initial activity.

For the cases where the measurements are normalized to the coherent scatter peak, the difference in the coherent scatter differential cross-sections of poP and cortical bone must be calculated. To do this, knowledge of material composition, incident photon energy and cross-section form factors must be available. Coherent scatter differential cross-section information has been calculated for both poP and cortical bone for a scattering angle of 180° . The procedure used to perform this calculation is outlined in Appendix A. The procedure to extract concentration from the calibration lines and to propagate all errors associated with a strontium measurement is outlined in Appendix B.

3.2.5 *In vivo* XRF measurements of Sr supplementing individuals

A self-medicating participant, who we will call Mary, was invited for a series of *in vivo* measurements spanning over half a year. Mary suffers from osteoporosis and has been self administering strontium citrate tablets since early October, 2007. Her first measurement was carried out in early April of 2008. At the time of her first measurement, Mary had been taking three 227 mg tablets of strontium citrate a day, at mid-afternoon, on an empty stomach; she reported that she only occasionally missed taking her daily dose. Mary was measured again in early May, early June and then not again until late October. Due to an impending medical procedure, Mary discontinued taking strontium medication completely in mid August and therefore, was over 2 months off medication at the time of her last bone strontium measurement. Each measurement was performed at about 11am-1pm with her last dose taken in the afternoon of the day before.

The parameters and conditions used to measure the poP phantoms were repeated for measuring Mary. Both finger and ankle measurements lasted 30 minutes. The finger positioning of an *in vivo* measurement was done in the same fashion as that for the *ex vivo*

cadaver finger measurements. In all four of the visits, the left index finger and right ankle were measured. Visits 1 and 2 were complemented with 8 MHz ultrasound readings of the ankle and finger soft tissue sites to determine overlying soft-tissue thickness so that Zamburlini soft-tissue corrections could be applied. A portable US system of 10 MHz maximum frequency was used during visit 4. The level of accuracy (6.6%), calculated in Chapter 2, of using this frequency of ultrasound was included in the propagation of error toward the estimate of bone strontium concentration. Ultrasound imaging was done to monitor any changes in skin and soft-tissue thickness over time. In visit 3, ultrasound was not available and so the tissue thickness was estimated as the average of the first two ultrasound measurements.

Analysis for $K_{\alpha}:K_{\beta}$ ratios was carried out and calculation for quantification of these measurements was applied. This was done using the procedure outlined as trial 1 involving a soft-tissue correction and coherent normalization. This was chosen as it is the most widely known theoretical means of obtaining quantification (Nie *et al.*, 2004a).

-

3.3 Results and Discussion

3.3.1 Strontium doped plaster of Paris calibration

The phantom calibration lines were created from the poP phantom measurements. Figure 3.6 is the calibration line constructed from the observed raw peak areas. Three measurements each of the seven phantoms were used to compute the average signal for each phantom. It is the average of three trials that is plotted in figure 3.6.

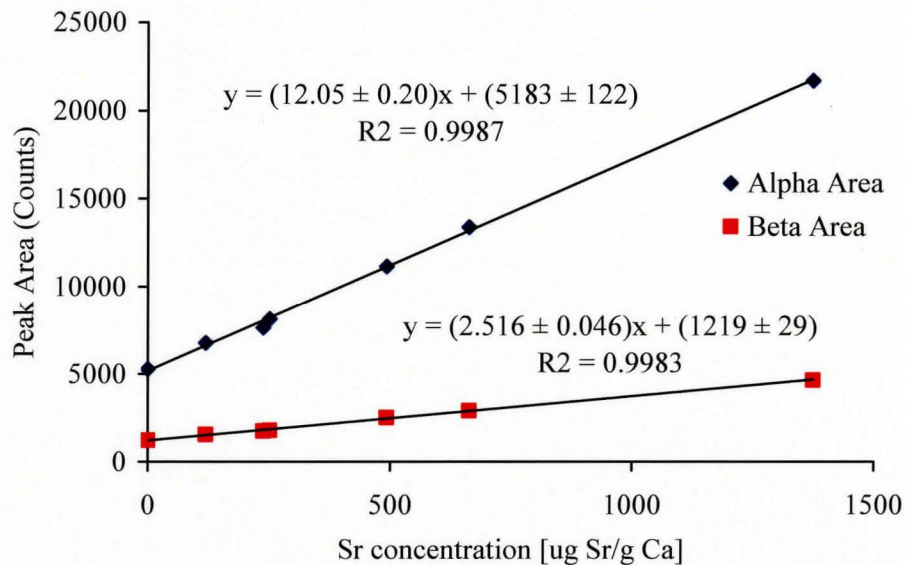


Figure 3.6: Sample plaster of Paris K_{α} and K_{β} calibration curves created from raw peak areas where each data point is the average of three measurements performed on each phantom

Minimum Detectable Limit is commonly reported as the element concentration that can produce a signal that is at least two times above the uncertainty of the signal from the zero phantom and is divided over the slope of the corresponding calibration line. This may be computed for both the K_{α} and K_{β} peaks using:

$$\text{MDL} = \frac{2 \times \sigma_{0ppm}}{\text{slope}} \quad [\mu\text{g Sr/g Ca}]$$

The MDL's calculated for both the K_{α} and K_{β} peak areas were found to be $22.5 \pm 2.3 \mu\text{g Sr/g Ca}$ and $88.5 \pm 7.9 \mu\text{g Sr/g Ca}$, respectively. The uncertainty is calculated both as the spread of multiple zero phantom measurements and the uncertainty of the calibration slope. It is not surprising that the MDL for the K_{β} is substantially higher than that of the K_{α} given that the K_{α} intensity is several times higher than the K_{β} intensity. The MDL_{α} and MDL_{β} may be pooled together to give a combined MDL using:

$$\left(\frac{1}{\text{MDL}}\right)^2 = \left(\frac{1}{\text{MDL}_{\alpha}}\right)^2 + \left(\frac{1}{\text{MDL}_{\beta}}\right)^2$$

The combined MDL calculated from the bare phantom calibration measurements is $21.8 \pm 2.2 \mu\text{g Sr/g Ca}$. This result is in agreement with the MDL reported by Zamburlini *et al.* (2007).

The strontium contamination in the zero added strontium plaster of Paris phantom has been estimated using both the K_{α} and K_{β} calibration lines. This was accomplished by dividing the y-axis intercept by the calibration slope. The K_{α} and K_{β} calibration lines suggested contamination to be $430 \pm 12 \mu\text{g Sr/g Ca}$ and $485 \pm 15 \mu\text{g Sr/g Ca}$, respectively. In taking the inverse variance weighted mean of these two values, a combined estimate of $453 \pm 9 \mu\text{g Sr/g Ca}$ is arrived at. Calculation of the inverse variance weighted mean and the associated uncertainty is illustrated in another example in Appendix B. The combined estimate of contamination is important to address because it suggests that the level of contamination may be similar or higher in concentration than that found in the skeleton of the population. If bone strontium levels are lower than contamination of the phantoms, than extraction of bone strontium concentration will require an extrapolation from the calibration curve generated above. This may be problematic if the linear relationship breaks down outside of the measurements taken. However, the high correlation between the plaster of Paris measurements, illustrated in figure 3.6, strongly suggest that this is not the case.

3.3.2 *Ex vivo* K_{α} and K_{β} properties and ratios

The relative intensities, calculated as the average of 10 signals, emerging from the 7 measured cadaver fingers, are illustrated in figure 3.7. The error bars here represent the standard deviation of the results ($K_{\alpha}/\text{coherent}$), from ten trials performed, per finger. Finger soft tissue thickness are displayed above the corresponding intensity in figure 3.7 and in successive data plots as well to elaborate that observed intensity may not necessarily be correlated to overlying soft tissue thickness as intersubject differences in bone strontium concentration are more likely to govern the strength of the observed signal. Hence, this illustrates that our system is capable of measuring differences in bone strontium concentration between individuals from the regular Caucasian population.

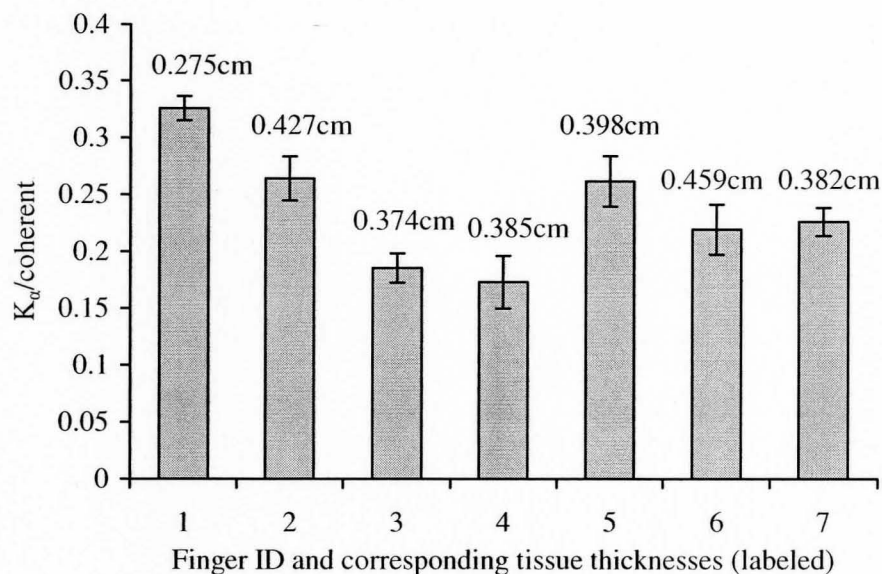


Figure 3.7: Relative strontium intensities of 7 measured cadaver fingers expressed as the K_{α} peak area normalized to the coherent scatter peak with associated overlying finger soft tissue thicknesses displayed above the corresponding intensity

The average $K_{\alpha}/\text{coherent}$ value obtained from the 7 measured cadaver fingers is 0.24. This is visibly lower than the Caucasian $K_{\alpha}/\text{coherent}$ average of approximately 0.40 from values observed by Zamburlini *et al.* (2007); living subjects were measured using

the same detection setup found in this experiment. It is possible that the values observed in this experiment are lower because the tissue thickness of the cadaver fingers is higher on average than those of the 22 individuals measured by Zamburlini *et al.* (2007). This would effectively lower the K_{α} area but produce much less of an effect on the coherent signal.

Zamburlini *et al.* (2007) have shown that the K_{α} : K_{β} ratio may be used as an indicator of the effectiveness of a soft-tissue correction. Figure 3.8 illustrates that there is a correlation between the observed K_{α} and K_{β} intensities from tissue intact *in vivo* strontium measurements. Throughout this manuscript, the t-test for correlation significance has been used. This is calculated using the regression correlation coefficient (R) for $(n - 2)$ degrees of freedom as follows:

$$t_{df=n-2} = R \sqrt{\frac{n-2}{1-R^2}}$$

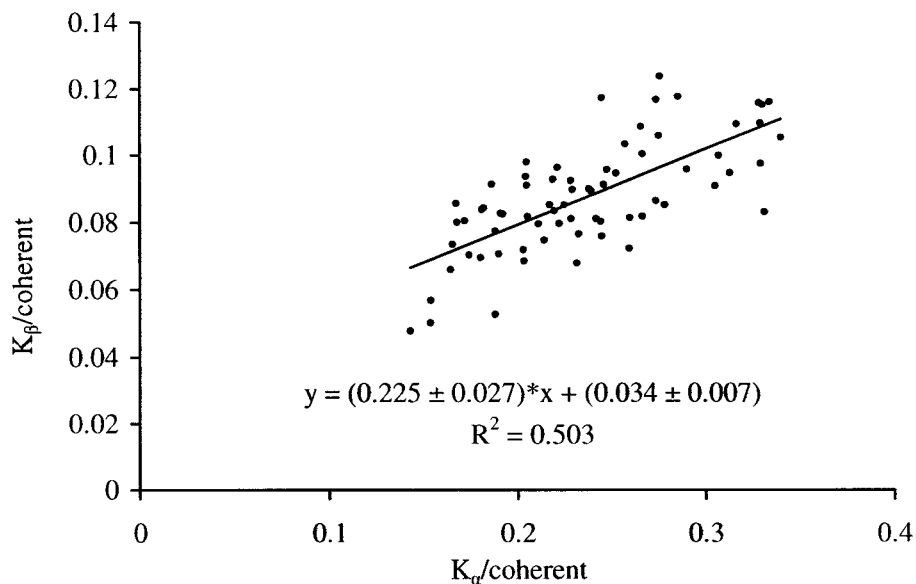


Figure 3.8: Tissue intact observed average K_{α} /coherent vs. average K_{β} /coherent

In figure 3.8, $t_{68} = 8.291$ which is a significant correlation at the 99.9% confidence level. The significance of the least squares linear fit to this data will be discussed with the data presented in figure 3.11 ahead.

The ratios observed from the 10 EDXRF trials performed on each finger are summarized in table 3.1. Tables 3.2 and 3.4 summarize the subsequent ratios observed after the Zamburlini soft-tissue correction has been applied to tissue-intact EDXRF measurements and those from bare bone measurements. The standard deviation (SD), standard error of the mean (SEM) and the full range of observed values are included to illustrate trends and variation in the observed ratios for each finger. The observed ratios are plotted in Figure 3.9.

Table 3.1: Observed $K_{\alpha}:K_{\beta}$ ratios from (N = 10) EDXRF measurements performed on cadaver fingers with tissue intact

Finger ID	Average $K_{\alpha}:K_{\beta}$ Ratio	SD	SEM	Observed Range
1	3.17	0.36	0.13	(2.84 - 3.99)
2	2.72	0.39	0.14	(2.08 - 3.26)
3	2.47	0.48	0.17	(2.04 - 3.58)
4	2.52	0.38	0.14	(1.96 - 3.07)
5	2.72	0.34	0.12	(2.23 - 3.27)
6	2.74	0.45	0.16	(2.25 - 3.59)
7	2.70	0.34	0.12	(2.18 - 3.22)
Combined Statistics	2.720	0.432	0.052	(1.96 - 3.99)

The combined statistics of all observed EDXRF trials on 7 fingers produced an average ratio of 2.72 ± 0.43 in the range of (1.96 - 3.99). Figure 3.9 illustrates the results in Table 3.1 with error bars representing the associated standard deviation of 10 EDXRF trials per finger. The uncertainties of the average ratio for each finger are large enough that each average of observed ratios overlaps with each other, within uncertainty. Although the size of the K_{α} is strongly correlated to the K_{β} , the broad range of uncertainty still indicates that the $K_{\alpha}:K_{\beta}$ ratio may not be used as a means to correct for soft tissue absorption of strontium K x-rays.

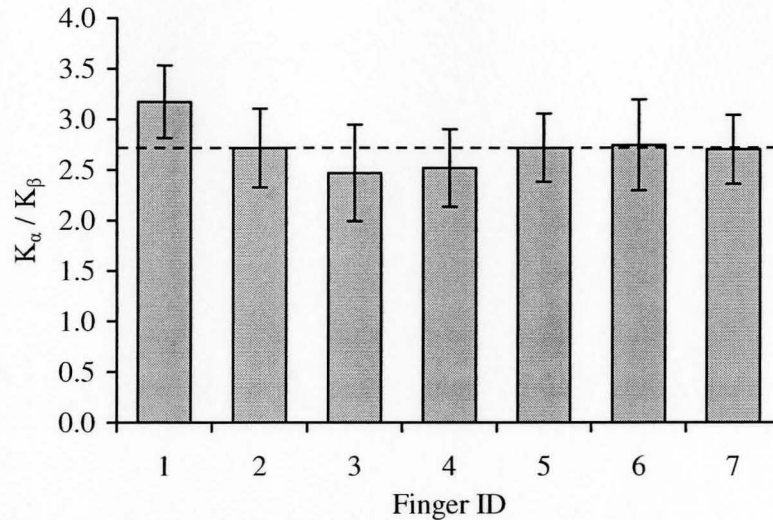


Figure 3.9: $K_\alpha:K_\beta$ ratio observed from intact cadaver fingers with error bars representing the one standard deviation in the spread of observed ratios

The dashed line drawn through the error bars in figure 3.9 represents the average ratio of 2.72 and serves to illustrate how close the observed $K_\alpha:K_\beta$ ratios are between fingers.

Previous suggestions that the $K_\alpha:K_\beta$ ratio may be used to correct for overlying soft-tissue thickness are strongly challenged given the results of the data in this manuscript. A first indicator is the broad range of observed ratios between measurements of the same finger. For example, finger 3 in table 3.1 has an observed ratio range of 2.04 - 3.58 which means that a trial with a ratio of $K_\alpha:K_\beta = 2.04$, would suggest a very large amount of overlying soft tissue thickness while a ratio of $K_\alpha:K_\beta = 3.58$ would suggest only minimal overlying soft-tissue thickness. Also, the range of 2.04 - 3.58 encompasses observed ratios from other cadaver fingers that are of different soft tissue thickness. Thus, the $K_\alpha:K_\beta$ ratio appears not to be sensitive enough to perform as an indicator of tissue thickness.

Figure 3.10 illustrates that there is only a weak correlation ($r = 0.286$) between observed $K_\alpha:K_\beta$ ratios and corresponding overlying soft-tissue thickness. It is also possible that significant correlation is observed only as a result of the contribution from the cadaver finger with 0.275 cm soft-tissue thickness. However, despite the apparent

correlation, there is still a broad range of ratios observed from measurements on individual fingers. This further supports that the $K_\alpha:K_\beta$ ratio may not be used as a means to correct for overlying soft-tissue thickness which is in agreement with the conclusion drawn by Zamburlini *et al.* (2007). Certainly, if there was a correlated pattern, the use of only seven subject cadaver fingers may not be sufficient to visualize this relationship. Additionally, the large uncertainty associated with the K_β peak area will ultimately put a large range of error on the resultant ratio. Regardless, the correlation produces $t_{68} = 2.456$ which is significant at 98% confidence.

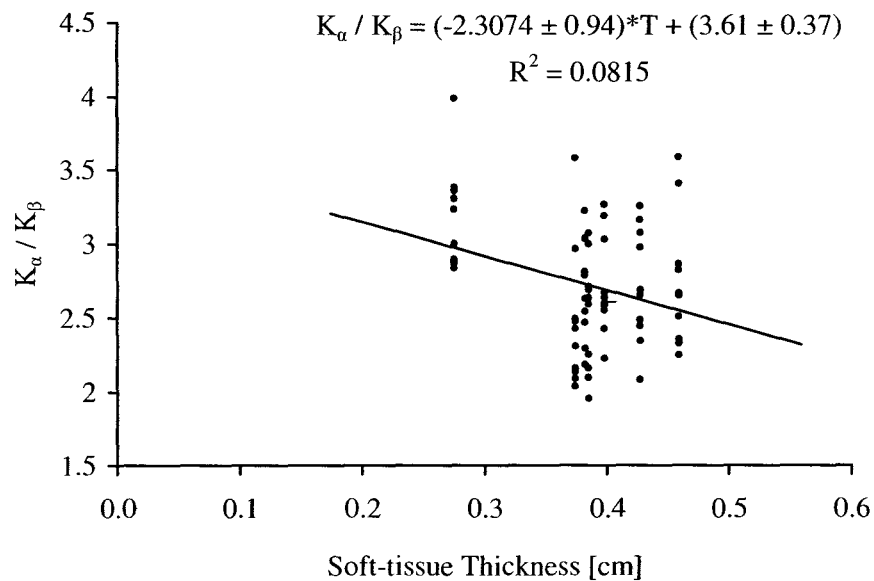


Figure 3.10: Observed K_α and K_β ratios from ten measurements performed on each of seven intact cadaver fingers plotted against corresponding soft-tissue thickness

Table 3.2 summarizes the tissue intact $K_\alpha:K_\beta$ ratios observed after soft-tissue correction using a Monte Carlo model by (Zamburlini, 2008). Although the observed ratios vary widely between 2.60 and 5.03, the average of all observed values deserves attention.

Table 3.2: Observed $K_{\alpha}:K_{\beta}$ ratios from EDXRF measurements performed on cadaver fingers with tissue intact and after soft-tissue thickness correction has been applied

Finger ID	Average $K_{\alpha}:K_{\beta}$ Ratio	SD	SEM	Observed Range
1	3.89	0.44	0.16	(3.48 - 4.89)
2	3.72	0.53	0.19	(2.85 - 4.46)
3	3.25	0.63	0.22	(2.69 - 4.72)
4	3.34	0.51	0.18	(2.60 - 4.08)
5	3.65	0.45	0.16	(2.99 - 4.38)
6	3.85	0.63	0.22	(3.15 - 5.03)
7	3.58	0.45	0.16	(2.89 - 4.27)
Combined Statistics	3.612	0.550	0.067	(2.60 - 5.03)

Monte Carlo modeling of a finger EDXRF measurement predicts a bare bone $K_{\alpha}:K_{\beta}$ ratio of 4.4 ± 0.4 (\pm SD) (Zamburlini, 2008). This suggests that if a soft-tissue correction is applied, the observed $K_{\alpha}:K_{\beta}$ ratio should be raised to this level. The average of the observed corrected ratio was found to be 3.61 ± 0.55 (\pm SD), as seen in table 2. A z-test for the difference of two means was used to verify that the Monte Carlo prediction of 4.4 ± 0.4 is significantly different than the average tissue corrected ratio of 3.61 ± 0.55 at over 99.9% confidence.

The lower observed $K_{\alpha}:K_{\beta}$ ratio suggests that either the soft tissue thickness estimated is too low, or that the coefficients of the exponential for attenuation are incorrect. To bring $K_{\alpha}:K_{\beta}$ ratio up to 4.4, the K_{α} coefficient of attenuation in the soft tissue correction model has to be strengthened or the K_{β} coefficient has to be lowered. Since it has been confirmed in chapter two that 55 MHz ultrasound measurements are providing an accurate reading of soft-tissue thickness, we may rule the first suggestion out.

Thus, it is possible that the model may not be sufficiently correcting for overlying soft-tissue. Alternatively, it had been suggested that Sr x-ray attenuation may be occurring as photons travel from the finger to the detector active volume. X-rays must pass through about 1 cm of air and through a 50 μ m beryllium window. Each of which have an effect on attenuation of photons and may cause a reduction in the observed $K_{\alpha}:K_{\beta}$ ratio. However, calculation of this attenuation indicates that attenuation of Sr K_{α} and K_{β} x-rays due to air and the Be window will only reduce the $K_{\alpha}:K_{\beta}$ ratio by 0.04%. This

does not nearly account for the full discrepancy between the observed and theoretical ratio. As yet, the disparity between the tissue corrected ratio and bare bone ratio is still a mystery.

The discrepancy between the predicted and observed ratio after soft-tissue correction is also seen in the estimates of strontium concentration predicted by the individual strontium K_α and K_β peaks. A general trend was observed that the concentration estimated by the K_β peak was higher than the K_α estimate for all seven fingers. This was observed in both bare bone and soft-tissue intact measurements after associated coherent normalizations and soft-tissue corrections were applied. To test the claim that the concentration of the average finger K_β is significantly higher than the average K_α ($\mu_\beta > \mu_\alpha$), the following t-statistic was used individually for each finger:

$$t = \frac{(\bar{K}_\beta - \bar{K}_\alpha) - (\mu_\beta - \mu_\alpha)}{\sqrt{\frac{(n_\alpha - 1)s_\alpha^2 + (n_\beta - 1)s_\beta^2}{n_\alpha + n_\beta - 2} \left(\frac{1}{n_\alpha} + \frac{1}{n_\beta} \right)}}, \text{ d.o.f.} = n_\alpha + n_\beta - 2$$

where, variances, s_α^2 and s_β^2 , of the respective K_α and K_β peaks, for each finger, were calculated using the spread of ten trials so that: $n_\alpha = n_\beta = 10$. Table 3.3 summarizes the average strontium concentrations estimated by the K_α and K_β peaks and indicates the overall significance found from agreement of each calculated finger t-statistic. Given that concentrations were extracted using the K_α and K_β lines from the same plaster of Paris phantoms, there should be no significant difference between average concentrations estimated by the *ex vivo* K_α and K_β peaks, i.e.: ($\mu_\beta \leq \mu_\alpha$).

Table 3.3: Comparison of average intact finger strontium concentration estimates from K_α and K_β peaks, after tissue correction and coherent normalization

Finger	Tissue Intact, $\mu\text{g Sr/g Ca}$		Bare Bone, $\mu\text{g Sr/g Ca}$	
	\bar{K}_α Conc.	\bar{K}_β Conc.	\bar{K}_α Conc.	\bar{K}_β Conc.
	($\pm s_1$), $n_1 = 10$	($\pm s_2$), $n_2 = 10$	($\pm s_1$), $n_1 = 10$	($\pm s_2$), $n_2 = 10$
1	452 \pm 15	560 \pm 63	556 \pm 30	596 \pm 47
2	633 \pm 46	823 \pm 111	647 \pm 24	707 \pm 73
3	367 \pm 26	553 \pm 95	510 \pm 15	565 \pm 52
4	356 \pm 48	520 \pm 106	470 \pm 16	533 \pm 58
5	565 \pm 48	748 \pm 108	745 \pm 25	830 \pm 51
6	589 \pm 59	740 \pm 86	717 \pm 39	827 \pm 77
7	461 \pm 25	619 \pm 53	710 \pm 22	779 \pm 46
Average	489 \pm 109	652 \pm 140	622 \pm 106	691 \pm 131
% Difference	33.3 % ($p < 0.0005$)		10.5 % ($p < 0.025$)	

Table 3 illustrates that for all fingers, in both bare bone and tissue intact measurements, the K_β estimate of concentration is significantly higher than that of the K_α . This strongly suggests the presence of an external factor that is causing the area of the K_β peak to become inflated. This discrepancy is appreciably larger in the tissue-intact measurements, at 33.3%, than found in the bare bone measurements, being only 10.5%. This is an interesting result because it implies that whatever is causing the difference is not solely linked to the presence of overlying soft-tissue but may have some dependency on it still.

One possible reason to explain why the K_β peak appears inflated would be if additional photons, of energy identical to Sr K_β x-rays, but from a different source, are accumulating in the spectrum. In this case, it must be considered that the human body is a store house of many different trace elements. If a trace element has a high Z or one similar in magnitude to strontium, then it may respectively emit L x-ray or K x-ray radiation at energies similar to strontium K_β x-rays. Artifact photons would not be discriminated by the EDXRF measurement system and would be consequently counted as though they were a strontium K_β photon. If said elements were present in both bone and soft-tissue, then this might explain why a difference is seen in bare bone measurements and an even stronger difference is seen in tissue-intact measurements.

However, more research would be required to either verify or rule out this possibility. Consideration would have to be given to the trace element composition in human soft-tissue and bone in order to find elements that could produce x-rays of this energy. It must also be determined if these elements exist in great enough concentrations to have a detectable effect on the observed peak area.

If the problem is not an artifact due to non-strontium photons, then it is possible that this may be an artifact of the curve fitting algorithm used to extract peak area. The same program and algorithm is used to extract peak area for poP phantoms, bare bone and tissue intact spectra. In the case of the tissue intact spectra, a greater proportion of Ag x-ray Compton scatter appears to the right of the Sr K_{β} x-ray peaks than in either the bare bone or plaster of Paris spectra. This may be attributed to the additional scatter from the overlying soft-tissue and is visualized as a steeper rising slope leading up to the Compton peak from the right side tail of the K_{β} peak.

The algorithm used in this experiment is designed so that the background under the Sr x-ray peaks is estimated using only the background between the Sr K_{α} and K_{β} peaks; the background on the right side of the K_{β} peak is not considered. This assumption may be limited in that it assumes the background to the right of the K_{β} peak is a direct continuation of the same slowly increasing exponential background to the left side of the K_{β} peak. This would have the effect of fitting the right side tail end of the K_{β} peak such that it terminates at a location lower than the true background of the spectrum. This would suggest a larger K_{β} peak area than the true area and would be a source of peak area inflation. This possibility could be examined further by incorporating the background of both sides of the K_{β} peak and comparing the resultant areas to those predicted by the formerly used algorithm.

Lastly, it is also possible that if the coefficients of the tissue correction model are not completely correct, then this might explain why the tissue intact K_{β} concentration estimates are proportionally so much higher than the bare bone case.

The K_{α} : K_{β} ratios observed coming from bare bone were examined in a fashion similar to the tissue corrected ratios in table 3.2. The results of EDXRF measurements

performed on bare bone further provide a comparison between model and experimental predictions. The bare bone $K_{\alpha}:K_{\beta}$ ratios are displayed in table 3.4.

Table 3.4: Observed $K_{\alpha}:K_{\beta}$ ratios from EDXRF measurements performed on cadaver fingers bare bones

Finger ID	Average $K_{\alpha}:K_{\beta}$ Ratio	SD	SEM	Observed Range
1	4.46	0.29	0.104	(3.87 - 4.35)
2	4.40	0.39	0.137	(3.67 - 4.93)
3	4.33	0.36	0.126	(3.88 - 4.99)
4	4.25	0.47	0.168	(3.51 - 5.33)
5	4.29	0.22	0.077	(3.95 - 4.56)
6	4.17	0.42	0.149	(3.57 - 4.85)
7	4.35	0.24	0.087	(3.86 - 4.72)
Combined Statistics	4.321	0.350	0.037	(3.51 - 5.33)

The observed ratios have a combined average of 4.32 ± 0.35 in the range of (3.51 – 5.33). Although the observed range varies widely, the combined average is well within the modeled theoretical range of 4.4 ± 0.4 (\pm SD). The agreement between theoretical and experiment further support the implication that more work is required to determine why the tissue corrected ratio is significantly less than the modeled bare bone ratio of 4.4 ± 0.4 .

Figure 3.11 illustrates the correlation between the K_{α} and K_{β} ratios observed from EDXRF measurements performed on bare finger bones. It is notable that trend for lower uncertainties, corresponding to bare bone measurements, manifests as an improvement of the correlation of the data in Figure 3.11 in comparison to the tissue intact K_{α} to K_{β} ratios observed in figure 3.8. The range of uncertainty of the combined average ratio of bare bone measurements is 8.0% which is much smaller than the 16% spread associated with the ratios from intact tissue measurements. This is likely because the soft-tissue imparts a greater level of uncertainty in a ratio calculation by reducing the quality of the K_{β} count statistics through photon absorption.

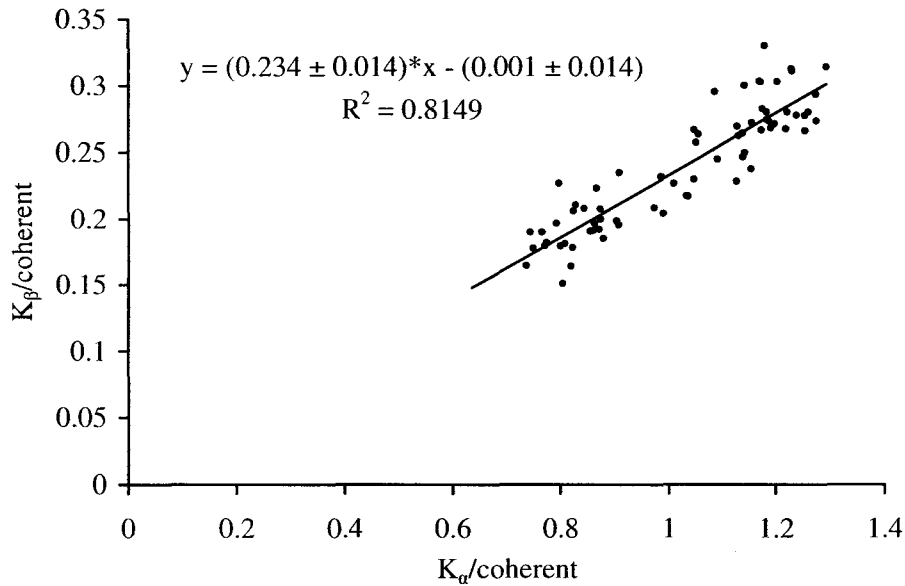


Figure 3.11: Observed K_β vs. K_α ratios from bare bone EDXRF measurements

It is interesting to note that the bare bone K_β vs. K_α slope of 0.234 ± 0.014 in figure 3.11 is within error of the tissue intact K_β vs. K_α slope of 0.225 ± 0.027 in figure 3.8. Taking the inverse of each of these produces $K_\alpha:K_\beta$ ratios 4.28 ± 0.25 and 4.44 ± 0.54 for bare bone and tissue intact readings respectively. Both of these ratios are in agreement with the modeled ratio of 4.4 ± 0.4 . One striking difference between the tissue intact and bare bone slopes is the value of the y-axis intercept. In the plot of bare bone $K_\alpha:K_\beta$ ratios, the slope intercept passes through zero within uncertainty. This is not the case in the tissue intact plot of figure 3.8 as it is observed that the linear fit passes through 0.034 ± 0.007 on the K_β axis. This was a trend also observed by Zamburlini *et al.* (2007) who suggested that an uneven radial distribution of strontium in bone might cause this behaviour. This idea was resolved when Zamburlini (2008) verified the presence of an even radial distribution of bone strontium in *ex vivo* finger bones. This further indicates that some additional factor is inflating the reading of the K_β peak in the soft-tissue case but is not affecting the K_α peak area. This is strongly suggested given that the intercept of the K_β does not pass through zero.

3.3.3 Creation of an experimental soft-tissue correction relationship

In chapter 2, a tissue correction relationship, created using modelling, was introduced. This was created by Zamburlini using the EGS5 Monte Carlo program and provided a theoretical estimation of the relationship of soft-tissue to the absorption of both ingoing photons and to a greater extent, outgoing strontium x-rays. This section summarizes an attempt to create a similar tissue correction relation, however, one that is based on the experimental data at hand. The Zamburlini tissue correction model required knowledge of the initial intensity from bone (I_0), the final intensity after passing through overlying soft tissue (I) and overlying tissue thickness (T). These parameters may be filled using the data observed from the EDXRF measurements, where T is the tissue thickness estimated by the most accurate modality, 55 MHz ultrasound, I is the intensity of strontium x-rays measured with cadaver finger soft-tissue intact and I_0 is the intensity from EDXRF measurements performed on bare bone. Both I and I_0 were normalized to 1800s live time.

The ratio of tissue intact to bare bone intensities was plotted as a function of tissue thickness and is displayed in figure 3.12. A semi logarithmic plot was used to extract a linear relationship. Figure 3.12 A) shows the ratio of soft-tissue to bare bone K_α intensities and B) shows that of the K_β intensities.

With all 70 data points plotted, the relationships in both 3.12 A) and 3.12 B) are significantly correlated at the 99.9% confidence level having t-scores of $t_{68} = 6.884$ and $t_{68} = 4.144$, respectively. Correlation is not entirely apparent given the lower R^2 values observed. However, if we plot only the average (I/I_0) of ten trials per finger, then the correlation is more apparent and hence, a more clearly visible relationship between ratio of intensities and tissue thickness is obtained. This collection of averages is plotted in Figure 3.13 for both the K_α and K_β ratios of observed intensities.

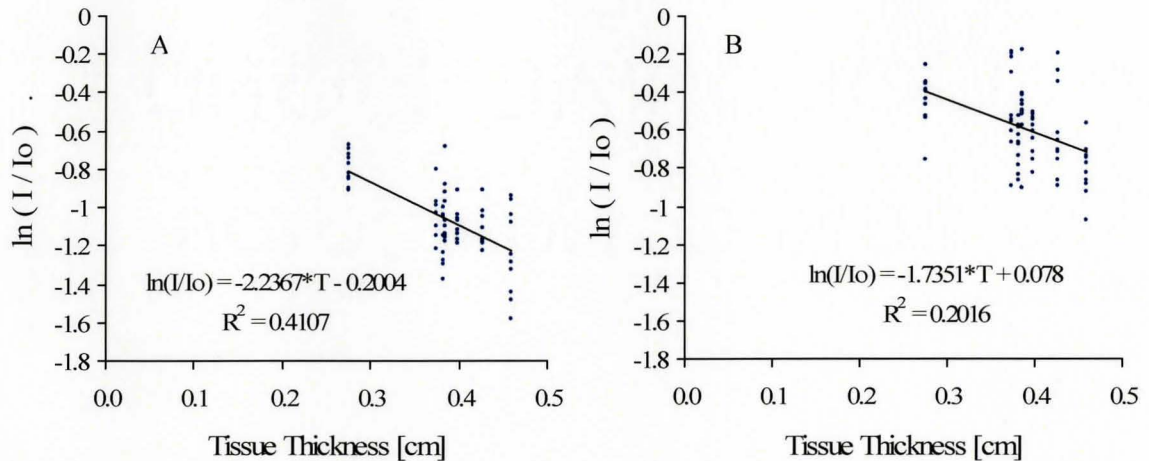


Figure 3.12: Semi-logarithmic plot of the ratio of all observed tissue intact intensities to bare bone intensities for K_α (A) and K_β (B), corrected for live time differences and plotted against overlying tissue thickness

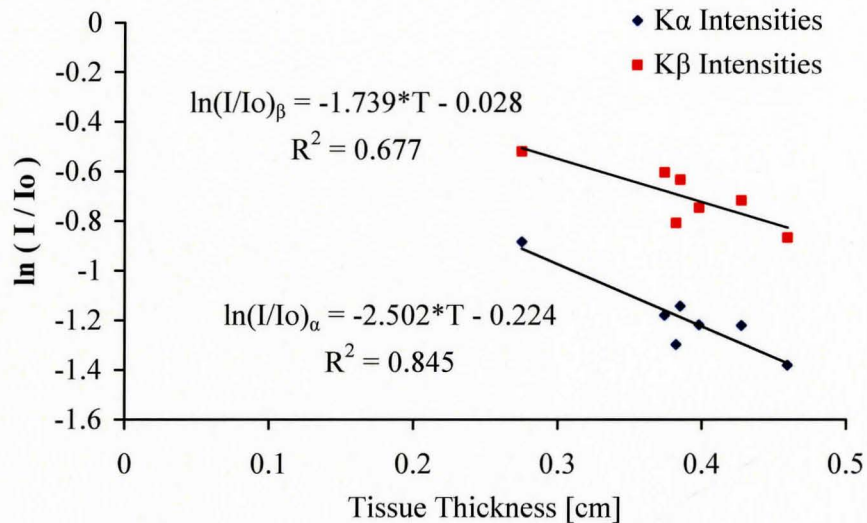


Figure 3.13: Experimental model of x-ray intensity on tissue thickness using EDXRF data from 7 cadaver finger measurements

In figure 3.13, the correlation of the ratio of observed intensities to tissue thickness is stronger in the K_α data at $R = 0.92$ than in the K_β data at $R = 0.82$. However, despite an improvement in the apparent correlation to the data, the t-scores are marginally diminished in comparison to those from figure 3.12 given that only 5 degrees of freedom

are used. The K_{α} tissue-correction model t-scores is $t_5 = 5.227$ which is significant at 99% confidence. Although the fit of the K_{β} model is marginally worse than the K_{α} , it is still significantly correlated at the 95% confidence level, with $t_5 = 3.237$. Thus, we can be quite confident that the K_{β} ratios of intensity, produced using the K_{β} signal, follow a logarithmic relationship similar to the K_{α} relationship. However, this relationship was only found after many measurements of the same finger were taken. The low count statistics and high associated statistical error of the K_{β} peaks are the likely causes of the reduced level of correlation.

The linear relationships derived from the data plotted in figure 3.13 are illustrated in E8 and E9 below. Uncertainties of the coefficients of the slope and intercepts are determined through regression analysis.

$$K_{\alpha}: \quad \ln\left(\frac{I}{I_0}\right) = (-2.50 \pm 0.48)T - (0.22 \pm 0.19) \quad (E8)$$

$$K_{\beta}: \quad \ln\left(\frac{I}{I_0}\right) = (-1.74 \pm 0.54)T - (0.03 \pm 0.21) \quad (E9)$$

Recalling that the theoretical Zamburlini models predicted K_{α} and K_{β} soft-tissue absorption of (E2) and (E3), we may directly compare the experimental models obtained in this work.

$$K_{\alpha}: \quad \ln\left(\frac{I}{I_0}\right) = (-3.58 \pm 0.04)T + (0.156 \pm 0.006) \quad (E2)$$

$$K_{\beta}: \quad \ln\left(\frac{I}{I_0}\right) = (-2.86 \pm 0.04)T + (0.162 \pm 0.006) \quad (E3)$$

A simple comparison of the slopes of the theoretical to experimental models will show that they do not match within uncertainty. The experimental model calculated in this work for both K_{α} and K_{β} Sr x-ray absorption predicts less x-ray attenuation per unit

tissue thickness relative to the theoretical model by Zamburlini. In figure 3.14, the experimental data points are plotted along side the theoretical relationships predicted by the models.

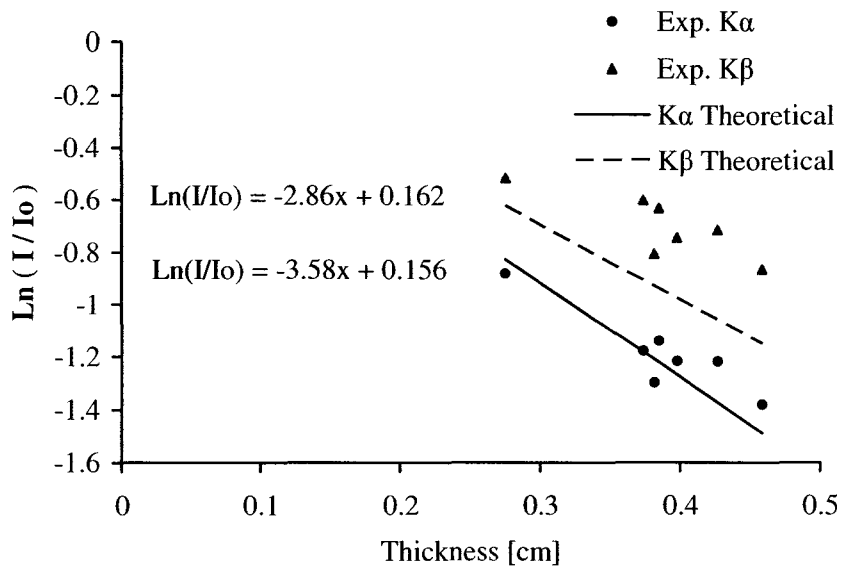


Figure 3.14: Experimental model data plotted with trend lines of the theoretical relationship data

Aside from the difference in slope coefficients in the K_α case, the relationships of experimental and theoretical are in partial alignment. In the case of the K_β relationships, the experimental data are entirely offset from the theoretical model and suggests that the two do not agree.

The ratio of the K_α coefficients between the theoretical model ($\mu_\alpha(T)$) to the experimental model ($\mu_\alpha(E)$) was calculated to be $(\mu_\alpha(T): \mu_\alpha(E)) = 1.25 \pm 0.06$. Similarly, the ratio of the K_β coefficients between the theoretical and experimental is $(\mu_\beta(T): \mu_\beta(E)) = 1.44 \pm 0.23$. Both ratios overlap within range of their respective uncertainties and suggest that these two ratios are not different from each other. Thus, it is possible that both experimental K_α and K_β coefficients are smaller than the theoretical coefficients as a result of a shared influential factor. The proportion of decrease of the slope coefficients from that of the theoretical to experimental model was also calculated. Relative to the

theoretical model, the experimental K_{α} and K_{β} slope coefficients saw a slope reduction of $30 \pm 13\%$ and $39 \pm 18\%$ respectively. Both increases are in agreement with each other and indicate that both K_{α} and K_{β} were estimated differently, by the same influencing factor.

Since this effect is manifest not just in the K_{β} model, but also in the K_{α} model, it is likely that the cause for this discrepancy is something other than poor count statistics of the K_{β} peak area. It may simply be the case that not enough data points have been used to produce an appropriate representation of an experimental tissue-correction relationship. It is difficult to make conclusive remarks on the observed experimental relationship given that only 7 data points are used to define the observed linear relationships. Also, there is question as to whether or not the y-intercept of the K_{α} least-squares line passes through zero as it theoretically should. The intercept and uncertainty, at one standard deviation, is 0.22 ± 0.19 giving a range (0.03, 0.41) which does not encompass zero. However at two standard deviations, the range increases to (-0.16, 0.60) which includes the possibility of passing through zero. Thus, we cannot conclude that the slope does or does not pass through zero.

Ultimately, this comparative analysis between the data constructed experimental models and the Monte Carlo theoretical models indicate that the two do not agree with each other. This might be further explained given that most of the data points are created using fingers that on average, have thicker overlying soft-tissue than the general population. This may have the effect of degrading the resultant count statistics obtained from bone Sr EDXRF measurements done with soft-tissue intact. The shape of the bone may also play a role in this disparity. The Monte Carlo model correction equations were constructed based on bone of perfect cylindrical shape. A true finger bone is only partially cylindrical in the centre of the bone and widens at the ends where the knuckles would be.

The compositional differences that exist between the fingers of living humans and fingers from embalmed cadavers may also play a role in affecting the observed attenuation which may affect the resultant experimental plotted slopes. Additionally,

cadaver fingers are stored in a preservation fluid consisting of 92% water which could introduce significant water content to the overall soft-tissue composition and consequently affect attenuation.

Future work would be to obtain more cadaver fingers to boost the sample size used to construct the experimental model. Additionally, index fingers with smaller overlying tissue thickness, such as 2-3 mm, would be beneficial in an effort to provide data points in the low end of the tissue thickness scale. If this could be carried out, then more conclusive statements of the discrepancy between experimental and theoretical models might be made. This might even allow for a proper experimental correction relationship to be constructed which might be used in favour of the theoretical model.

3.3.4 Attempts to quantify *ex vivo* bone strontium using Monte Carlo soft-tissue correction model

This section presents the results of an attempt to quantify bone strontium in human cadaver fingers using the Zamburlini soft tissue correction model and the four correction trials outlined above. In each trial, a comparison of EDXRF measurements on bare bone is made to measurements on fingers tissue intact. Table 3.5 summarizes the results of trial 1 in which both tissue correction and coherent scatter normalization have been used. Uncertainties presented with the data represent the larger of either the average propagated uncertainty, of the full quantification process outlined in Appendix B, or the standard deviation of the ten measurements per finger. Figure 3.15 illustrates these results and provides overlying soft-tissue thickness readings of each cadaver finger above the bars of the histogram. The error bars represented in figures 3.15 to 3.18 also represent the larger of either the propagated uncertainties or the standard deviations spread of the ten EDXRF trial results. A calculation of the difference in coherent scattering differential cross section between plaster of Paris and cortical bone for 35.5 keV reveals that the cross section is 1.4 times greater for plaster of Paris. This has been taken into account for corrections where coherent normalization has been used.

The EDXRF measurements on the fingers with tissue intact are compared directly to the measurements performed on bare bone in terms of concentration of strontium per gram of calcium and finally per gram of wet bone using a calcium/wet bone proportion of 0.225 (Woodard and White, 1986). The average of all trials presented is meant to illustrate an estimate of the average human strontium concentration where the uncertainty is the standard deviation spread of all 70 measurements.

Table 3.5: Comparison of tissue intact to bare bone EDXRF quantifications using soft-tissue correction and coherent normalization

Finger ID (N = 10)	Bare Bone	Tissue Intact	Percentage Difference, %
	Strontium Conc., $\mu\text{g Sr/g Ca}$	Strontium Conc., $\mu\text{g Sr/g Ca}$	
1	563 \pm 24*	471 \pm 28	-16.2
2	660 \pm 26	671 \pm 48	1.7
3	518 \pm 23	393 \pm 33	-24.1
4	479 \pm 21	379 \pm 53*	-20.8
5	764 \pm 31	598 \pm 52*	-21.6
6	736 \pm 30*	616 \pm 52	-16.3
7	724 \pm 30	487 \pm 37	-32.8
Average (\pm SD) (all trials)	635 \pm 110 ($\mu\text{g Sr/g Ca}$) 143 \pm 25 ($\mu\text{g Sr/g wet bone}$)	516 \pm 113 ($\mu\text{g Sr/g Ca}$) 116 \pm 25 ($\mu\text{g Sr/g wet bone}$)	-18.6

* standard deviation of spread used instead of propagated error (N = 10)

The average percentage propagated uncertainty associated with a complete soft-tissue and coherent scatter correction and quantification of 70 EDXRF trials was found to be 7.65 % in the range of (5.73 to 9.40%). This calculation includes the propagated errors of the following factors: the Monte Carlo tissue model slope and intercept, tissue thickness estimation from imaging, peak area statistics from Sr K x-rays and coherent scatter and calibration slope. In this case, tissue correction was accomplished using 55 MHz ultrasound having an inherent 3.2% uncertainty. The uncertainty with the Zamburlini tissue correction model was also factored in. Uncertainties associated with bare bone measurements are smaller as the error in the Monte Carlo correction model and the tissue thickness estimate do not apply. It was found that the propagated uncertainty

was similar in magnitude to the spread of values at one standard deviation for ten trials. The procedure used to arrive at the values in table 3.5 is explained in Appendix B.

The histograms in figure 3.15 show that the estimations using soft-tissue correction of tissue intact measurements is on average about 18.6% lower, of range (-32.8 to 1.7 %), in concentration than bare bone measurements. Both are calculated using coherent normalization. Only in finger 2, did the bare bone to tissue measurements match within uncertainty but this may be due to chance alone. The reason behind this overall discrepancy may be the result of not taking into account the soft-tissue absorption of the incoming and outgoing 35 keV coherent scatter photons. Soft-tissue absorption of these photons is small but cannot be considered negligible. For example, a rudimentary calculation using the coefficients from table 2.1 indicates that 4.5 mm of overlying skin will attenuate the 35 keV coherent scatter signal by upwards of 14%. However, this absorptive effect does not occur in the case of bare bone or phantom normalization. Hence, this may account for the disparity of directly comparing bare bone to tissue-intact, coherently normalized measurements.

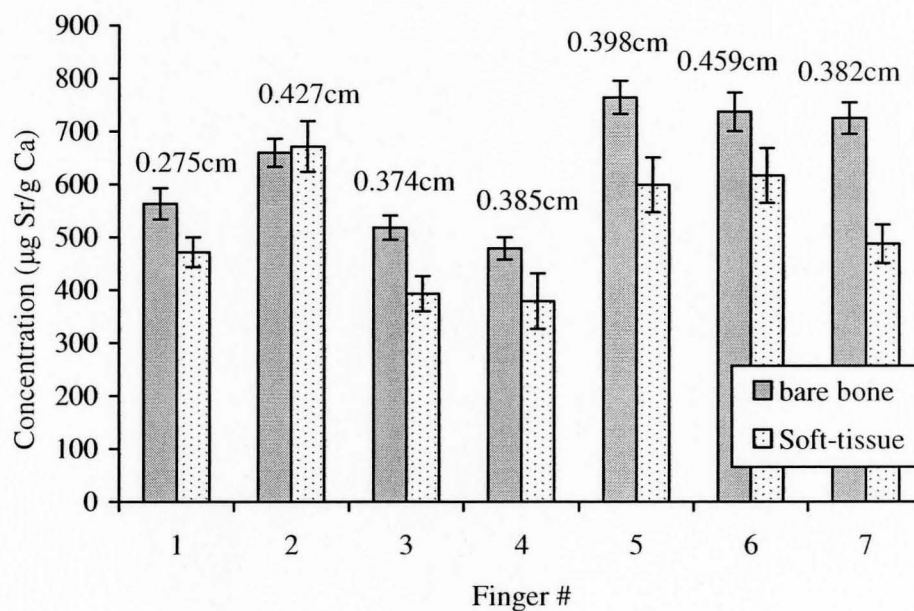


Figure 3.15: Comparison of tissue intact to bare bone EDXRF quantifications using soft-tissue correction and coherent normalization

In Chapter 2, the accuracy of the examined imaging modalities had to be calculated in the absence of a reference soft tissue thickness value. This was done by using the tissue thickness readings of all other modalities to approximate a true tissue thickness. Given that there is no reference value to compare the quantification results presented in this section, the method used in chapter 2 was implemented to examine the accuracy of the *in vivo* strontium EDXRF system used in this experiment. This was done by summing the square of the differences between a single measurement of a finger and the average computed by the other 9 trials for that finger. In this case however, instead of having 6 imaging modalities estimating a parameter, we have 10 ($j = 1..10$) EDXRF trials estimating a concentration. So a computation of accuracy is a calculation of the accuracy received for just one trial on all seven fingers. Since each trial is symmetrical with the next, the final accuracy of the system is obtained by taking the average of all 10 Accuracy readings.

$$\text{Accuracy}_{\text{TRIAL}(j)} = \left[\frac{\sum_{i=1}^{7 \text{ fingers}} \left(\text{Mod}_{i,j} - \left(\frac{\sum_{k=1, k \neq j}^6 \text{Mod}_{i,k}}{N_k - 1} \right) \right)^2}{N_i} \right]^{1/2} \quad [\mu\text{g Sr/g Ca}]$$

$$\text{Accuracy}_{\text{EDXRF System}} = \frac{1}{10} \sum_{j=1}^{10} \text{Accuracy}_{\text{TRIAL}(j)}$$

The Accuracy of this system, as estimated using the coherent scatter and soft tissue correction and coherent scatter normalization, is 11.3 % relative uncertainty. This value represents the expected level of uncertainty associated with using this particular correction procedure and EDXRF system to quantify an *in vivo* bone strontium measurement. As was the case in the accuracy determined for the imaging modalities in

chapter 2, this value represents an upper limit to the uncertainty in performing a measurement.

When creating calibration lines using strontium doped plaster of Paris phantoms, the method of coherent normalization has been used repeatedly to improve the correlation of the data to the line of best fit. This is so because it effectively corrects for differences in phantom geometry and positioning. In turn, it is reasonable to assume that it will effectively correct for the same said differences in measuring and quantifying bare finger bones. Thus, the quantification values reported in table 3.5 under bare bone strontium concentrations may be considered our best estimate of true bone strontium concentration in the human population. In this case, the average human bone strontium concentration was taken from 7 human cadaver fingers and is estimated to be $635 \pm 110 \mu\text{g Sr/g Ca}$ or $143 \pm 25 \mu\text{g Sr/g wet bone}$.

Table 3.6 represents the second correction trial where soft-tissue correction, coherent normalization and correction for source activity differences have been applied. It was found that the average bare bone strontium concentration estimated using this method did not drastically change from the amount suggested using the first correction trial. Table 3.5 reports a combined average bare bone concentration (\pm SD) of $609 \pm 116 \mu\text{g Sr/gCa}$ from trial 2 and is in close agreement with the estimate from trial 1 being $635 \pm 110 \mu\text{g Sr/g Ca}$. Hypothesis testing using a student t-test indicates that there is not enough evidence to suggest that the combined average bare bone concentration estimates, using correction trials 1 and 2, are statistically different from each other at the 80% confidence level. However, the differences between these trials are always in the same direction for all 7 fingers. All bare bone measurements in trial 1 are higher than in trial 2, by an average $32 \pm 7 \mu\text{g Sr/g Ca}$ difference. This suggests that there is something small but systematic that is affecting the final estimates of concentration as a result of taking differences of source activity into account.

Table 3.6: Comparison of tissue intact to bare bone EDXRF quantifications using soft-tissue correction, source activity correction and coherent normalization

Finger ID (N = 10)	Bare Bone	Tissue Intact	Percentage Difference, %
	Strontium Conc., $\mu\text{g Sr/g Ca}$	Strontium Conc., $\mu\text{g Sr/g Ca}$	
1	536 \pm 42*	539 \pm 51*	0.5
2	627 \pm 53*	765 \pm 63*	21.9
3	498 \pm 48*	450 \pm 43*	-9.5
4	460 \pm 37*	437 \pm 80*	-4.9
5	734 \pm 60*	690 \pm 75*	-6.0
6	709 \pm 71*	715 \pm 100*	0.8
7	697 \pm 66*	565 \pm 49*	-19.0
Average (\pm SD) (all trials)	609 \pm 116 ($\mu\text{g Sr/g Ca}$) 137 \pm 26 ($\mu\text{g Sr/g wet bone}$)	594 \pm 138 ($\mu\text{g Sr/g Ca}$) 134 \pm 31 ($\mu\text{g Sr/g wet bone}$)	-2.3

* standard deviation of spread used instead of propagated error (N = 10)

The average percentage propagated uncertainty of all 70 quantification trials using the tissue correction with live time normalization on intact tissue measurements was 7.58 % with a range of (5.63 to 9.33 %). System accuracy was calculated for using this correction method and found to be 14.3% relative uncertainty which is slightly worse than the 11.3% uncertainty calculated for trial 1. It is also interesting to note that the standard deviation was larger than the propagated uncertainty in all cases of this trial. These observations are likely a result of the large range of concentration values observed with this trial; this observation is discussed in greater detail in section 3.3.5. Using this correction procedure, the overall average bone strontium concentration calculated for both bare bone and tissue intact measurements were very close in agreement. The difference in the combined averages was found to be -2.3%, of range (-19.0 to 21.9%). Figure 3.16 illustrates the results of table 3.6.

Out of the 7 finger estimates of bone strontium, 5 were within error of each other as visualized by the overlapping of the uncertainty ranges in figure 3.16. Of the five that overlap, hypothesis t-testing indicates that for fingers 1, 4 and 6, there is not enough evidence to suggest that there is any difference between bare bone and tissue intact average estimates of bone strontium, at the 95% confidence level. This provides a strong indication of agreement and suggests that quantification may be achieved using the

conditions of trial 2. Of the two outliers, the finger 2 bare bone estimate was lower than the tissue corrected estimate by about 21.9% while bare bone was higher than tissue corrected by 19.0% for finger 7.

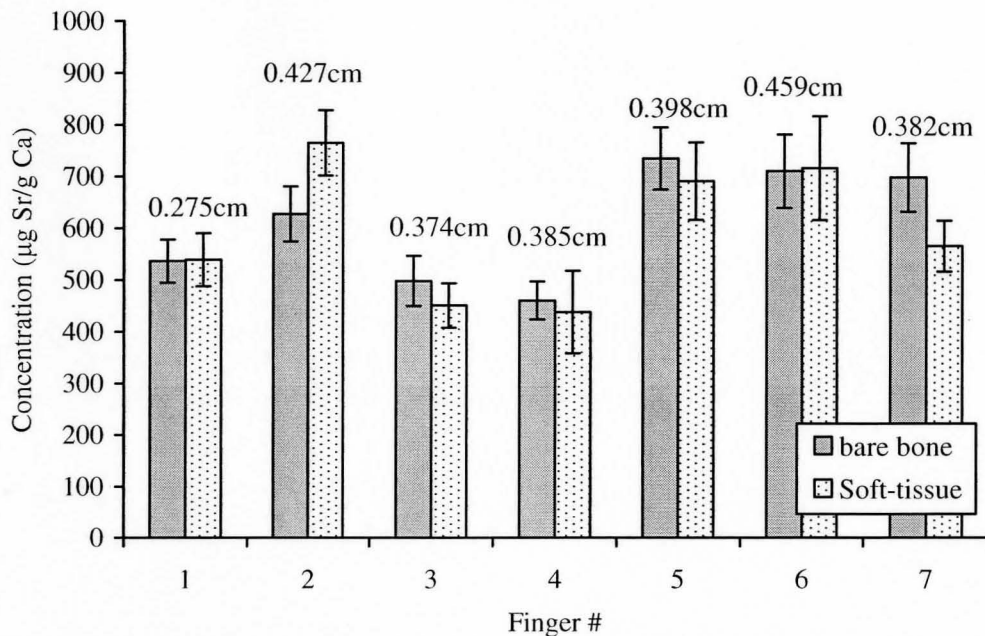


Figure 3.16: Comparison of tissue intact to bare bone EDXRF quantifications using soft-tissue correction, source activity correction and coherent normalization

Given the encouraging results of trial 2, it appears that correcting for source activity, in addition to coherent scatter correction, produces an improved agreement between bare bone and soft-tissue corrected concentration estimates over trial 1. This is in contradiction to the generally accepted idea that coherent normalization corrects for differences in source activity. If this were true, then applying an additional source activity correction would result in an over correction and as a result, we would not expect to find agreement between bare bone and tissue intact measurements. It is possible that there is some other systematic factor involved in a finger EDXRF measurement that is coincidentally corrected for using the source activity correction.

One possible explanation might lie in the high detector dead time associated with the tissue intact measurements on each finger. The observed dead times of these

measurements were between 35-50% and as a result, may contribute high uncertainty in a concentration estimate even if coherent normalization is performed. In speculating, we might consider that coherent normalization corrects only partially for the effect of source activity. We may further assume that source activity is inversely proportional to observed live time, so that the two are considered correlated. If both of these are so, then it may be possible that correcting for source activity will improve or complement the partial source activity correction from the coherent scatter normalization and bring tissue corrected readings to within uncertainty of bare bone readings.

An examination of z scores was done for each finger to compare how the overall bare bone to tissue intact measurements match. The z-score for finger j is calculated as follows:

$$z_j = \left(\frac{\Delta_j}{\sigma_{\Delta_j}} \right) = \left(\frac{Sr_{j,1} - Sr_{j,2}}{\sqrt{(\sigma Sr_{j,1})^2 + (\sigma Sr_{j,2})^2}} \right)$$

where: $Sr_{j,1} \pm \sigma Sr_{j,1}$ - is the concentration and uncertainty of bare bone measurements of finger j

$Sr_{j,2} \pm \sigma Sr_{j,2}$ - is the concentration and uncertainty of tissue-intact measurements of finger j

The final result is presented as the average of all fingers as follows:

$$\bar{z} \pm \sigma(\bar{z}) = \frac{1}{N} \sum_{j=1}^7 z_j \pm SD(z_1, \dots, z_7)$$

where N is the number of fingers used and $\bar{z} \pm \sigma(\bar{z}) = 0.19 \pm 0.99$. This may be compared directly to the ideal situation of $\bar{z} \pm \sigma(\bar{z}) = 0.00 \pm 1.00$ in which the average difference between two trials is 0.00. The computed average z-score overlaps with the

ideal situation well in the range of (-0.80 to 1.00) and suggests that trial 2 provides a close overall match between tissue intact to bare bone measurements.

It is possible that the mismatch between tissue intact and bare bone measurements of fingers 2 and 7 results from possible extreme positioning differences or excessive coherent scatter contribution from soft tissue of large fingers such as these. Modeling of large finger soft-tissue thicknesses (≥ 4.0 mm) was found to produce large amounts of variation in the expected normalized signal. This effect may be manifest in the cases of both finger 2 and 7 (Zamburlini *et al.*, 2008b). Alternatively, it is possible that the elemental composition of cadaver fingers is different from living human fingers. If this is so, then our calculation of strontium x-ray absorption may not be representative of that observed in a cadaver finger. However, until further such studies are taken to verify these results, this does suggest that it is possible to quantify *in vivo* bone strontium measurement performed on the non-supplementing Caucasian population.

In trial 3, further examination was undertaken to estimate bone strontium concentration in the absence of the coherent scatter correction. Table 3.7 summarizes an attempt to carry out quantification of bone strontium using only soft-tissue correction and correction for differences in measurement live time. In this trial, the bare bone and tissue intact estimates of the average human strontium concentration was found to be 381 ± 71 and 470 ± 101 $\mu\text{g Sr/g Ca}$, respectively.

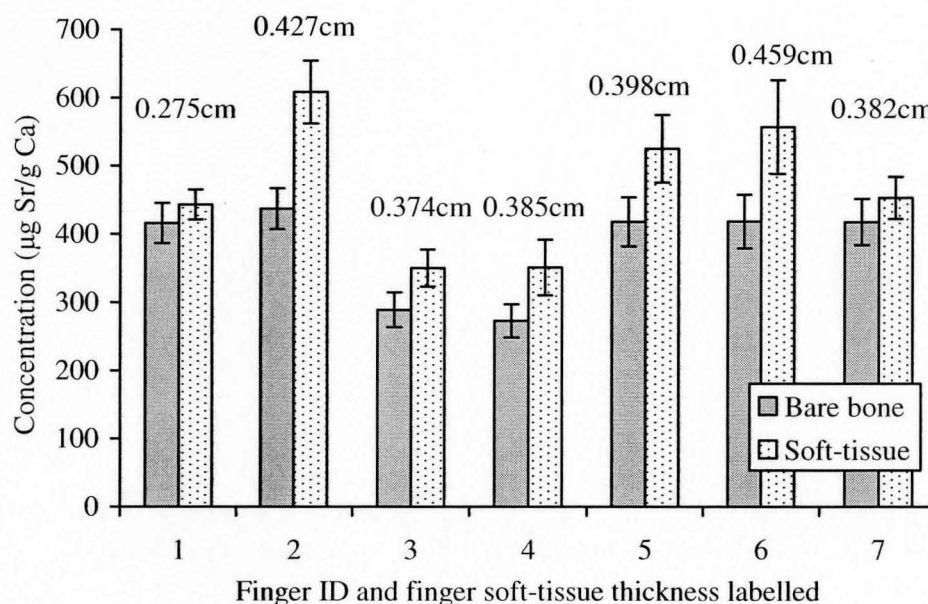
The average percentage propagated uncertainty of all 70 quantification trials using the tissue correction with live time normalization on intact tissue measurements was 6.91 % with a range of (4.68 to 8.76 %). In this trial, the tissue corrected signal was on average 23.3%, in the range of (6.5 to 39.1%), higher than the reading of bare bone strontium concentration. To make a comparison, both bare bone and tissue intact measurements had to be corrected in the same way, by live time only. Similarly, the plaster of Paris calibration line was also corrected for live time to allow a direct concentration extraction.

Table 3.7: Comparison of tissue intact to bare bone EDXRF quantifications using soft-tissue correction and live time correction

Finger ID (N = 10)	Bare Bone	Tissue Intact	Percentage Difference, %
	Strontium Conc., $\mu\text{g Sr/g Ca}$	Strontium Conc., $\mu\text{g Sr/g Ca}$	
1	416 \pm 29*	443 \pm 22	6.5
2	437 \pm 30*	608 \pm 46*	39.1
3	288 \pm 25*	350 \pm 27	21.2
4	272 \pm 24*	351 \pm 41*	28.6
5	418 \pm 36*	525 \pm 50*	25.6
6	418 \pm 39*	557 \pm 69*	33.2
7	418 \pm 34*	453 \pm 31	8.5
Average (\pm SD) (all trials)	381 \pm 71 ($\mu\text{g Sr/g Ca}$) 86 \pm 16 ($\mu\text{g Sr/g wet bone}$)	470 \pm 101 ($\mu\text{g Sr/g Ca}$) 106 \pm 23 ($\mu\text{g Sr/g wet bone}$)	23.3

* standard deviation of spread used instead of propagated error (N = 10)

It is suspected by this author that the difference in calculated concentration values are the result of not taking sample positioning into account, especially considering that the coherent normalization has not been used to correct for these factors. Figure 3.17 illustrates the results of table 3.6.

**Figure 3.17:** Comparison of tissue intact to bare bone EDXRF quantifications using soft-tissue correction and live time correction

These results indicate that quantification cannot be achieved using live time corrections alone. Therefore, this method was not examined any further.

The fourth and last correction trial is summarized in table 3.8. This correction utilized both a correction for live time and source decay in the absence of coherent normalization. It was in this correction that the greatest level of disparity between bare bone and tissue intact measurements was observed. The tissue intact estimation of bone strontium content was ($540 \pm 122 \mu\text{g Sr/g Ca}$) while that of bare bone was ($364 \pm 62 \mu\text{g Sr/g Ca}$). This indicates that the tissue intact estimates are on average 48.5% higher than the bare bone estimates, with an observed difference range of (27.9 to 67.4%).

Table 3.8: Comparison of tissue intact to bare bone EDXRF quantifications using soft-tissue correction, live time correction and source activity correction

Finger ID (N = 10)	Bare Bone Strontium Conc., $\mu\text{g Sr/g Ca}$	Tissue Intact Strontium Conc., $\mu\text{g Sr/g Ca}$	Percentage Difference, %
1	396 ± 22	$505 \pm 37^*$	27.9
2	415 ± 22	$694 \pm 74^*$	67.4
3	-276 ± 16	$401 \pm 38^*$	45.4
4	261 ± 15	$404 \pm 58^*$	54.8
5	400 ± 22	$603 \pm 41^*$	50.9
6	401 ± 22	$646 \pm 104^*$	61.3
7	400 ± 22	$525 \pm 50^*$	31.5
Average (\pm SD) (all trials)	364 ± 62 ($\mu\text{g Sr/g Ca}$) 82 ± 14 ($\mu\text{g Sr/g wet bone}$)	540 ± 122 ($\mu\text{g Sr/g Ca}$) 122 ± 27 ($\mu\text{g Sr/g wet bone}$)	48.5

* standard deviation of spread used instead of propagated error (N = 10)

The average percentage propagated uncertainty of all 70 quantification trials using the tissue correction with live time normalization on intact tissue measurements was 6.92% with a range of (4.70 to 8.77%). In this case, it is possible that the large disagreement of concentration estimates is a result of performing both live time and source activity corrections separately. If source activity is inversely proportional to live time where an increased activity may effectively decrease the live time of a counting trial, then these may be said to be related as one affects the other. However, if this is true, our correction of both factors separately would constitute an over-correction for these factors which

could translate into the observed disparity. Similar to the results of the third correction trial, differences in positioning may also play a role in the mismatching of calculated bone strontium estimates. Figure 3.18 illustrates the discrepancies between bare bone and tissue intact estimates.

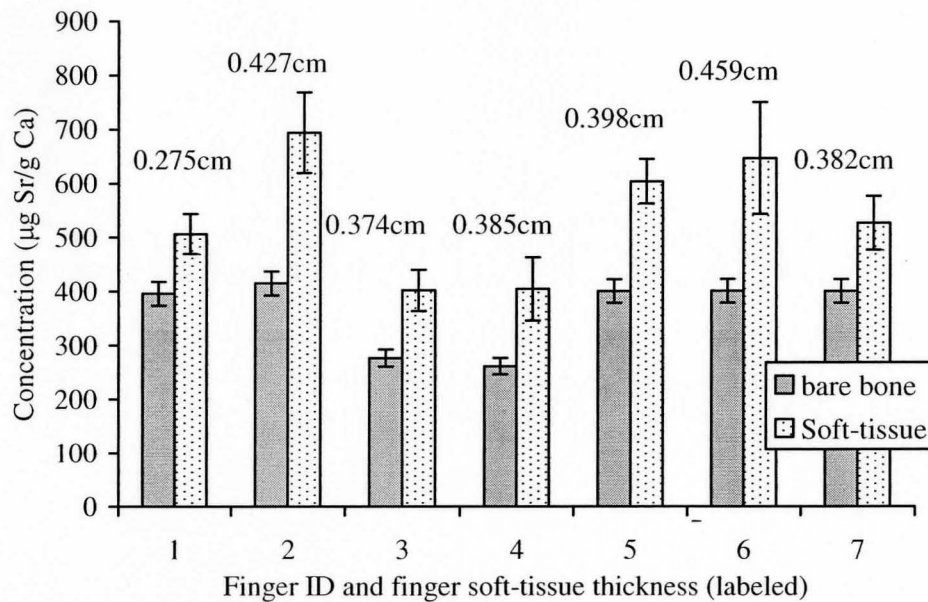


Figure 3.18: Comparison of tissue intact to bare bone EDXRF quantifications using soft-tissue correction, live time correction and source activity correction

In the case of calculations made in the absence of the use of coherent normalizations, estimates of bone strontium between bare bone and tissue intact measurements do not match. This is likely due to so many aforementioned factors that may affect the observed signal intensity. This disagreement indicates that quantification may not be achieved using only live time and source decay corrections. It further supports that the use of coherent normalization, even at energies pertaining to strontium, is necessary to correct for the many variables associated with a measurement.

3.3.5 Evaluation of system performance and measurement reproducibility

The results from each of the four trials may be used to further examine the system performance in estimating bone strontium. Table 3.9 illustrates the full scale range of quantification estimates obtained from performing ten measurements and associated trial corrections on each finger.

Table 3.9: Comparison of the range of finger bone strontium concentration estimates obtained using each of the four correction trials

Finger #	min - max Sr _μ range, (μg Sr/g Ca) % relative to average conc.			
	Trial 1	Trial 2	Trial 3	Trial 4
1	(436 - 492) 11.7	(476 - 613) 25.4	(407 - 465) 13.0	(463 - 580) 23.0
2	(600 - 759) 23.6	(664 - 855) 25.0	(569 - 688) 19.5	(596 - 853) 37.0
3	(347 - 445) 25.0	(401 - 518) 26.0	(320 - 394) 21.0	(352 - 488) 34.0
4	(303 - 489) 49.1	(323 - 612) 66.1	(298 - 421) 35.1	(322 - 507) 45.8
5	(528 - 669) 23.5	(576 - 812) 34.2	(441 - 583) 26.9	(548 - 657) 18.0
6	(557 - 716) 25.8	(593 - 888) 41.2	(430 - 678) 44.6	(457 - 841) 59.5
7	(456 - 515) 12.1	(519 - 645) 22.3	(416 - 484) 14.9	(465 - 614) 28.5
Average, %	24.4	34.3	25.0	35.1

It is interesting to note that despite the superior match of tissue intact to bare bone estimates of trial 2, the range of observed concentration values at 34.3% is still higher than those of trial 1 (24.3%). Additionally, this effect is seen between trials 3 and 4 where correction using source activity increases the observed range from 25.1%, in trial 3, to 35.1% in trial 4. However, this analysis is based on full scale range of observed values only and may not provide the best indicator as to how much observed values vary about their mean. To try to understand this effect further, the coefficient of variation (CV) of each finger for each trial was calculated. These results are presented in table 3.10. The average CV of each trial were calculated to determine the degree by which the measurements vary about their respective means for each trial.

Table 3.10: Comparison of the coefficient of variation associated with using each correction trial for tissue intact measurements

Finger #	Tissue intact CV (σ/μ), %			
	Trial 1 Coherent	Trial 2 Coh. & activity	Trial 3 Live time	Trial 4 Live time and activity
1	4.1	9.5	4.1	7.3
2	6.7	8.2	7.6	10.7
3	7.3	9.5	7.7	9.5
4	14.0	18.2	11.6	14.5
5	8.7	10.8	9.4	6.9
6	8.3	14.0	12.3	16.0
7	3.6	8.7	5.2	9.4
Average CV, %	7.5	11.3	8.3	10.6

Analysis of coefficient of variation indicates that trial one has a superior level of variation about the mean, at 7.5%, compared to all other trials. It is interesting to note that trial 2 had the highest level of variation, at 11.3%, of all 4 trials and that trial 4 is similarly elevated. Since both trials 2 and 4 involved correction for source activity, it is possible that in performing the source activity correction operation, the observed range of concentration values diverge from the average estimate. If this is the case, then the correction method of trial two may need to be used with caution. The observation that the results of trial 2 would have a broad range was insinuated by the calculations of system accuracy performed for trials 1 and 2. Recall that trial 1 had a predicted range of accuracy of 11.3% while correction using trial 2 conditions would give a poorer accuracy of 14.3% uncertainty.

Given the range of estimates observed in trial 2, it is recommended that a minimum of three measurements, at 30 – 60 minutes each, be taken of a single individual. A sample size of three would improve the overall estimate of bone strontium compared to performing just one measurement. Also, if the obtained measurement is an extreme maximum or minimum estimate of the true concentration, then a follow-up measurement would likely catch this effect and indicate that the true concentration is substantially different from the initial reading.

In summary, it seems that the use of the coherent normalization may still be positively relied upon in the calculation of bone strontium concentration given that it

appears to correct for so many unknown factors. The encouraging results of trial 2 suggest that coherent normalization might be used in combination with correction for source activity and overlying soft-tissue thickness to arrive at *in vivo* bone strontium concentrations. Further study to confirm these results is warranted.

3.3.6 *In vivo* XRF measurements of a strontium supplementing individual

A total of four EDXRF measurements were performed, over a six month period, on a strontium supplementing individual who we call Mary. A comparison of Mary's $K_{\alpha}:K_{\beta}$ ratios were made to examine the possible radial distribution of strontium in bone of a strontium medicating individual. Ratios were calculated using both the raw peak areas before and after soft-tissue correction. These results are displayed in table 3.11

Table 3.11: $K_{\alpha}:K_{\beta}$ ratios from an *in vivo* bone strontium XRF measurement of a strontium supplementing individual before and after soft-tissue correction

Visit #	Before Correction		After Correction	
	Ankle	Finger	Ankle	Finger
1	4.75	4.39	5.25	5.49
2	4.62	5.14	5.22	6.31
3	4.86	4.41	5.43	5.47
4	4.44	3.95	5.07	4.79
Average \pm SD	4.66 \pm 0.18	4.47 \pm 0.49	5.24 \pm 0.15	5.52 \pm 0.62

The $K_{\alpha}:K_{\beta}$ ratios observed from Mary's spectra before soft-tissue correction are similar to the ratio of 4.4 for non-supplementing individuals, after tissue correction, as predicted by Zamburlini (2008) and to those confirmed experimentally in this work for bare bone. After soft-tissue correction, these ratios are increased to 5.24 and 5.52 in the ankle and finger respectively. Since this is higher than values expected in the case of non-supplementing individuals, it is reasonable to conclude that strontium, from supplementation, has been predominantly deposited on the outer bone surface in Mary's case. This is suggested by all four measurements taken.

Despite the encouraging results of trial 2, without further verification, it is not completely certain if we can reliably calculate bone strontium concentration in absolute amounts. The results of Mary's measurements have been reported in a similar fashion to the cadaver finger quantification results of trial 1 in which only soft-tissue correction and coherent normalization have been applied. This is the same procedure illustrated in Appendix B. This will at least provide an idea of the associated concentrations of strontium found in the bones of strontium supplementing individuals so that we may compare directly to the levels found in the non-supplementing Caucasian population. Both sets of measurements from finger and ankle are reported and can be interpreted as concentrations found largely in cortical and trabecular bone, respectively. Although a small amount of cortical bone (<0.5mm) overlies the trabecular bone in the ankle, it is still likely that the primary contribution to the observed signal originates from trabecular bone. The finger and ankle measurement results are summarized in table 3.12 and illustrated graphically in figures 3.19 and 3.20.

Table 3.12: Bone strontium concentration estimates of finger and ankle measurement sites of a strontium supplementing individual

Time elapsed, days	Ankle		Finger	
	Conc., $\mu\text{g Sr/g Ca}$	% Error	Conc., $\mu\text{g Sr/g Ca}$	% Error
180	5129 ± 218	4.2	2996 ± 218	7.3
214	4267 ± 185	4.3	2854 ± 197	6.9
242	5216 ± 230	4.4	2677 ± 182	6.8
385	4058 ± 189	4.6	2522 ± 192	7.6

Figure 3.19 displays the results of the calculations of bone strontium content from the four finger measurements. To calculate bone strontium concentration in the ankle, the exact procedure used to quantify bone strontium from an index finger measurement was used. The Zamburlini finger soft-tissue correction model was used for the ankle soft-tissue correction as there are no readily available existing models for the correction of an ankle measurement when ankle geometry is taken into consideration. Therefore, ankle concentration estimates should be considered somewhat arbitrary in comparison to the estimates of finger bone strontium. Still, the approximate magnitude of both finger and

ankle concentrations provide a rough indication of the amount of strontium in a person supplementing strontium medication versus a person from the average Caucasian population.

The average of Mary's four measurements was calculated for both the ankle and finger site to approximate her average bone strontium levels (\pm SD). These were found to be $(4.67 \pm 0.59) \times 10^3$ and $(2.76 \pm 0.21) \times 10^3$ $\mu\text{g Sr/g Ca}$ in the ankle and finger respectively. The average strontium concentration estimated by the seven cadaver fingers suggested a skeletal concentration of 635 ± 110 $\mu\text{g Sr/g Ca}$ and hence, indicates that Mary's cortical and trabecular levels are about 4.4 ± 0.8 and 7.4 ± 1.6 times greater, respectively, than the average Caucasian population. This is assuming that strontium is evenly distributed in all trabecular and cortical bone of the population.

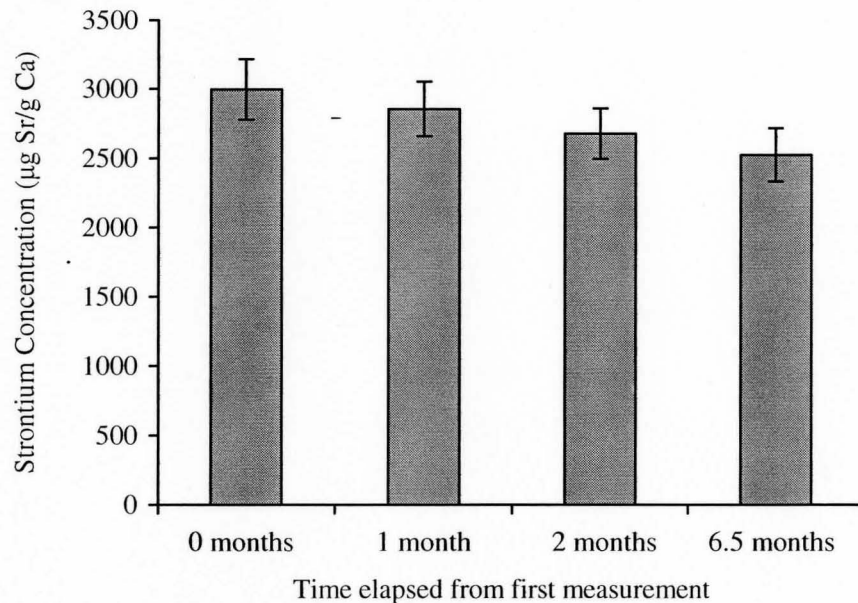


Figure 3.19: Concentration estimates of strontium in finger bone measured starting six months after strontium supplementation was begun

When consideration is given to the uncertainty associated with each measurement, the data suggest that Mary's strontium levels have reached a plateau or are only marginally beginning to decrease in cortical bone. Even more fascinating is the result of

the 4th measurement which was taken over 2 months past the day of the last self-administered dose. Despite being off her strontium medication for that period of time, there has been no significant change in her bone strontium levels. This suggests that the process of clearance of strontium from cortical bone is very slow acting and may not be visibly observed after only several months.

The biological clearance of administered strontium from long term bone storage compartments has been estimated by various groups to be on the order of several years. Cohn *et al.* (1962) and Newton *et al.* (1977) measured biological halflives of the long term compartment corresponding to strontium release from the bone matrix to be 843 and 1118 ± 450 days, respectively. However, these values are the rates found in the population. Smith *et al.* (1967) studied the retention of strontium in osteoporotic individuals and ultimately found the biological half-life of bone strontium clearance to be much shorter at 178 days in the range of (122 to 256 days). Given that the errors of the finger measurement are so high, calculation of a meaningful biological half-life clearance is not feasible. Mary informed us that she will begin taking strontium medication at the conclusion of the fourth measurement. Hence, it will not be possible to continue monitoring cortical bone clearance. However, it will still be of value to continue monitoring this individual to determine if her strontium levels remain at a plateau or change over time.

The studies mentioned above involve measuring clearance from the whole skeletal system and so the reported clearance times were estimated from the combined release of strontium from both cortical and trabecular bone. Analysis of the ankle bone might produce a reference as to how trabecular bone, in an osteoporotic individual, retains strontium.

Figure 3.20 illustrates the data on the four ankle measurements. An interesting anomaly is observed in the second measurement where the value dropped by 17% relative to the first measurement. Since Mary had confirmed that she had continued to take her medication as regularly as always, this decrease may not necessarily be associated as a drop in her actual bone strontium levels, but rather an error in the measurement taking. In

visit three, the strontium levels appeared to match with those of the first visit. However, in visit four, a reduced signal was again observed. This one was attributed to the discontinuation of the supplementation.

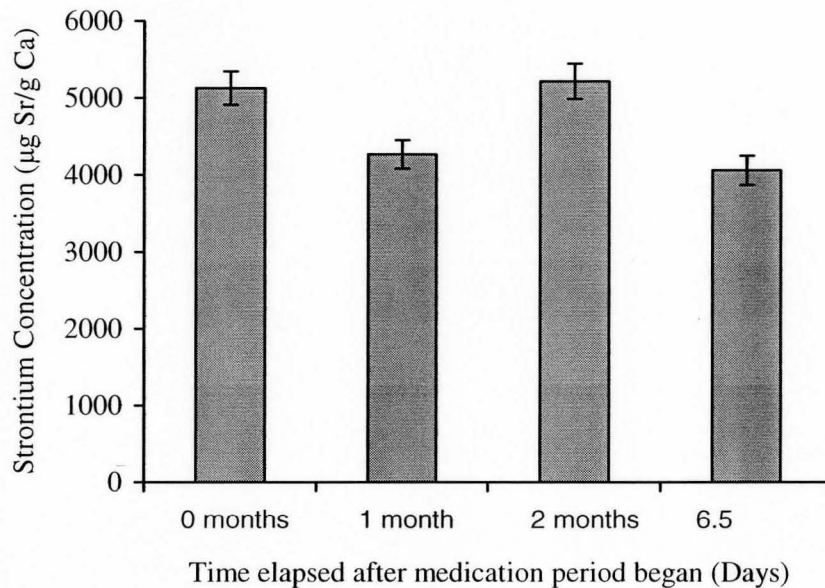


Figure 3.20: Concentration estimates of strontium in ankle bone measured starting six months after strontium supplementation began

A crude calculation of strontium biological half-life can be done for trabecular bone in the ankle using the assumption that the quantity present at the third measurement is the same quantity present on the last day of supplementing. A drop of 22.2% in the between the third and fourth measurement is observed and so this may be considered the drop that occurred over 70 days up to the last measurement. Using the ratio of observed intensities between ankle measurements 3 and 4, and a time difference of $t = 70$ days, the half-life is calculated to be 193 ± 72 days. This is substantially shorter than the literature estimates for whole bone clearance from the population, but is in closer agreement with the clearance time predicted by Smith *et al.* (1967) for osteoporotic individuals of 178 days. In general, it can be expected that strontium clearance from the ankle bone will be faster than that from finger bone, for any healthy or osteoporotic individual. This is mainly because the ankle is largely composed of trabecular bone and receives a greater

flow of blood which will accelerate the exchange of ions at the bone surface. However, since only two data points were used to make this calculation, further investigation is warranted to understand trends in osteoporotic bone strontium clearance rates.

In summary, an examination of $K_{\alpha}:K_{\beta}$ ratios from a strontium supplementing individual indicated that strontium in bone is more highly concentrated on the outer bone surface than throughout the inner bone matrix. Measurement results indicate that the strontium levels of a supplementing individual may be many times higher than a non-supplementing Caucasian individual and that concentrations found in trabecular bone are higher than in cortical bone. This is consistent with study findings involving the administration of strontium supplements. These results furthermore support findings that clearance of ions such as calcium and strontium from bone is faster in trabecular bone than in cortical bone.

Chapter 4

CONCLUSIONS AND FUTURE WORK

4.1 Conclusions

Interest toward the effects of strontium in the human body gained precedence in the 1950's. This was initiated when it was discovered that radioactive strontium was formed as a fall-out product of atomic bomb testing and later reinforced when it was discovered that strontium may potentially be used in the treatment of bone diseases such as osteoporosis (Shorr and Carter, 1952; McCaslin and Janes, 1959). A renewal of interest of the therapeutic effects of strontium has surged with the large scale, ongoing studies of TROPOS (Reginster *et al.*, 2008) AND SOTI (Meunier *et al.*, 2004) in which an increase in bone mineral density and a decrease in fracture incidence have been observed. The advent of this new therapy has warranted the development of a diagnostic technique to measure *in vivo* bone strontium levels and changes, non-invasively. Pejović-Milić *et al.* (2004) and Zamburlini *et al.* (2007) met this challenge through the development and optimization of an EDXRF system designed to measure bone strontium in humans, *in vivo*.

The bulk of the work in this manuscript has been to overcome some of the obstacles presented in attempting to use this system to quantify bone strontium absolutely. The first was to determine if estimation of soft tissue thickness could be optimized through comparison of several different medical imaging systems and to determine if the currently used 8 MHz ultrasound system was grossly misrepresenting the true tissue thickness, as was suspected. Later, attempts to quantify *ex vivo* bone strontium measurements were performed to examine the feasibility of using this system to achieve quantification of *in vivo* bone strontium measurements.

4.1.1 Soft-tissue correction using imaging modalities

In chapter 2, a cross-examination of imaging modalities was presented. This was done in an effort to determine the efficacy of each modality to provide an accurate and precise soft-tissue thickness estimate for use in soft-tissue correction of an *in vivo* bone strontium measurement. Results indicated that of the modalities tested, 55 MHz ultrasound would provide the most accurate measurement of finger soft-tissue thickness at 3.2% relative uncertainty for a given measurement with 1 Tesla MR as the runner-up. An examination of the other modalities tested suggested that the CT method had a tendency to underestimate finger soft-tissue thickness while the other ultrasound and MR imaging modalities were not significantly different than the computed average soft tissue thickness.

The 8 MHz ultrasound system used in previous studies was found to have a 6.6% uncertainty in the estimate of soft-tissue thickness. A re-examination of 9 individuals was done to examine if the ultrasound measurements of a study from 2006 were performed correctly by comparing to the measurements of 2008. This comparison suggested that the ankle thickness was measured correctly in 2006 while the measurement of finger soft-tissue thickness was underestimated in the 2006 study by an average of 17.7%. Ultimately, since the ankle measurements were not underestimated in 2006, we could rule out the hypothesis that an underestimation of overlying soft-tissue would produce the lower than expected observed $K_{\alpha}:K_{\beta}$ ratios. The finger underestimation of 2006 may have been the result of tissue compression during the measurement or as a result of mistaking the tendon sheath for bone during the thickness measurement.

In either case, care must be taken to minimize compression during image acquisition and to center carefully the position measurement tool cross-hairs directly on the bone-tissue and tissue-air boundaries. The only foreseen shortcoming of the 8 MHz system is the marginally poorer associated precision of measurement in comparison to the 55 MHz system. Still, if measurement procedures are meticulously and correctly performed, then the current 8 MHz ultrasound system has the capability to measure finger soft-tissue thickness accurately with an acceptable range of uncertainty.

4.1.2 Analysis of observed K_{α} and K_{β} ratios

Experimental data were acquired from EDXRF measurements performed on cadaver fingers both with soft-tissue intact and then removed. The average of the observed tissue-intact K_{α} : K_{β} ratios was calculated as 2.72 ± 0.43 which is similar to the findings of (Zamburlini *et al.*, 2007). The average of the tissue corrected ratio was 3.61 ± 0.55 which does not match predictions by the theoretical model or bare bone ratios of 4.4 ± 0.4 . This indicates that some additional factor might be influencing the lowering of this ratio. One proposed idea was that some factor was inflating the area under the K_{β} peak in the case of tissue-intact measurements. This was suggested after it was observed that the concentration estimates found using the K_{β} peak were on average, 33% higher than the estimates from the K_{α} peak, from tissue-intact measurements. This was significant given that concentration extraction was done from K_{α} and K_{β} calibration lines produced using the same phantoms.

The idea that the observed K_{α} : K_{β} ratios could be used to correct for overlying soft-tissue was examined and ultimately found not to be feasible due to the broad range of observed K_{α} : K_{β} ratios that may be observed within a single subject. A plot of K_{α} : K_{β} vs. tissue thickness indicated only a very weak correlation which was not enough to create the desired correction relationship.

4.1.3 Creation of an experimental soft-tissue correction model

An attempt was made to create an experimental based soft-tissue correction model to compare with the currently used theoretical model constructed by Zamburlini, through Monte Carlo modeling. This was done by plotting the logarithm of the ratio of tissue intact to bare bone observed intensities to the finger soft-tissue thickness reported by 55 MHz ultrasound. The correlation of these data was significant but not overly strong. A comparison between the theoretical and experimental models indicated that the two did not agree within uncertainty. This may be attributed to using a small sample size of only 7 fingers, six of which, have generally high overlying soft-tissue thickness. As yet, this

model is not sufficient to be used to correct for overlying soft-tissue. Future work might include further measurements on additional cadaver fingers to see if correlation may be improved. This may determine ultimately if the theoretical and experimental relationships match. It would be beneficial to incorporate measurements from fingers of thin overlying soft tissue thickness to see if this improves our estimate of the current experimental absorption coefficients.

4.1.4 Attempts to quantify *ex vivo* bone strontium

The attempts to quantify bone strontium *ex vivo* were carried out in four separate trials using the data set from measurements performed on fingers with soft-tissue intact and on bare bone. All trials incorporated Zamburlini soft-tissue correction. In trial 1, all signals were normalized to the coherent scatter peak and concentrations in micrograms strontium per gram calcium were extracted from strontium doped plaster of Paris calibration lines. Bare bone trials estimated an average human bone strontium concentration of $635 \pm 110 \mu\text{g Sr/g Ca}$ or $143 \pm 25 \mu\text{g Sr/g wet bone}$ which is similar to levels estimated by the previous studies summarized in Chapter 1. In this case, tissue intact concentrations were on average 18.6% lower than bare bone concentrations and did not match within uncertainty. This may be the result of not considering the soft-tissue attenuation of the 35 keV coherent scatter photons in the full calculation for bone strontium quantification.

A similar gross mismatching was observed between bare bone and tissue intact estimates in trials 3 and 4 where the coherent normalization was not used; only correction for live time in trial 3 and live time and source activity in trial 4 was calculated. In trial 2, the use of coherent scatter normalization and source activity corrections produced the best overall agreement between bare bone and tissue intact measurements at only 2.3% average difference. As yet it is uncertain if this is due to the necessity of correcting for source activity or that this method simply corrected for an additional systematic, yet unknown, factor that coincidentally brought the results into agreement. However, these results do suggest that the coherent scatter normalization is necessary to extract

meaningful information from a bone strontium measurement. Given the encouraging results of trial 2, it would be advantageous to carry out further cadaver finger measurements to verify if this correction procedure is capable of extracting valid estimates of bone strontium concentration. This may ultimately determine if source activity must be externally corrected in addition to coherent normalization.

4.1.5 Evaluation of system performance and measurement reproducibility

An examination of system accuracy was carried out to determine the maximum spread of measurements expected from using the current EDXRF system in conjunction with the correction procedures outlined in trials 1 and 2. Although trial 2 produced superior agreement of bare bone to tissue intact concentrations, its accuracy at 14.3% relative uncertainty was found to be slightly worse than the 11.3% uncertainty calculated for trial 1. Further analysis of the maximum spread and coefficient of variation of measurements within each finger supported this trend and suggests that the correction using source decay may cause a broadening in the spread of individual concentration estimates about the average. Thus, the use of trial 2 as a means to quantify *in vivo* strontium should be used cautiously or include multiple measurements to ensure that individual readings are not simply outliers.

4.1.6 *In vivo* XRF measurements of a strontium supplementing individual

In vivo EDXRF measurements were performed on an individual self-administering strontium citrate medication. Soft-tissue correction and normalization according to the procedure of trial 1 were performed on both finger and ankle measurements of this individual. This was done to illustrate the approximate difference in levels observed between individuals from the population and individuals taking strontium based medication. Results indicated that strontium concentrations were 4.6 ± 0.8 and 7.4 ± 1.6 times greater in the finger and ankle, respectively, of this individual than in the average Caucasian population. A comparison between $K_{\alpha}:K_{\beta}$ ratios observed

between Mary and the average population suggests that Mary's bone strontium is predominantly deposited on the surface of her bone which is consistent with the findings of strontium distribution in monkeys that were fed strontium supplements.(Boivin *et al.*, 1996) Analysis of the biological clearance of bone strontium from the ankle site produced a clearance half-life of 193 ± 72 days which is consistent with the clearance rates found in osteoporotic individuals (Smith *et al.*, 1967). Both ankle and finger measurements seem to indicate that at the time of her first measurement, Mary's strontium levels were already at a plateau. This suggests that the time taken to reach a plateau is on the order of several months or less after administration begins.

4.2 Future Work

There are currently several obstacles standing in the way of quantifying an *in vivo* bone strontium measurement reliably using EDXRF. One aspect which may be confirmed, and potentially improved upon, is the use of the current Zamburlini Monte Carlo soft-tissue correction model. Further modelling of the finger EDXRF bone strontium measurement might indicate if the current model is more than adequate enough or improvements can be made. Further study toward the creation of an experimental soft-tissue correction model is also warranted as this may ultimately prove superior to the current Monte Carlo based model. The acquisition of additional cadaver fingers to accomplish this goal would invite further investigation into the unexplained trends seen in the observed $K_{\alpha}:K_{\beta}$ ratios. EDXRF measurements of cadaver fingers may verify if quantification might be achieved using Zamburlini soft-tissue corrections, coherent scatter normalization and source activity correction.

4.2.1 Finger bone composition analysis

If we consider that quantification trials 1 and 2 have produced the most accurate estimates of bone strontium concentration, then it would be interesting to verify these results further and determine how close the EDXRF measurement estimates are to the

true value. A true value might be approached if further composition analysis of each finger bone is undertaken. Currently, plans are in motion to have three separate tests performed: wavelength dispersive x-ray fluorescence (WDXRF), inductively coupled plasma atomic emission spectroscopy (ICPAES) and powder x-ray diffraction (XRD). Bones will be sent to Ryerson University where these instruments are readily available. Eric Da Silva, a Ryerson graduate student, will prepare the bone samples and perform each test. Each test will involve alteration of the bone samples into a form required to carry out the test. Steps such as these are necessary to produce concentration estimates of precision greater than the current EDXRF system. For example, the current WDXRF system is expected to yield results with an uncertainty of only several parts per million which would constitute a marked improvement in measurement precision.

4.2.2 Creation of a new calibration standard

One problem observed in our efforts to quantify bone strontium is the strontium contamination inherent within the plaster of Paris phantoms used for concentration extraction. As yet, the extraction of strontium concentration from a poP calibration curve requires manipulation of the curve such as setting the intercept equal to zero. This technique has the limitation in that it may introduce additional uncertainty in an extraction of bone strontium. If a calibration line could be constructed using phantoms with no contamination, this would solve this problem. However, this is a difficult goal to achieve.

As part of his Master of Science research, Eric Da Silva is attempting to perfect a set of hydroxyapatite based phantoms. The construction material of these phantoms have been rigorously purified so that strontium contamination is down to only a few parts per million. This appears to be a promising solution to the problem of the non-zero calibration intercept indicative of contamination. Additionally, the use of this material, over plaster of Paris, may be thought to more closely model the composition of bone given that hydroxyapatite is the fundamental constituent of the mineralized portion of bone. To account for the compositional differences between plaster of Paris and cortical

bone, a calculation of the ratio of coherent scatter differential cross-section between these materials is necessary to produce meaningful concentration extraction. This calculation depends strongly on knowledge of material composition and hence, if the material is inaccurately represented, then this may add uncertainty to extraction of concentration. However, if the hydroxyapatite phantoms could be formed so that they are far more representative of the composition of human cortical bone, then this may reduce uncertainty and improve estimations of bone strontium. The application of these phantoms would not be limited to *in vivo* measurements of strontium but could extend to measurement of all other *in vivo* bone trace element measurements.

4.2.3 Optimization of a new DCC x-ray optical system

The quest to quantify and reproduce *in vivo* bone strontium measurements warrants continued investigation into new procedures and technologies that may accomplish this goal. Recently, a new x-ray optical system has been installed at McMaster University with the intended use to measure and quantify *in vivo* bone strontium. Complemented with this system is a brand new Ketek Silicon Drifted Detector (SDD). The Ketek SDD has the advantage of portability owing to its small size and, in contrast to Si(Li) and HPGe systems, does not require electronic cooling. Also, the SDD can measure count rates much higher than the current Si(Li) detectors are capable of handling. However, the smaller crystal size means a lower expected efficiency than a Si(Li) system. The x-ray system is a doubly-curved crystal (DCC) x-ray optical system that utilizes a power supplied, operator chosen anode target as the excitation source. This system has already undergone preliminary optimization tests by Zamburlini (2008) to determine the feasibility of its use for measuring bone strontium *in vivo*.

This system provides the advantage of a simplifying the spectrum and decreasing background under the strontium peaks since a homogeneous anode source is used. The use of a silver anode was found to optimize the conditions of a bone strontium measurement (Zamburlini, 2008). The DCC provides several additional advantages over the current EDXRF system. First, it permits filtering of the anode photons according to

energy so that only photons of known energies, such as the Ag K_{α} x-rays, may be selected and used as an excitation source. This includes filtration of most of the Bremsstrahlung continuum. Second, it permits the user to control the photon fluence and beam size incident on a subject. This provides a prospective advantage of eliminating the need for coherent scatter normalization in the quantification procedure. The use of this device imparts only a marginally inflated dose to the subject receiving the measurement. However, this dose is still well within acceptable limits so that a non-occupationally exposed individual may receive a bone strontium measurement with no appreciable increase in risk. Given that the benefits seem to outweigh the costs of using this system, it would be worthwhile to invest in the continued development and full implementation of this system as a possible superior replacement of the current EDXRF system.

4.2.4 Measurement of strontium kinetics in strontium supplementing individuals

In Chapter 3 it was discussed how there is a growing number of women and men with bone diseases such as osteoporosis who are beginning to take strontium based medications in effort to treat these diseases. Over that past decade, these individuals have come to represent an interesting new sub-group of the population in which the particulars of their condition, and therapy by administration of strontium, have spawned many questions. Several of these questions are: how does the strontium metabolism of strontium supplementing individuals compare to that of the population? Do strontium levels rise indefinitely or eventually plateau in supplementing individuals? What sort of strontium clearance rates may be observed between healthy and osteoporotic individuals? Is there a level of strontium exposure that is detrimental to skeletal health? What effect does strontium supplementation have on observed bone mineral density? Is there a correlation between fracture risk and bone strontium supplementation?

Questions such as these may be answered if subjects from this unique pool of individuals may be recruited and measured on our current EDXRF system. Helen Moise, a graduate student of Ryerson University will soon recruit these individuals to begin a series of measurements that may help answer some of these questions. This study will

focus on understanding the incorporation and retention of strontium in the human body. Ultimately, these answers may help to inform and educate health practitioners about the use of strontium as a treatment of bone disease and may further lead to its use as a standardized therapy for osteoporosis.

References

- Ahlgren L, Lidén K, Mattsson S, Tejning S. (1976) X-ray fluorescence analysis of lead in human skeleton *in vivo*. *Scand. J. Work Environ. Health.* **2** (2): 82-86.
- Alexander GV and Nusbaum RE. (1959) The relative retention of strontium and calcium in human bone tissue. *J. Biol. Chem.* **234** (2): 418-421.
- Aras NK, Yilmaz G, Korkusuz F, Olmez I, Sepici B, Eksioglu F, Bode P. (2000) Multielement analysis of iliac crest bone by neutron activation. *J. Radioanal. Nucl.* **244** (1): 185-188.
- Berger MJ, Hubbell JH, Seltzer SM, Chang J, Coursey JS, Sukumar R and Zucker DS. (2005) XCOM: Photon Cross Sections Database (Version 1.3). National Institute of Standards and Technology, Gaithersburg, MD. Retrieved: August, 2008 from <http://physics.nist.gov/libaccess/lib.mcmaster.ca/XCOM>
- Bevington PR. *Data Reduction and Error Analysis for the Physical Sciences*. McGraw-Hill, New York, 1969.
- Boivin G, Deloffre P, Perrat B, Panczer G, Boudeulle M, Mauras Y, Allain P, Tsouderos Y, Meunier PJ. (1996) Strontium distribution and interactions with bone mineral in monkey iliac bone after strontium salt (S 12911) administration. *J. Bone Miner. Res.* **11** (9): 1302-1311.
- Brand S, Weiss EC, Lemor RM, Kolios MC. (2008) High frequency ultrasound tissue characterization and acoustic microscopy of intracellular changes. *Ultrasound Med. Biol.* **34** (9): 1396-1407.
- Cabrera WE, Schrooten I, De Broe ME, D'Haese PC. (1999) Strontium and bone. *J. Bone Miner. Res.* **14** (5): 661-668.
- Canalis E, Hott M, Deloffre P, Tsouderos Y, Marie PJ. (1996) The divalent strontium salt S12911 enhances bone cell replication and bone formation *in vitro*. *Bone.* **18** (6): 517-523.
- Carvalho ML, Brito J, Barreiros MA. (1998) Study of trace element concentrations in human tissues by EDXRF spectrometry. *X-Ray Spectrom.* **27** (3): 198-204.
- Christoffersen J, Christoffersen MR, Kolthoff N, Bärenholdt O. (1997) Effects of strontium ions on growth and dissolution of hydroxyapatite and on bone mineral detection. *Bone.* **20** (1): 47-54.

- Cohen-Solal M. (2002) Strontium overload and toxicity: impact on renal osteodystrophy. *Nephrol. Dial. Transplant.* **17** (Suppl 2): 30-34.
- Cohn SH, Spencer H, Samachson J, Robertson JS. (1962) The turnover of strontium-85 in man as determined by whole-body counting. *Radiat. Res.* **17** 173-185.
- Comar CL, Russell RS, Wasserman RH. (1957) Strontium-calcium movement from soil to man. *Science.* **126** (3272): 485-492.
- Dahl SG, Allain P, Marie PJ, Mauras Y, Boivin G, Ammann P, Tsouderos Y, Delmas PD, Christiansen C. (2001) Incorporation and distribution of strontium in bone. *Bone.* **28** (4): 446-453.
- D'Haese PC, Schrooten I, Goodman WG, Cabrera WE, Lamberts LV, Elseviers MM, Couttenye MM, De Broe ME. (2000) Increased bone strontium levels in hemodialysis patients with osteomalacia. *Kidney Int.* **57** (3): 1107-1114.
- Firestone RB. (2005) LBNL Isotopes Project Nuclear Data Dissemination Home Page. Ernest Orlando Lawrence Berkeley National Laboratory, Berkeley, U.S.A. Retrieved: September 2008 from <http://ie.lbl.gov/libaccess.lib.mcmaster.ca/toi.html>
- Gordon CL, Webber CE, Chettle DR. (1994) The reproducibility of ¹⁰⁹Cd-based x-ray fluorescence measurements of bone lead. *Environ. Health Perspect.* **102** (8): 690-694.
- Grynepas MD, Hamilton E, Cheung R, Tsouderos Y, Deloffre P, Hott M, Marie PJ. (1996) Strontium increases vertebral bone volume in rats at a low dose that does not induce detectable mineralization defect. *Bone.* **18** (3): 253-259.
- Hodges RM, MacDonald NS, Nusbaum R, Stearns R, Ezmirlan F, Spain P, McArthur C. (1950) The strontium content of human bones. *J. Biol. Chem.* **185** (2): 519-524.
- Hubbell JH and Øverbø I. (1979) Relativistic atomic form-factors and photon coherent scattering cross-sections. *Journal of Physical and Chemical Reference Data.* **8** (1): 69-105.
- Hurlbut CS, Jr. and Sharp WE. *Dana's Minerals and How to Study Them.* 4th ed. John Wiley & Sons Inc., 605 Third Avenue, New York, NY, USA, 1998.
- Inglis D, Pui M, Ioannidis G, Beattie K, Boulos P, Adachi JD, Webber CE, Eckstein F. (2007) Accuracy and test-retest precision of quantitative cartilage morphology on a 1.0 T peripheral magnetic resonance imaging system. *Osteoarthritis Cartilage.* **15** (1): 110-115.

- International Commission on Radiological Protection (ICRP). (2002) Basic anatomical and physiological data for use in radiological protection: reference values. *ICRP Publication 89*. Pergamon Press, Oxford.
- International Commission on Radiological Protection (ICRP). (1975) Report of the Task Group on Reference Man. *ICRP Publication 23*. Pergamon Press, Oxford.
- Kereiakes JG and Rao DV. (1992) Auger electron dosimetry: report of AAPM Nuclear Medicine Committee Task Group No. 6. *Med. Phys.* **19** (6): 1359.
- Knoll GF. *Radiation Detection and Measurement*. 3rd ed. John Wiley & Sons, Inc., United States of America, 1999.
- Lederer CM, Hollander JM and Perlman I. *Table of Isotopes*. 6th ed. John Wiley & Sons, Inc., New York, NY, 1967.
- Lentle B and Worsley D. (2006) Osteoporosis redux. *J. Nucl. Med.* **47** (12): 1945-1959.
- MacDonald NS, Ezmirlan F, Spain P, McArthur C. (1951) The ultimate site of skeletal deposition of strontium and lead. *J. Biol. Chem.* **189** (1): 387-399.
- Marie PJ. (2006) Strontium ranelate: a dual mode of action rebalancing bone turnover in favour of bone formation. *Curr. Opin. Rheumatol.* **18** (Suppl 1): S11-5.
- Marie PJ, Ammann P, Boivin G, Rey C. (2001) Mechanisms of action and therapeutic potential of strontium in bone. *Calcif. Tissue Int.* **69** (3): 121-129.
- Marie PJ, Garba MT, Hott M, Miravet L. (1985) Effect of low doses of stable strontium on bone metabolism in rats. *Miner. Electrolyte Metab.* **11** (1): 5-13.
- McCaslin FE, Jr. and Janes JM. (1959) The effect of strontium lactate in the treatment of osteoporosis. *Proc. Staff Meet. Mayo Clin.* **34** (13): 329-334.
- Meunier PJ, Roux C, Seeman E, Ortolani S, Badurski JE, Spector TD, Cannata J, Balogh A, Lemmel EM, Nielsen SP, Rizzoli R, Genant HK, Reginster JY. (2004) The effects of strontium ranelate on the risk of vertebral fracture in women with postmenopausal osteoporosis. *N. Engl. J. Med.* **350** (5): 459-468.
- Newton D, Rundo J, Harrison GE. (1977) The retention of alkaline earth elements in man, with special reference to barium. *Health Phys.* **33** (1): 45-53.
- Nie HL, Chettle DR, Stronach I, Arnold M, Huang SB, McNeill F, O'Meara JM. (2004) A study of MDL improvement for the *in vivo* measurement of lead in bone. *Nucl. Instrum. Methods Phys. Res. Sect. B-Beam Interact. Mater. Atoms.* **213** 579-583.

- Nie HL, Chettle DR, McNeill FE, O'Meara JM. (2004a) An investigation of the ^{109}Cd γ -ray induced K-x-ray fluorescence (XRF) bone-lead measurement calibration procedure. *Phys. Med. Biol.* **49** N325-N334
- Nielsen SP, Barenholdt O, Barenholdt-Schioler C, Mauras Y, Allain P. (2004) Noninvasive measurement of bone strontium. *J. Clin. Densitom.* **7** (3): 262-268.
- Nielsen SP. (2004a) Review: The biological role of strontium. *Bone.* **35** (3): 583-588.
- Nielsen SP, Slosman D, Sørensen OH, Basse-Cathalinat B, De Cassin P, Roux C, Meunier PJ. (1999) Influence of strontium on bone mineral density and bone mineral content measurements by dual x-ray absorptiometry. *J. Clin. Densitom.* **2** (4): 371-379.
- NIST. (2005) Composition of Tissue, Soft (ICRP). National Institute of Standards and Technology, Gaithersburg, MD. Retrieved: July, 2008 from <http://physics.nist.gov/libaccess/lib.mcmaster.ca/cgi-bin/Star/compos.pl?matno=261>
- Nouveau-Richard S, Monot M, Bastien P, de Lacharriere O. (2004) *In vivo* epidermal thickness measurement: ultrasound vs. confocal imaging. *Skin Res. Technol.* **10** (2): 136-140.
- O'Meara JM, Chettle DR, McNeill FE, Webber CE. (1997) The feasibility of measuring bone uranium concentrations *in vivo* using source excited K x-ray fluorescence. *Phys. Med. Biol.* **42** (6): 1109-1120.
- O'Flaherty, EJ. (1992) Modeling bone mineral metabolism, with special reference to calcium and lead. *Neurotoxicology.* **13** (4): 789-797.
- Özgür S, Sümer H, Koçoğlu G. (1996) Rickets and soil strontium. *Arch. Dis. Child.* **75** (6): 524-526.
- Paschalis EP, Betts F, DiCarlo E, Mendelsohn R, Boskey AL. (1997) FTIR microspectroscopic analysis of human iliac crest biopsies from untreated osteoporotic bone. *Calcif. Tissue Int.* **61** (6): 487-492.
- Pecher C. (1941) Biological investigations with radioactive calcium and strontium. *Proc Soc Exp Biol Med.* **46** 86-91.
- Pejović-Milić A, Stronach IM, Gyorffy J, Webber CE, Chettle DR. (2004) Quantification of bone strontium levels in humans by *in vivo* x-ray fluorescence. *Med. Phys.* **31** (3): 528-538.
- Pejović-Milić A, Brito JA, Gyorffy J, Chettle DR. (2002) Ultrasound measurements of overlying soft tissue thickness at four skeletal sites suitable for *in vivo* x-ray fluorescence. *Med. Phys.* **29** (11): 2687-2691.

- Pors Nielsen S. (2004) The biological role of strontium. *Bone*. **35** (3): 583-588.
- Reginster JY, Felsenberg D, Boonen S, Diez-Perez A, Rizzoli R, Brandi ML, Spector TD, Brixen K, Goemaere S, Cormier C, Balogh A, Delmas PD, Meunier PJ. (2008) Effects of long-term strontium ranelate treatment on the risk of nonvertebral and vertebral fractures in postmenopausal osteoporosis: Results of a five-year, randomized, placebo-controlled trial. *Arthritis Rheum*. **58** (6): 1687-1695.
- Rosenthal HL, Cochran OA, Eves MM. (1972) Strontium content of mammalian bone, diet and excreta. *Environ. Res*. **5** (2): 182-191.
- Samudralwar DL and Robertson JD. (1993) Determination of major and trace-elements in bones by simultaneous PIXE/PIGE analysis. *Journal of Radioanalytical and Nuclear Chemistry-Articles*. **169** (1): 259-267.
- Schroeder HA, Tipton IH, Nason AP. (1972) Trace metals in man: strontium and barium. *J. Chronic Dis*. **25** (9): 491-517.
- Schrooten I, Cabrera W, Goodman WG, Dauwe S, Lamberts LV, Marynissen R, Dorrine W, De Broe ME, D'Haese PC. (1998) Strontium causes osteomalacia in chronic renal failure rats. *Kidney Int*. **54** (2): 448-456.
- Shorr E and Carter AC. (1952) The usefulness of strontium as an adjuvant to calcium in the remineralization of the skeleton in man. *Bull. Hosp. Joint Dis*. **13** (1): 59-66.
- Smith DA, Speirs CF, Shimmins J. (1967) The long-term skeletal retention and recirculation of ⁸⁵Sr in man. *Calcif. Tissue Res*. **1** (2): 144-152.
- Snyder RE and Secord DC. (1982) The *in situ* measurement of strontium content in bone using x-ray fluorescence analysis. *Phys. Med. Biol*. **27** (4): 515-529.
- Sobel AE, Cohen J, Kramer B. (1935) The nature of the injury to the calcifying mechanism in rickets due to strontium. *Biochem. J*. **29** (12): 2640-2645.
- Somervaille LJ, Chettle DR, Scott MC. (1985) *In vivo* measurement of lead in bone using x-ray fluorescence. *Phys. Med. Biol*. **30** (9): 929-943.
- Takahashi N, Sasaki T, Tsouderos Y, Suda T. (2003) S 12911-2 inhibits osteoclastic bone resorption *in vitro*. *J. Bone Miner. Res*. **18** (6): 1082-1087.
- Thurber DL, Kulp JL, Hodges E, Gast PW, Wampler JM. (1958) Common strontium content of the human skeleton. *Science*. **128** (3318): 256-257.
- Turekian KK and Kulp JL. (1956) Strontium content of human bones. *Science*. **124** (3218): 405-407.

- Verberckmoes SC, Behets GJ, Oste L, Bervoets AR, Lamberts LV, Drakopoulos M, Somogyi A, Cool P, Dorrine W, De Broe ME, D'Haese PC. (2004) Effects of strontium on the physicochemical characteristics of hydroxyapatite. *Calcif. Tissue Int.* **75** (5): 405-415.
- WHO. (1994) Study Group on Assessment of Fracture Risk and its Application to Screening for Postmenopausal Osteoporosis. *Technical Report Series (World Health Organization)*. WHO, Geneva.
- Wielopolski L, Vartsky D, Yasumura S, Cohn SH. (1983) Application of XRF to measure strontium in human-bone *in vivo*. *Advances in X-Ray Analysis.* **26** 415-421.
- Woodard HQ and White DR. (1986) The composition of body tissues. *Br. J. Radiol.* **59** (708): 1209-1218.
- Woodard HQ. (1962) The elementary composition of human cortical bone. *Health Phys.* **8** (0017-9078): 513-517.
- Zaichick V. (2006) INAA of Ca, Cl, K, Mg, Mn, Na, P, and Sr contents in the human cortical and trabecular bone. *J. Radioanal. Nucl.* **269** (3): 653-659.
- Zamburlini M. (2008) *In vivo* measurement of bone strontium with x-ray fluorescence. Ph.D. Dissertation. McMaster University.
- Zamburlini M, Pejović-Milić A, Chettle DR. (2008a) Spectrometry methods for *in vivo* bone strontium measurements. *X-Ray Spectrom.* **37** (1): 42-50.
- Zamburlini M, Pejović-Milić A, Chettle DR. (2008b) Coherent normalization of finger strontium XRF measurements: feasibility and limitations. *Phys. Med. Biol.* **53** (15): N307-N313.
- Zamburlini M, Pejović-Milić A, Chettle DR, Webber CE, Gyorffy J. (2007) *In vivo* study of an x-ray fluorescence system to detect bone strontium non-invasively. *Phys. Med. Biol.* **52** (8): 2107-2122.
- Zamburlini M, Pejović-Milić A, Chettle DR. (2006) Evaluation of geometries appropriate for I-125 *in vivo* bone strontium x-ray fluorescence measurement. *J. Radioanal. Nucl.* **269** (3): 625-629.

Appendix A

COHERENT SCATTER DIFFERENTIAL CROSS- SECTIONS

Calculation of differential cross-section of a material relies on the Thompson formula of a classical scattering cross-section and the atomic form factor $F(x,Z)$ of the associated material. Here, x is a function of both the scattering angle and the photon energy represented in wavelength form:

$$x = \frac{1}{\lambda} \sin\left(\frac{\theta}{2}\right) \quad [\text{\AA}^{-1}] \quad (\text{A1})$$

where: θ = photon scattering angle from incident pathway
 λ = wavelength of the scattering photon [\AA strom]
 Z = atomic number of the scattering atom

Values of the atomic form factors have been interpolated from reference values of x that have been tabulated extensively by (Hubbell and Øverbø, 1979). To extract a form factor for a precise energy and element, approximately 5-7 values given around this energy were plotted as $F(x,Z)$ vs. x . Depending on the energy and element from which a form factor is being interpolated, the relationship was plotted as either: log-log, linear-log, log-linear or linear-linear depending on the relationship that produced the best correlation for a least-squares fit through these points.

The Thompson Differential cross-section of a single photon in the presence of a single electron is given as:

$$\frac{d\Omega}{d\sigma} = \left(\frac{r_e^2}{2}\right)(1 + \cos^2(\theta)) \quad [\text{cm}^2\text{sr}^{-1}/\text{atom}] \quad (\text{A2})$$

Where: $r_e = 2.8178 \text{ fm}$ is the classical electron radius
 θ = photon scattering angle from incident pathway

To include the effect of the specific incident photon energy and the scattering contribution from multiple electrons from an atom with $Z > 1$, the Rayleigh differential cross-section is then given as the Thompson cross-section multiplied by the square of the atomic form factor.

$$\frac{d\Omega}{d\sigma} = \left(\frac{r_e^2}{2}\right)(1 + \cos^2(\theta)) \cdot |F(x, Z)|^2 \quad [\text{cm}^2\text{sr}^{-1}] \quad (\text{A3})$$

This expression calculates the differential cross-section for any given, single Z , homogeneous material. In the case of calculating the differential cross-section for a heterogeneously composed material, such as bone or soft-tissue, the Rayleigh differential cross-section must be computed for all elements present in the composition. The abundance of each element in a mixed material must be taken into account in the full calculation.

The following expression represents the contribution to the differential cross-section from a single element, per gram of total composite material:

$$\frac{d\Omega}{d\sigma}(Z) = \left(\frac{\text{fract.wt}(Z) \cdot N_A}{A(Z)}\right) \cdot \left(\frac{r_e^2}{2}\right)(1 + \cos^2(\theta)) \cdot |F(x, Z)|^2 \quad [\text{cm}^2\text{sr}^{-1}\text{g}^{-1}] \quad (\text{A4})$$

Where: N_A = Avogadro's number
 $A(Z)$ = molar mass of element

$fract.wt(Z)$ = fractional weight of element Z to total medium

To account for contribution to differential cross-section from all elements in 1 gram of medium, the expression above is computed individually for each element and summed together to give the total differential cross-section. The final expression is illustrated below in A5.

$$\frac{d\Omega}{d\sigma} = N_A \cdot \left(\frac{r_e^2}{2}\right) (1 + \cos^2(\theta)) \cdot \sum_Z^{\text{All Z in mixture}} |F(x, Z)|^2 \cdot \left(\frac{fract.wt(Z)}{A(Z)}\right) \quad [\text{cm}^2\text{sr}^{-1}] \quad (\text{A5})$$

A direct comparison of differential cross-sections between different materials is done by comparing the calculated differential cross-sections as follows:

$$\text{Ratio} = \left(\frac{d\Omega}{d\sigma}\right)_{\text{BONE}} / \left(\frac{d\Omega}{d\sigma}\right)_{\text{SOFT TISSUE}} \quad (\text{A6})$$

Note that this calculation does not account for geometry of solid angle of material contribution to scattering. This is an additional calculation that would need to be done in order to understand fully how great a contribution skin and soft tissue has to coherent 35 keV scatter in comparison to bone in a finger. Due to the specific geometry of a human finger, such a calculation is not easily done analytically but might be possible to carry-out through Monte Carlo modelling.

The sources for the compositions of wet cortical bone and human soft-tissue used in calculation of coherent scattering cross-sections are (Woodard, 1962) and (NIST, 2005), respectively. The composition of the plaster of Paris was very simply taken as to be its chemical formula. Considering the level of strontium contamination inherent in plaster of Paris, the chemical formula may not be entirely representative of the true composition as there may be many other trace elements present in gypsum ($\text{CaSO}_4 \cdot 2\text{H}_2\text{O}$), the building material of plaster of Paris. A chemical analysis of a

sample phantom may provide a better representation of the true composition for this analysis.

Appendix B

STRONTIUM QUANTIFICATION AND ERROR PROPAGATION

B.1 Soft-tissue correction and bone strontium quantification calculations

Extraction of strontium concentration may be accomplished using both the K_{α} (x_1) and K_{β} (x_2) strontium K x-ray peak areas. The peak area observed directly from the EDXRF measurement may be corrected for live time or source decay prior to making any further calculations. A calibration line for extraction of each was made using 3 XRF measurement trials on each of the 7 plaster of Paris phantoms. If coherent normalization is to be used then division over the coherent scatter may be done as a first step. The normalization of x-ray peak area (x_i) to the coherent scatter peak may be described as B1:

$$N_i = \frac{x_i}{coh} \quad (B1)$$

Where the uncertainty of the normalized peak area is the statistical uncertainty of the K x-ray peak area added in quadrature to the statistical uncertainty of the coherent scatter peak calculated as:

$$\sigma N_i = \sigma \left(\frac{x_i}{coh} \right) = \frac{x_i}{coh} \sqrt{\left(\frac{\sigma x_i}{x_i} \right)^2 + \left(\frac{\sigma coh}{coh} \right)^2} \quad (B2)$$

In the case of *in vivo* bone strontium measurements, a soft-tissue correction is required to quantify *in vivo* bone strontium. This step is done prior to concentration extraction from a phantom calibration line. The soft-tissue correction relationships for

both K_{α} and K_{β} Sr x-rays used in this work were created by Zamburlini (unpublished work) and were introduced in chapter 2 in E2 and E3. These relationships have the format illustrated in B3.

$$\ln\left(\frac{I_i}{I_{o,i}}\right) = -M_i \cdot T + b_i \quad (\text{B3})$$

Where:

- $I_i \pm \sigma(I_i)$ = measured x-ray peak (i), normalized = $N_i \pm \sigma N_i$
- $I_{o,i} \pm \sigma(I_{o,i})$ = intensity of x-ray peak i before soft-tissue absorption, (initial intensity)
- $M_i \pm \sigma(M_i)$ = slope coefficient of soft tissue correction for x-rays of energy $E(x_i)$
- $T \pm \sigma(T)$ = overlying soft-tissue thickness
- $b_i \pm \sigma(b_i)$ = intercept coefficient of soft-tissue correction x-rays of energy $E(x_i)$

All quantities associated with this calculation have inherent uncertainties. The correction formula may be rearranged into a more useful format for extracting initial peak area as seen in B4.

$$I_{o,i} = \frac{I_i}{\exp(-M_i \cdot T) \cdot \exp(b_i)} \quad (\text{B4})$$

Equation B4 may be rewritten as follows:

$$I_{o,i} = I_i \cdot \exp(M_i \cdot T) \cdot \exp(-b_i) \quad (\text{B5})$$

The variance associated with B5 is illustrated in B6 according to the method outlined in Bevington (1969). This method involves partial differentiating the unattenuated strontium signal $I_{o,i}$ with respect to each variable seen in B5. The partial differentials are multiplied by the variance of the matching variable. Since the slope and intercept of the tissue correction equation are dependent on each other, the covariance between these variables is included as they may have an affect on the final uncertainty.

$$\begin{aligned} \sigma^2(I_{o,i}) = & \left(\frac{\partial I_{o,i}}{\partial I_i}\right)^2 \sigma^2(I_i) + \left(\frac{\partial I_{o,i}}{\partial M_i}\right)^2 \sigma^2(M_i) + \left(\frac{\partial I_{o,i}}{\partial T}\right)^2 \sigma^2(T) + \dots \\ & \dots + \left(\frac{\partial I_{o,i}}{\partial b_i}\right)^2 \sigma^2(b_i) + 2\left(\frac{\partial I_{o,i}}{\partial M_i}\right)\left(\frac{\partial I_{o,i}}{\partial b_i}\right) \text{COV}(M_i, b_i) \end{aligned} \quad (\text{B6})$$

where: $\text{COV}(M_i, b_i)$ is the covariance between slope and intercept. Partial differentiation yields the following terms:

$$\begin{aligned} \frac{\partial I_{o,i}}{\partial I_i} &= \exp(M_i T) \exp(-b_i) \\ \frac{\partial I_{o,i}}{\partial M_i} &= T \exp(M_i T) \exp(-b_i) \\ \frac{\partial I_{o,i}}{\partial T} &= M_i \exp(M_i T) \exp(-b_i) \\ \frac{\partial I_{o,i}}{\partial b_i} &= -I \exp(M_i T) \exp(-b_i) \end{aligned}$$

Introducing the partial differentials back into B6 and putting the uncertainty in terms of the relative uncertainty allows equation B6 simplify to B7.

$$\frac{\sigma^2(I_{o,i})}{I_{o,i}^2} = \frac{\sigma^2(x_i)}{x_i^2} + \frac{\sigma^2(coh)}{coh^2} + T^2\sigma^2(M_i) + M_i^2\sigma^2(T) + \dots$$

$$\dots + \sigma^2(b_i) - 2T \cdot \text{COV}(M_i, b_i) \quad (\text{B7})$$

where:

$$\text{COV}(M_i, b_i) = \sigma^2(M_i) \cdot \frac{1}{N} \sum_i^N X_i \quad (\text{B8})$$

- N is the number of data points used to construct the tissue correction relationship
- X_i is the i^{th} data point reading from the x-axis of the tissue correction plot

The final uncertainty of $I_{o,i}$ is shown in B9.

$$\sigma(I_{o,i}) = I_{o,i} \sqrt{\frac{\sigma^2(x_i)}{x_i^2} + \frac{\sigma^2(coh)}{coh^2} + T^2\sigma^2(M_i) + M_i^2\sigma^2(T) + \dots}$$

$$\dots + \sigma^2(b_i) - 2T \cdot \sigma^2(M_i) \frac{1}{N} \sum_i^N X_i \quad (\text{B9})$$

The covariance requires knowledge of the data points used to create the calibration line in order to calculate this quantity. Unfortunately, the original data plots from which the Zamburlini K_α and K_β tissue correction relationships were created, were not available to this study. This means that the calculation of covariance was not done for any of the quantification uncertainty estimates presented in Chapter 3. Hence:

$$\left(2T \cdot \sigma^2(M_i) \frac{1}{N} \sum_i^N X_i \right) = 0 \quad (\text{B10})$$

Given that the quantity B10 would be subtracted from the total uncertainty calculation, it would influence the final uncertainty by reducing it compared to the case where it was not included at all. Hence, by not calculating it, the uncertainties corresponding to estimates of strontium concentration presented in this paper are all upper bound limits on the expected range of uncertainty.

Note that since the quantification process for bare bone does not require soft-tissue correction, the expression in B9 simplifies to only the Sr x-ray peak uncertainty and the coherent scatter peak uncertainty as seen in B2.

The quantity calculated in B4 may be used to extract strontium concentration from the phantom calibration line. The calibration line has the formula seen in B11.

$$I_{o,i} = \frac{1}{DC} \cdot (m_i Sr_i + C_i) \quad (\text{B11})$$

Where:

DC = poP to wet cortical bone ratio of coherent scatter differential cross-sections at 35.5 keV and 180° coherent scatter

$I_{o,i} \pm \sigma(I_{o,i})$ = tissue corrected, normalized peak area

$Sr_i \pm \sigma(Sr_i)$ = bone strontium concentration in $\mu\text{g Sr/g Ca}$

$C_i \pm \sigma(C_i)$ = intercept of calibration line

$m_i \pm \sigma(m_i)$ = slope of calibration line

Equation B11 can be rearranged to solve explicitly for bone strontium concentration, as displayed in B12.

$$Sr_i = DC \cdot \left(\frac{I_{o,i}}{m_i} - \frac{C_i}{C_i} \right) \quad (\text{B12})$$

To account for uncertainties of $I_{o,i}$, m_i , C_i and the covariance that exists between the intercept and slope ($\sigma_{m_i C_i}^2$), the method outlined by Bevington (1969) is again used. The procedure to propagate associated uncertainties and quantify strontium *in vivo* was modeled after the work of Gordon *et al.* (1994). The variance of a strontium concentration, $\sigma^2(Sr_i)$, extracted from a calibration line is calculated according to B13.

$$\sigma^2(Sr_i) = \left(\frac{\partial Sr_i}{\partial I_{o,i}}\right)^2 \sigma^2(I_{o,i}) + \left(\frac{\partial Sr_i}{\partial m_i}\right)^2 \sigma^2(m_i) + \left(\frac{\partial Sr_i}{\partial C_i}\right)^2 \sigma^2(C_i) + \sigma_{m_i C_i}^2 \quad (\text{B13})$$

However, consideration for the uncertainty of the intercept and calculation of covariance is not necessary in this case since the intercept has been set equal to zero, ($C_i = 0$).

Artificially setting the slope to zero has been done to counteract the interfering effect of the inherent strontium contamination in the plaster of Paris phantoms. Figure B.1 shows the effect that contamination can impart to extracting concentration information from peak areas with fewer counts than those observed from zero phantom measurements.

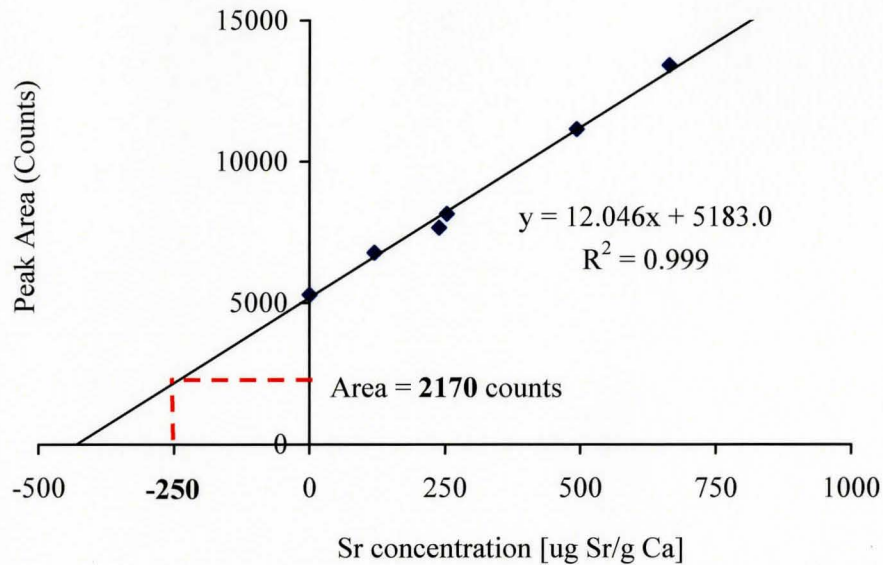


Figure B.1: An example extraction of strontium concentration from a plaster of Paris K_{α} calibration line, with a non-zero intercept, using a low count peak area

In figure B.1, a K_{α} peak area of 2170 counts is less than the intercept of the calibration line and extraction of concentration corresponds to a negative concentration (-250 $\mu\text{g Sr/g Ca}$). This is intuitively not possible. Considering that the bone strontium levels found in humans may be similar to the level of strontium contamination found in the plaster of Paris, this effect must be corrected extract meaningful estimates of concentration. This is done by setting the value of the intercept equal to zero while leaving the value of the slope unchanged. The effect of doing this is illustrated in figure 3.22 where a peak area of 2170 counts now corresponds to a positive concentration.

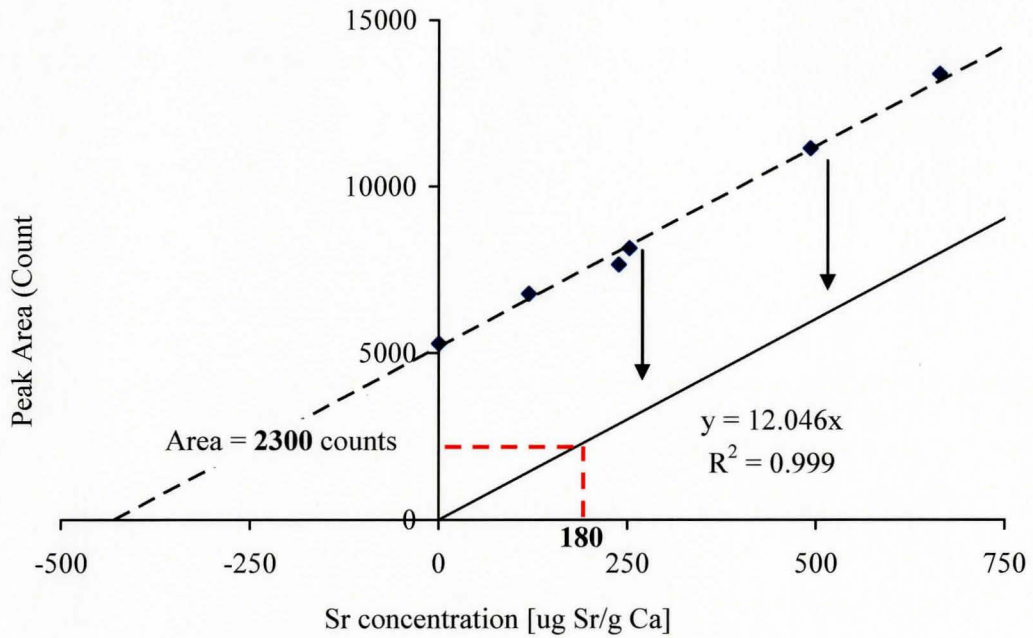


Figure B.2: An example extraction of strontium concentration from a plaster of Paris K_{α} calibration line, with a zero intercept, using a low count peak area

Since the calibration line intercept is no longer involved, equations B12 and B13 simplifies to B14 and B15, respectively.

$$Sr_i = DC \cdot \frac{I_{o,i}}{m_i} \quad (\text{B14})$$

Consideration of the uncertainty in the intercept and covariance between slope and intercept is not needed in the propagation of total error.

$$\sigma^2(Sr_i) = \left(\frac{\partial Sr_i}{\partial I_{o,i}} \right)^2 \sigma^2(I_{o,i}) + \left(\frac{\partial Sr_i}{\partial m_i} \right)^2 \sigma^2(m_i) \quad (\text{B15})$$

where: $\frac{\partial Sr_i}{\partial I_{o,i}} = \frac{DC}{m_i}$

$$\frac{\partial Sr_i}{\partial m_i} = \frac{-DC \cdot I_{o,i}}{m_i^2}$$

Substituting these two partial differentials back into B15 gives B16 which simplifies to B17.

$$\sigma^2(Sr_i) = \left(\frac{DC}{m_i}\right)^2 \sigma^2(I_{o,i}) + \left(\frac{-DC \cdot I_{o,i}}{m_i^2}\right)^2 \sigma^2(m_i) \quad (B16)$$

$$\sigma^2(Sr_i) = DC^2 \left[\left(\frac{\sigma(I_{o,i})}{m_i}\right)^2 + \left(\frac{I_{o,i} \cdot \sigma(m_i)}{m_i^2}\right)^2 \right] \quad (B17)$$

Equation B17 calculates the variance of the uncertainty of the absolute quantity of strontium as estimated by peak i , with consideration for the uncertainty of the calibration line slope. In the case of *in vivo* bone strontium measurement, two peaks, K_α and K_β , may be used to quantify bone strontium. It may be considered that two peaks estimating a quantity will provide a better estimate of bone strontium concentration than one alone and hence, the combined concentration estimation from the K_α and K_β analysis will provide the best indication of bone strontium concentration.

Considering that the K_α peak provides greater count statistics and hence, a lower range of error than the K_β peak, the estimate of bone strontium should be calculated as an average of K_α and K_β estimates, but, weighted in favour of the K_α peak estimate. This concentration will be denoted as Sr_μ and is calculated using an inverse variance weighted mean calculation as seen in B18.

$$Sr_\mu = \frac{\sum_i \frac{Sr_i}{\sigma_{Sr_i}^2}}{\sum_i \frac{1}{\sigma_{Sr_i}^2}}, \quad (B18)$$

Where: $i = 1$ and 2 for K_α and K_β , respectively. Similarly, the combined strontium concentration variance $\sigma_{Sr_\mu}^2$ will be calculated as seen in B19.

$$\sigma_{Sr_\mu}^2 = \left(\sum_i \frac{1}{\sigma_{Sr_i}^2} \right)^{-1} \quad (\text{B19})$$

Note that all concentrations of bone strontium reported in this work are in terms of $Sr_\mu \pm \sigma(Sr_\mu)$ as calculated from the steps outlined in this Appendix.

A sample calculation is provided as follows:

B.2 Ex-vivo bone strontium concentration estimation example

The First measurement of finger 1, of thickness $T = 0.275$ cm, was fitted with our in-house, non-linear least-squares Marquardt fitting routine which produced the following information:

$$\begin{aligned} \text{Area}(K_\alpha) &= x_1 \pm \sigma(x_1) = & 2807.3 \pm 107.4 \\ \text{Area}(K_\beta) &= x_2 \pm \sigma(x_2) = & 974.92 \pm 92.167 \\ \text{Area}(K_{coh}) &= coh \pm \sigma(coh) = & 8404 \pm 118.28 \end{aligned}$$

The Zamburlini soft-tissue correction relationships, provides the necessary values used in this calculation.

$$K_\alpha: \quad \ln\left(\frac{I}{I_0}\right) = (-3.58 \pm 0.04)T + (0.156 \pm 0.006) \quad (\text{E2})$$

$$K_\beta: \quad \ln\left(\frac{I}{I_0}\right) = (-2.86 \pm 0.04)T + (0.162 \pm 0.006) \quad (\text{E3})$$

The calibration line illustrated in chapter 3 was modified so that phantom measurements were normalized to their coherent scatter peaks. That way, the normalized, tissue-corrected peak areas ($I_{o,i}$) could be used directly to extract concentration information.

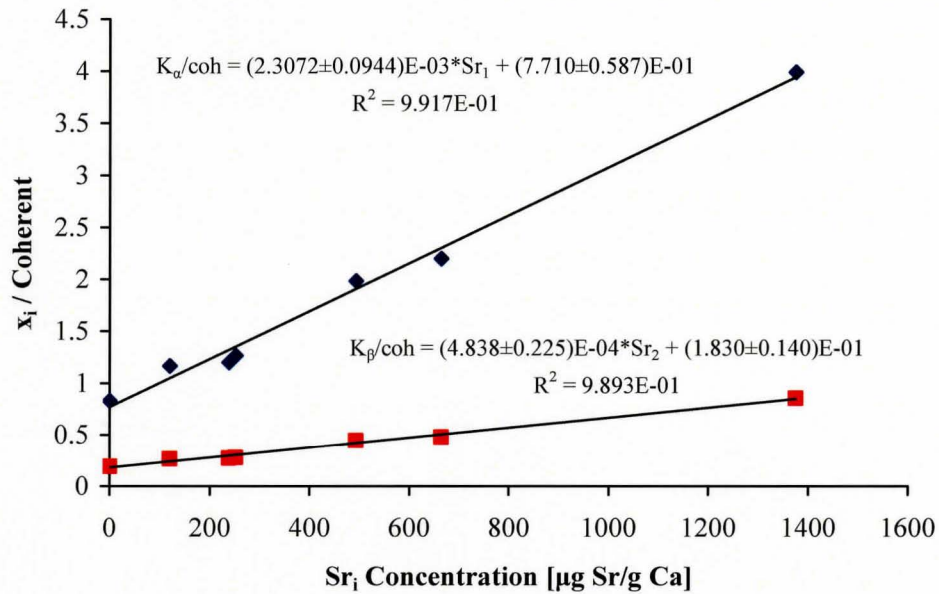


Figure B.3: Plaster of Paris phantom calibration line of K x-ray peak area normalized to coherent scatter peak area versus added strontium

K_α peak calculation:

$$I_1 = \frac{x_1}{coh} = \frac{2807.3}{8404} = 0.334043$$

Substitute I_1 into equation B5

$$I_{o,1} = 0.334043 \cdot \exp(3.58 \text{ cm}^{-1} \cdot 0.275 \text{ cm}) \cdot \exp(-0.156) = 0.764937 \quad (\text{B20})$$

The uncertainty of $I_{o,1}$ may be calculated by substituting all corresponding values into equation B9.

$$\sigma(I_{o,1}) = I_{o,1} \sqrt{\frac{\sigma^2(x_1)}{x_1^2} + \frac{\sigma^2(coh)}{coh^2} + T^2\sigma^2(M_1) + M_1^2\sigma^2(T) + \dots}$$

$$\dots + \sigma^2(b_1) - 2T \cdot \sigma^2(M_1) \frac{1}{N} \sum_i^N X_i$$

$$\sigma(I_{o,1}) = 0.764937 \times \sqrt{\left(\frac{107.4}{2807.3}\right)^2 + \left(\frac{92.167}{974.92}\right)^2 + (0.275\text{cm})^2 (0.04\text{cm}^{-1})^2 + \dots}$$

$$\dots + (3.58\text{cm}^{-1})^2 (0.032 \cdot 0.275\text{cm})^2 + (0.006)^2$$

$$\sigma(I_{o,1}) = 0.040558 \quad (\text{B21})$$

To extract strontium concentration, B20 and B21 are substituted into equations B14 and B17, respectively.

$$Sr_1 = DC \cdot \frac{I_{o,1}}{m_1}$$

$$Sr_1 = 1.4 \cdot \frac{0.764937}{2.3072 \times 10^{-3}} = 464.1597 \text{ } \mu\text{g Sr/g Ca} \quad (\text{B22})$$

$$\sigma^2(Sr_1) = 1.4^2 \left[\left(\frac{\sigma(I_{o,1})}{m_1} \right)^2 + \left(\frac{I_{o,1} \cdot \sigma(m_1)}{m_1^2} \right)^2 \right]$$

$$\sigma^2(Sr_1) = 1.96 \left[\left(\frac{0.040558}{2.3072 \times 10^{-3}} \right)^2 + \left(\frac{0.764937 \cdot 9.4359 \times 10^{-5}}{(2.3072 \times 10^{-3})^2} \right)^2 \right] = 966.0136$$

$$\sigma(Sr_1) = \sqrt{966.0136}$$

$$\sigma(Sr_1) = 31.0808 \mu\text{g Sr/g Ca} \quad (\text{B23})$$

Therefore, $Sr_1 \pm \sigma(Sr_1) = 464 \pm 31 \mu\text{g Sr/g Ca}$. Note that although they are not displayed, the extra decimal places are carried through into the inverse variance weighted mean calculations to arrive at the final estimate of bone strontium concentration. The K_β peak area strontium extraction procedure is calculated in the same format as the K_α , as illustrated below.

K_β peak calculations:

$$I_2 = \frac{x_2}{coh} = \frac{974.92}{8404} = 0.116007$$

Substitute I_2 and associated quantities into equation B5 gives:

$$I_{o,2} = 0.116007 \cdot \exp(2.86\text{cm}^{-1} \cdot 0.275\text{cm}) \cdot \exp(-0.162) = 0.2165 \quad (\text{B24})$$

The uncertainty of $I_{o,1}$ may be calculated by substituting all corresponding values into equation B9.

$$\sigma(I_{o,2}) = I_{o,2} \sqrt{\frac{\sigma^2(x_2)}{x_2^2} + \frac{\sigma^2(coh)}{coh^2} + T^2 \sigma^2(M_2) + M_2^2 \sigma^2(T) + \dots}$$

$$\dots + \sigma^2(b_2) - 2T \cdot \sigma^2(M_2) \frac{1}{N} \sum_i X_i$$

$$\sigma(I_{o,2}) = 0.2165 \times \sqrt{\left(\frac{92.167}{974.92}\right)^2 + \left(\frac{118.28}{8404}\right)^2 + (0.275\text{cm})^2 (0.04\text{cm}^{-1})^2 + \dots}$$

$$\dots + (2.86\text{cm}^{-1})^2 (0.032 \cdot 0.275\text{cm})^2 + (0.006)^2$$

$$\sigma(I_{o,2}) = 0.021567 \quad (\text{B25})$$

To extract strontium concentration, B24 and B25 are substituted into equations B14 and B17, respectively.

$$Sr_2 = DC \cdot \frac{I_{o,2}}{m_2}$$

$$Sr_2 = 1.4 \cdot \frac{0.216477}{4.8382 \times 10^{-4}} = 626.402 \text{ } \mu\text{g Sr/g Ca} \quad (\text{B26})$$

$$\sigma^2(Sr_2) = 1.4^2 \left[\left(\frac{\sigma(I_{o,2})}{m_2} \right)^2 + \left(\frac{I_{o,2} \cdot \sigma(m_2)}{m_2^2} \right)^2 \right]$$

$$\sigma^2(Sr_2) = 1.96 \left[\left(\frac{0.021567}{4.8382 \times 10^{-4}} \right)^2 + \left(\frac{0.216477 \cdot 2.2486 \times 10^{-5}}{(4.8382 \times 10^{-3})^2} \right)^2 \right] = 4742.180$$

$$\sigma(Sr_2) = \sqrt{4742.180}$$

$$\sigma(Sr_2) = 68.864 \text{ } \mu\text{g Sr/g Ca} \quad (\text{B27})$$

Therefore, $Sr_2 \pm \sigma(Sr_2) = 626 \pm 69 \text{ } \mu\text{g Sr/g Ca}$. Finally, a calculation of the inverse variance weighted mean is performed to combine the K_α and K_β estimates of peak area. The calculated quantities B22, B23, B26 and B27 are substituted into B18.

$$Sr_\mu = \frac{\sum_{i=1}^2 \frac{Sr_i}{\sigma_{Sr_i}^2}}{\sum_{i=1}^2 \frac{1}{\sigma_{Sr_i}^2}} \quad (\text{B18})$$

$$S_{r_{\mu}} = \frac{\frac{S_{r_1}}{\sigma^2(S_{r_1})} + \frac{S_{r_2}}{\sigma^2(S_{r_2})}}{\frac{1}{\sigma^2(S_{r_1})} + \frac{1}{\sigma^2(S_{r_2})}}$$

$$S_{r_{\mu}} = \frac{\frac{464.1597}{966.0136} + \frac{626.402}{4742.180}}{\frac{1}{966.0136} + \frac{1}{4742.180}}$$

$$S_{r_{\mu}} = 491.616 \mu\text{g Sr/g Ca}$$

The uncertainty of this quantity is the combined uncertainty calculated from the K_{α} and K_{β} soft tissue estimate using equation B19 as seen below.

$$\sigma_{S_{r_{\mu}}}^2 = \left(\sum_{i=1}^2 \frac{1}{\sigma_{S_{r_i}}^2} \right)^{-1}$$

$$\sigma^2(S_{r_{\mu}}) = \left(\frac{1}{\sigma^2(S_{r_1})} + \frac{1}{\sigma^2(S_{r_2})} \right)^{-1}$$

$$\sigma^2(S_{r_{\mu}}) = \left(\frac{1}{966.0136} + \frac{1}{4742.180} \right)^{-1}$$

$$\sigma^2(S_{r_{\mu}}) = 802.533$$

$$\sigma(S_{r_{\mu}}) = \sqrt{802.533} = 28.329$$

Therefore, the final strontium concentration reported based on strontium K_{α} and K_{β} peak areas acquired from a single EDXRF measurement is:

$$S_{r_{\mu}} + \sigma(S_{r_{\mu}}) = 492 \pm 28 \mu\text{g Sr/g Ca}$$

where the uncertainty is calculated from the propagation of all uncertainties associated with individual measurements, tissue thickness readings, soft-tissue corrections and slope concentration extraction. This is the method by which all 70 of the tissue intact concentration extractions were calculated. Recall that this is an upper limit estimate of the true uncertainty given that the covariance of the tissue correction relationship was not included. Also not included is consideration of the uncertainty that may be associated with the ratio of coherently scattered differential cross-section between bone and poP and calculation of the absorption of the ^{125}I 35keV coherently scattered photons used in the normalization.

B.3 Examination of the influence of ignoring the uncertainties inherent to the soft-tissue calibration line

If we ignore the uncertainty associated with the tissue correction relationship all together, then we might arrive at a lower limit estimate of the true uncertainty. This would effectively provide a range of possible uncertainty in which the true uncertainty would be found, if covariance were taken into account. This range is calculated for the example given above.

If all tissue correction uncertainties are ignored, than the quantity B9 simplifies as several quantities are eliminated. This is illustrated below where a subscript L is used to denote quantities associated with the lower limit of uncertainty.

$$\sigma_L(I_{o,i}) = I_{o,i} \sqrt{\frac{\sigma^2(x_i)}{x_i^2} + \frac{\sigma^2(coh)}{coh^2} + \cancel{T^2 \sigma^2(M_i)} + M_i^2 \sigma^2(T) + \dots}$$

$$\dots + \cancel{\sigma^2(b_i)} - \cancel{2T \cdot \sigma^2(M_i) \frac{1}{N} \sum_i X_i}$$

$$\sigma_L(I_{o,i}) = I_{o,i} \sqrt{\frac{\sigma^2(x_i)}{x_i^2} + \frac{\sigma^2(coh)}{coh^2} + M_i^2 \sigma^2(T)}$$

Using the concentration extraction procedure outlined above, the concentration uncertainty estimated from trial 1 on finger 1 are recalculated without taking the uncertainty of the tissue correction relationship into account. Note that the quantities B21 and B25 decrease as indicated by the arrows below:

$$\sigma(I_{o,1}) = 0.040558 \rightarrow \sigma_L(I_{o,1}) = 0.039409$$

$$\sigma(I_{o,2}) = 0.021567 \rightarrow \sigma_L(I_{o,2}) = 0.021396$$

This results in a consequent change in the uncertainties of the calculated strontium concentrations as illustrated below:

$$\sigma(Sr_1) = 31.081 \mu\text{g Sr/g Ca} \rightarrow \sigma_L(Sr_1) = 30.532 \mu\text{g Sr/g Ca}$$

$$\sigma(Sr_2) = 68.864 \mu\text{g Sr/g Ca} \rightarrow \sigma_L(Sr_2) = 68.415 \mu\text{g Sr/g Ca}$$

A change in the concentration uncertainty will result in a change in both the final combined estimate of strontium concentration and its uncertainty as follows:

$$Sr_{L,\mu} = \frac{\frac{Sr_1}{\sigma_L^2(Sr_1)} + \frac{Sr_2}{\sigma_L^2(Sr_2)}}{\frac{1}{\sigma_L^2(Sr_1)} + \frac{1}{\sigma_L^2(Sr_2)}}$$

$$Sr_{L,\mu} = \frac{\frac{464.1597}{932.1889} + \frac{626.402}{4680.577}}{\frac{1}{932.1889} + \frac{1}{4680.577}}$$

$$Sr_{L,\mu} = 491.105 \mu\text{g Sr/g Ca}$$

The final uncertainty is calculated as follows:

$$\sigma^2(Sr_\mu) = \left(\frac{1}{932.1889} + \frac{1}{4680.577} \right)^{-1} = 777.368$$

$$\sigma(Sr_\mu) = \sqrt{777.368} = 27.881$$

Thus, dropping the tissue correction model uncertainties changes the final concentration and uncertainty as follows:

$$Sr_\mu \pm \sigma(Sr_\mu) = 491.6 \pm 28.3 \quad \rightarrow \quad Sr_{L,\mu} \pm \sigma(Sr_{L,\mu}) = 491.1 \pm 27.8$$

This represents only a 0.1% decrease in the final strontium concentration estimate and a decrease in the final uncertainty by only 1.8%. This indicates that the effect of including the calculation of covariance would only play a very small role in altering the calculated error and estimated concentration. This difference is representative of the difference seen in the remaining 69 trials. Therefore, it is of minimal consequence that the covariance was not used in this study.